AD-A067 937　　REGIS COLL　WESTON MASS　　　　　　　　　　　　　　F/G 4/2
METEOROLOGICAL STUDIES--ATMOSPHERIC ANALYSIS, AUTOMATED WEATHER--ETC(U)
FEB 79　S L BURKE　　　　　　　　　　　　　　　　　　　F19628-77-C-0010
UNCLASSIFIED　　　　　　　　　　　　AFGL-TR-79-0047　　　　　　NL

1 OF 2
AD
A067937

12
B.S.

AFGL-TR-79-0047

LEVEL II

AD A067937

DDC FILE COPY

METEOROLOGICAL STUDIES
Atmospheric Analysis
Automated Weather System Development
Satellite Studies

S. Leonarda Burke

Regis College
235 Wellesley Street
Weston, Massachusetts 02193

28 February 1979

Final Report for Period 28 September 1976 - 30 November 1978

Approved for public release; distribution unlimited

DDC
RECEIVED
APR 27 1979
A

AIR FORCE GEOPHYSICS LABORATORY
AIR FORCE SYSTEMS COMMAND
UNITED STATES AIR FORCE
HANSCOM AFB, MASSACHUSETTS 01731

79 04 26 413

Qualified requestors may obtain additional copies from the Defense Documentation Center. All others should apply to the National Technical Information Service.

UNCLASSIFIED

SECURITY CLASSIFICATION OF THIS PAGE (When Data Entered)

(19)

REPORT DOCUMENTATION PAGE

READ INSTRUCTIONS BEFORE COMPLETING FORM

1. REPORT NUMBER (18) AFGL-TR-79-0047 ✓

2. GOVT ACCESSION NO.

3. RECIPIENT'S CATALOG NUMBER (9)

4. TITLE (and Subtitle) (6)
METEOROLOGICAL STUDIES - -
Atmospheric Analysis,
Automated Weather System Development,
Satellite Studies.

5. ~~TYPE OF REPORT & PERIOD~~ COVERED
Final Report.
[redacted]

6. ~~PERFORMING ORG. REPORT NUMBER~~
28 Sep 76-30 Nov 78

7. ~~AUTHOR(s)~~ (10)
S. Leonarda/Burke

8. ~~CONTRACT OR GRANT NUMBER(s)~~ (15)
F19628-77-C-0010 ✓

9. PERFORMING ORGANIZATION NAME AND ADDRESS
Regis College ✓
235 Wellesley Street
Weston, Massachusetts 02193

10. PROGRAM ELEMENT, PROJECT, TASK AREA & WORK UNIT NUMBERS
PE: 62101F; 61102F
Task: 667008, 10; 2310G2
JOCAS: 2310G2AF

11. CONTROLLING OFFICE NAME AND ADDRESS
Air Force Geophysics Laboratory
Hanscom AFB, Massachusetts 01731
Monitor/Peter A. Giorgio/LY

12. ~~REPORT DATE~~ (11)
28 Feb[redacted]y 1979

13. NUMBER OF PAGES
185

14. MONITORING AGENCY NAME & ADDRESS(if different from Controlling Office)
(12) 188p.

15. SECURITY CLASS. (of this report)
UNCLASSIFIED

15a. DECLASSIFICATION/DOWNGRADING SCHEDULE

16. DISTRIBUTION STATEMENT (of this Report)

Approved for public release; distribution unlimited.

(16) 6670, 2310

(17) 667008, 2310G2

17. DISTRIBUTION STATEMENT (of the abstract entered in Block 20, if different from Report)

18. SUPPLEMENTARY NOTES

19. KEY WORDS (Continue on reverse side if necessary and identify by block number)

lapse stratification
stable stratification
rough links z_0
extinction coefficient
slant visual range
Harris Disk Monitor
spectral signature
annular
Koschmieder's Law
SRI models
Allard's Law

20. ABSTRACT (Continue on reverse side if necessary and identify by block number)

This report details research efforts undertaken by the Regis College Research Center in three areas of meteorology, atmospheric analysis, automated weather system development and satellite studies. In atmospheric analysis, a number of modeling experiments were performed which explored the flux-profile relationships in the atmospheric surface layer. In mesoscale forecasting, automated procedures were developed to: (1) specify the type and intensity of surface weather phenomena and (2) exploit indirect methods to specify and predict landing zone slant visual range. In satellite studies, data acquired by the McIDAS

(over)

DD FORM 1 JAN 73 1473 EDITION OF 1 NOV 65 IS OBSOLETE

UNCLASSIFIED

SECURITY CLASSIFICATION OF THIS PAGE (When Data Entered)

301000

LB

Block 20 (continued)

(Man-computer Interactive Data Access System) were used to perform analyses in the following areas: the physical properties of clouds; the objective extraction of satellite-sensed vertical surroundings; the use of imagery data for investigating automated short range forecasting techniques; the objective specification of cloud type from DMSP (Defense Meteorological Satellite Program) very high resolution satellite imagery.

ACCESSION for

NTIS	White Section	☑
DDC	Buff Section	☐
UNANNOUNCED		☐

JUSTIFICATION ....

BY ....

DISTRIBUTION/AVAILABILITY CODES

Dist.	AVAIL. and/or SPECIAL
A	

TABLE OF CONTENTS

Section		Page
	Introduction	6
1.0	ATMOSPHERIC ANALYSIS	7
1.1	Errors of Estimates in the Atmospheric Surface Layer	7
1.1.1	Introduction	7
1.1.2	Experiments	9
1.1.3	Optimization of the gradient equations	11
1.1.4	Uses of the gradient equations	14
1.1.4.1	Estimation of wind and temperature with the aid of micrometeorological measurements	15
1.1.4.2	Estimation of eddy fluxes with the aid of multi-level measurements of wind and temperature	16
1.1.4.3	Estimation of wind and temperature with the aid of micrometeorological estimates	21
1.1.5	Conclusions	22
	Appendix	24
	References	26
	Tables	27
	Figures	37
1.2	A Contour Analysis of the Temperature Forecast Errors in the Boundary Layer Model	41
1.2.1	Introduction	41
1.2.2	Technique of analysis	43
1.2.2.1	General contour features and qualities	43

TABLE OF CONTENTS (Continued)

Section		Page
1.2.2.2	Measures	44
1.2.3	Results of analysis	45
1.2.3.1	Models "C", "H" and "V"	45
1.2.3.2	Model 6	46
1.2.3.3	Similarity comparisons	46
	Tables	48
	Figures	51
2.0	AUTOMATED WEATHER SYSTEM DEVELOPMENT	53
2.1	Introduction	53
2.2	Weather Test Facility Site Description	54
2.3	Data Reduction and Analysis	59
	Figures	61
2.4	Automation of Visual Present Weather Observations	74
2.5	Remote Tower Slant Visual Range Studies	78
2.5.1	Background	78
2.5.2	Initial data analysis	79
2.5.3	Analysis technique formulation	80
2.5.4	Results	82
	Tables	85
2A	APPENDIX: Interactive Graphics Program Description	87
2A-1	Introduction	87
2A-1.1	Four program decks	87
2A-1.2	Ready	87

TABLE OF CONTENTS (Continued)

Section		Page
2A-1.3	Graphic overlays in the system	88
2A-2	Overlay (0,0)	88
2A-3	Overlay (1,0)	88
2A-4	Overlay (2,0)	89
2A-4.1	Option One	90
2A-4.2	Option Three	91
2A-4.3	Option Four	91
2A-5	Overlay (3,0)	91
2A-6	Overlay (4,0)	92
2A-7	Overlay (5,0)	93
2A-8	Overlay (6,0)	93
2A-9	Overlay (7,0)	93
2A-10	Overlay (8,0)	95
2A-11	Overlay (9,0)	96
2A-12	Overlay (10,0)	96
2A-13	Limitations	97
2A-14	Original list for graphics	98
3.0	SATELLITE STUDIES	99
3.1	Introduction	99
3.2	McIDAS Support	99
3.2.1	McIDAS operations	99
3.2.2	McIDAS software	102
	Tables	105

TABLE OF CONTENTS (Continued)

Section		Page
3.3	Vertical Sounding Evaluation	109
	Tables	114
	Figures	119
3.4	Automated Cloud Identification by Second Order Statistical Methods	121
3.4.1	Introduction	121
3.4.2	Nature of the problem	122
3.4.3	The Fast Fourier Transform (FFT)	122
3.4.4	Computation of power spectra	124
3.4.5	Normalized averaged power spectra (NAA) computation	126
3.4.6	A study of two cloud areas	127
3.4.7	Conclusions	129
3.5	Estimates of Cloud Properties derived from Satellite Sensors	129
3.5.1	Visible and infrared radiation in cloudy atmospheres	129
3.5.2	Satellite measurements	133
3.5.3	Aircraft measurements	134
	Tables	136
3.5.4	Analysis of variance	137
	Figures and Tables	138
3.5.5	Multiple regression	147
	Figures	148
3.5.6	Conclusions	151
3.6	Objective Prediction of Cloud Cover and Precipitation	152
3.6.1	Introduction	152

TABLE OF CONTENTS (Continued)

Section		Page
3.6.2	Objective	152
	Figures	153
3.6.3	Data sample	154
3.6.4	Data corrections	155
	Figures	156
3.6.5	Data sampling	157
3.6.6	Brightness analysis	159
	Tables	160
	Figures	162
3.6.7	Conclusions	163
	Figures	164
3.7	Cloud Pattern Motion Vectors	170
3.7.1	Introduction	170
3.7.2	Three significant steps to motion vector analysis	172
3.7.3	Computational details of motion vector model	174
	Figures	179
	Tables	181
3.7.4	Summary	182
	References	183
	Acknowledgment	185

INTRODUCTION

This report describes the results achieved by the Regis College Research Center during a 26-month contract with the Air Force Geophysics Laboratory (AFGL). The scientific disciplines under investigation were varied and all of them paralleled some of the efforts undertaken by the Meteorology Division, AFGL. The Research Center worked on three general areas: atmospheric analysis, mesoscale forecasting, and satellite meteorology.

In atmospheric analysis we performed a number of modeling experiments to explore flux-profile relationships in the atmospheric surface layer. In mesoscale forecasting we concentrated on the development of automated procedures for specifying the type and intensity of surface weather phenomena and the development of indirect methods for specifying and predicting landing zone slant visual range. In satellite studies, we used data acquired by the Man-computer Interactive Data Access System (McIDAS) to perform analyses in the following areas: the physical properties of clouds, the objective extraction of satellite sensed vertical soundings, the use of imagery data for investigating automated short range forecasting techniques, and the objective specification of cloud type from the Defense Meteorological Satellite Program (DMSP) very high resolution satellite imagery by advanced statistical methods. This last effort in DMSP imagery was conducted in collaboration with the Air Force Global Weather Central (AFGWC) and was undertaken because of AFGWC's need for assistance in this area.

1.0 ATMOSPHERIC ANALYSIS

1.1 Errors of Estimates in the Atmospheric Surface Layer

1.1.1 Introduction

Many, if not all, empirical formulas in the physical sciences are determined by some optimization procedure applied to sets of measurements. A frequently used procedure, for example, is the method of least squares in which the best formula is the one rendering the sum of squares of the differences between estimated and measured values a minimum for a given set of measurements. The best formula obtained in this manner is thus subject to variations due to changes in the set of measurements employed in the optimization and to changes in the variable optimized. It is therefore no mere idle curiosity either to ask how good a best-fit empirical formula is or to examine how sensitive such a formula is to differences in the optimization procedure. The answers to these questions are important not only in determining the accuracy of the formulas but also in assessing the utility of the formulas.

Businger, Wyngaard, Izumi and Bradley (1971) proposed the following set of formulas for the relationship between the vertical gradients of the mean wind and potential temperature and the eddy fluxes within the atmospheric surface layer:

(1) lapse stratification

$$\frac{dV}{dz} = \frac{u_*}{.35} z^{-1} \left(1 + 15 \frac{z}{L}\right)^{-\frac{1}{4}} \qquad (1.1)$$

$$\frac{d\Theta}{dz} = .74\, \theta_* z^{-1} \left(1 + 9 \frac{z}{L}\right)^{-\frac{1}{2}} \qquad (1.2)$$

(2) stable stratification

$$\frac{dV}{dz} = \frac{u_*}{.35} z^{-1} (1 + 4.7 \frac{z}{L}) \tag{1.3}$$

$$\frac{d\Theta}{dz} = \theta_* z^{-1} (.74 + 4.7 \frac{z}{L}) \tag{1.4}$$

in which V is wind speed, Θ potential temperature, and z the height above the ground at which V and Θ are referred. Three micrometeorological parameters u_*, θ_* and L are defined, respectively, by

$$u_* = (\frac{\tau_0}{\rho})^{\frac{1}{2}} = (-\overline{uw})^{\frac{1}{2}} \tag{1.5}$$

$$\theta_* = \frac{H_0}{c_p} / .35 u_* = \frac{\overline{w\theta}}{.35 u_*} \tag{1.6}$$

$$L = - \frac{u_*^3 \overline{\Theta}}{.35 g \overline{w\theta}} \tag{1.7}$$

where u_* is the friction velocity, θ_* the scaling temperature and L is the Monin-Obukhov length. $\overline{\Theta}$ is the mean potential temperature of the atmospheric surface layer.

$\overline{uw}$ and $\overline{\theta w}$ are the covariance between the longitudinal and vertical components of wind and the covariance between the potential temperature and the vertical component of wind, respectively.

These formulas were derived in accordance with the principle of least squares using the results of measurements taken in the Kansas 1968 Field Program of the Air Force Cambridge Research Laboratories. A complete report on the measurements taken and the data collected in the field program has been prepared by Izumi (1971) in the Kansas 1968 Field Program Data Report (hereafter referred to as the Report). The veracity and significance of the formulas rest both on the careful measurements and the meticulous analyses of the data, and are highly appreciated by the scientific community (Panofsky (1974)).

Ironically, it is this recognition of excellence that has led us to raise the question concerning the utility of these formulas. For, in almost any other perceivable situation, in which some applications of the formulas are desired, we would not expect to have the sophistication of instrumentation and the accuracy of measurements as those that were present in the Kansas 1968 Field Program. It is more likely that the formulas would be utilized in conjunction with data that are obtained in a less refined manner. A few inevitable questions then are: Can these formulas still be used with the same degree of confidence? What reservations should be kept in applying these formulas?

The work reported below is our attempt to answer these questions without the benefit of another field program. By depriving ourselves of some of the measurements obtained in the field program and employed in the derivation of Eq. (1), we constructed a hypothetical set of measurements that might be obtained with less complete yet practical instrumentation. We then sought the best-fit formulas, in those that would give the least square errors of estimate in a slightly different but equally sound manner as that employed by Businger et al. Comparisons were made among various choices of values of parameters in these formulas by calculating the square errors of estimate as defined here using the data available in the field program as appeared in the Report.

1.1.2 Experiments

While adhering to the same assumption about the surface layer and to the same notion about optimality as those adopted by Businger et al., we have chosen variations to two major decisions they took in the course of arriving at Eq.(1). These deviations resulted in the use of different data for estimating values of the parameters and different objective functions for minimizing the difference between estimated and measured values. We shall elaborate upon these differences in this section.

On the basis of analyses by Haugen, Kaimal and Bradley (1971), Businger et al. assume that the heat and momentum fluxes remain constant with height in the atmospheric surface layer and, therefore, parameters u_*, θ_* and L in Eq.(1) are constant in each sample case. However, in order to reconcile the measurements of the Reynolds stress by drag plates at the ground and by the sonic anemometers on the tower, they recognized the trend of variation of the measured $\overline{uw}$ with height between 5.66 m- and 22.63 m-level and, took the latter into account in estimating the surface value of the stress. The *friction velocity* u_* characteristic of the surface layer was calculated from this surface value of the stress. On the other hand, they thought it best to average the values of heat flux measured at three different levels (5.66, 11.32 and 22.63 m) in defining the value of the surface layer heat flux.

We imagine that we set up the required instrumentation a posteriori to the assumption that the fluxes remain constant with height. It would therefore be natural, for reasons of economy, to measure each flux at one level. This we do at the lowest level available in the Report. Thus, for the momentum flux we take the average of two drag-plate measurements, corrected for the difference between the plates and the sonic anemometers. It is the same as that used by Businger et al. For the heat flux, however, we take the value of $\overline{w\theta}$ measured at $z = 5.66$ m as the value representative of the surface layer, in contradistinction to that of Businger et al. Likewise, while Businger et al. used the value of θ at $z = 4$m as the estimate of $\overline{\theta}$ in the expression of L, we employ the value of θ at $z = 2$m for $\overline{\theta}$.

In minimizing the difference between estimate and observation, Businger et al. chose for the objective function of minimization the sum of squares of differences between the estimated and observed vertical gradients. Since the vertical gradients were never measured directly in practice, they resorted to an alogarithm to obtain the so-called observed values (Businger et al. (1971)).

As shown in Appendix 1.1, since the assumed vertical-gradient equations may be readily integrated with respect to height to yield the difference between any two levels above ground, we choose for the objective function of minimization the weighted sum of squares of differences between estimated and observed differences between two consecutive levels. The weights are chosen to be proportional with the difference in logarithm of the height. Thus, all the sublayers between 2m- and 32m-levels considered in this study, from 2m to 4m, from 4m to 8m, from 8m to 16m, and from 16m to 32m, have the same weight.

1.1.3 Optimization of the gradient equations

We assume that the vertical-gradient equations are given by

(1) lapse stratification

$$\frac{d\hat{V}}{dz} = \frac{u_*}{k_V} z^{-1} \left(1 + \gamma_V \frac{z}{L}\right)^{-1/n_V} \tag{3.1}$$

$$\frac{d\hat{\theta}}{dt} = \frac{\theta_*}{k_H} z^{-1} \left(1 + \gamma_H \frac{z}{L}\right)^{-1/n_H} \tag{3.2}$$

(2) stable stratification

$$\frac{d\hat{V}}{dz} = \frac{u_*}{k_V} z^{-1} (\beta_V + \delta_V z) \tag{3.3}$$

$$\frac{d\hat{\theta}}{dz} = \frac{\theta_*}{k_H} z^{-1} (\beta_H + \delta_H z) \tag{3.4}$$

in which (k_V, γ_V, n_V), (k_H, γ_H, n_H) under lapse stratification and (β_V, δ_V) (β_H, δ_H) under stable stratification are to be determined such that quantities such as

$$\sum_{n=1}^{N} \sum_{k=2}^{5} \left[(\hat{V}_k - \hat{V}_{k-1}) - (V_k - V_{k-1})\right]_n^2$$

where symbol ^ is used to denote the estimate, are minimized. Here, integer index k denotes the level in the vertical, with k=1 referring to the lowest, z = 2m and k=5 to the highest, z = 32m. Each value of integer index n identifies one sample case which is a 15 minute period during which a set of concurrent measurements on V, Θ, $\overline{uw}$ and $\overline{w\theta}$ is available (see Tables 1.1 and 1.2 of the Report). We shall call these the universal constants of the flux-profile relationships.

Excluding runs 46 and 47 (as called in the Report) in view of missing data of $\overline{uw}$ and $\overline{w\theta}$ at z = 22.63 m, we find altogether 68 cases with lapse stratification and 42 cases with stable stratification. Each group has been treated as one sample group characteristic of the respective stratification,after the initial trial of dividing the groups into subgroups of approximately twenty cases failed to reveal any sign of consistency in the optimal values of the universal constants among different subgroups.

The optimal sets of the universal constants are sought within the following confines:

(1) k_V and k_H are positive real numbers with two decimal places,

(2) γ_V and γ_H are real integers,

(3) n_V and n_H are real integers,

(4) β_V, δ_V, β_H and δ_H are real numbers with one decimal place.

It is readily recognized that all the values proposed by Businger et al. fall within the above restrictions. That these restrictions have a sufficiently fine resolution for the given set of measurements may be seen from the values of root-mean-square errors of estimate tabulated in Tables 1.1a, 1.1b and 1.1c.

Table 1.1 is presented to demonstrate the structure of topography of the root-mean-square errors of estimate. Each of the tables gives a three-dimensional cross-section on a hyperplane defined by n_V = const. The entry in the last column under $\overline{(2.32)}$, where the overbar signifies average, gives the value of the objective function of optimization at a given set of (k_V, γ_V) which defines the coordinates of the valley of the topography. Each entry in other columns is the root-mean-square error of estimate of the wind-speed difference between the two levels bounding the sublayer. The smallest value in each column is underlined for easy recognition.

It appears from these tables that there are a number of equally acceptable choices for the optimal set of universal constants. By using the values of mean square error of estimate, however, it is possible to discriminate further among them to choose the set defined by

$$n_V = 4, \; k_V = .34, \; \gamma_V = 17.$$

The finer structure of topography of the average square of error of estimate in the vicinity of the optimal set is given in Table 1.2. A comparison of the values of the average square errors between this set and that of Businger et al. shows that the difference is insignificant. Similar procedures are followed in the determination of the optimal sets for other categories. The results for lapse stratification are summarized in Table 1.3a and those for stable stratification in Table 1.4a. Accompanying each set is the recommended set of the universal constants which is obtained when the optimality of the objective function in the optimal set is given up for uniformity of values of constants. The values of the root-mean-square errors of estimate are included in the table to show the effect of such a trade-off.

Tables 1.5 and 1.6 are prepared to exhibit finer details of these selected sets of the universal constants as well as of the sets proposed by Businger et al. Superscripts r, o and b are entered in appropriate places to designate the rows referring to the recommended sets, the optimal sets, and the sets of Businger et al, respectively. It is clear from these tables that, measured in terms of the objective function employed in this study, the sets of Businger et al. differ little from the other two in both wind speed and potential temperature under lapse stratification. This, however, is not the case under stable stratification. In both wind speed and potential temperature they are associated with considerably larger errors of estimate, particularly in the upper two sublayers.

1.1.4 Uses of the gradient equations

There are two practical uses to which the vertical gradient equations can be put. One is to estimate wind speed and/or potential temperature within the surface layer at a level away from the level of measurement. This may be accomplished by integrating the gradient equations if there are measurements or estimates of the micrometeorological parameters together with the measurement of wind and/or temperature at one level. The other is to estimate the values of eddy fluxes from multi-level measurements of wind and temperature. This is done by inverting the integrals of the gradient equations. The application for such purposes of the gradient equations obtained in the previous section are discussed in the following.

1.1.4.1 Estimation of wind and temperature with the aid of micrometeorological measurements.

A comparison of errors of estimate, which are obtained with the use of the data in the Report, is made using three different methods of estimating wind and temperature at various levels from the measurements taken at $z = 2$m.

The micrometeorological method makes use of the value of u_* and θ_* calculated from the measurements of the momentum flux at the ground and of the heat flux at $z = 5.66$ m. The value at level z_k, $F(z_k)$, is estimated by

$$F(z_k) = F(z_1) + \int_{z_1}^{z_k} \frac{dF}{dz}\, dz \qquad (4.1)$$

where $z_1 = 2$m and $\frac{dF}{dz}$ is the vertical gradient defined by one of Eqs (3.1) ∿ (3.4) with the corresponding optimal set of the universal constants.

The method of linear regression estimates $F(z_k)$ by

$$F(z_k) = A_k + B_k F(z_1) \qquad (4.2)$$

where A_k, B_k are determined by linear regression. The method of polynomial-in-logarithm assumes that

$$F(z_k) = F(z_1) + P_4(\ln \frac{z_k}{z_1}) \qquad (4.3)$$

in which $P_4(x)$ is the fourth-order polynomial in x. The values of all constants in the polynomial are determined in accordance with the least-squares principle, with the aid of the same set of data, as were A_k and B_k in the method of linear regression, that is used in the micrometeorological method.

The results are summarized in Table 1.7. It shows that, at least, with the set of measurements available there is no evidence suggesting that the micrometeorological method is superior to the other two, as far as the accuracy of estimation is concerned. On the contrary, the errors in stable stratification are considerably larger than those of the other two methods. This may be due to the fact that the thickness of the surface layer can be much less than 32 meters under stable stratification and, consequently, the flux-profile relationships used are no longer valid in the layer above z = 8m.

1.1.4.2 Estimation of eddy fluxes with the aid of multi-level measurements of wind and temperature

With the use of definitions of friction velocity u_* and scaling temperature θ_* given, respectively, by

$$\frac{\tau_o}{\rho} = {u_*}^2 \tag{4.4}$$

and

$$\frac{H_o}{\rho c_p} = -k_v u_* \theta_* \tag{4.5}$$

where ρ is the air density and c_p the specific heat of air at constant pressure, the problem of estimating the momentum flux τ_o and the heat flux H_o in the surface layer is reduced to that of estimating u_* and θ_*.

In designing the schemes of estimating u_* and θ_* from multi-level measurements of wind and temperature that are described below, we have followed the sequential procedure in which the parameters are estimated one at each step uniquely and the value of a parameter estimated at a later step depends on the values of those estimated at earlier steps.

(a) Scheme I - This method assumes no knowledge of the roughness length z_o and requires measurements of wind at three different levels and of temperature at two different levels. Let these be denoted by $V_i = V(z_i)$, $i = 1, 2, 3$ and $\theta_j = \theta(z_j)$, $j = 1,2$, respectively. The estimation procedure runs as follows:

Step 1: Obtain ratio R_1 defined by

$$R_1 = \frac{V_3 - V_2}{V_2 - V_1}$$

Step 2: Estimate the Monin-Obukhov length L from R_1 with identity

$$R_1 = \frac{I_V(z_2,\ z_3;\ \hat{L})}{I_V(z_1,\ z_2;\ \hat{L})}$$

where $I_V(z_1,\ z_2;\ \hat{L})$ is the integral of the gradient for wind with respect to height from level z_1 to level z_2 with the value of the Monin-Obukhov length $\hat{L}$.

Step 3: Estimate u_* from V_1, V_2, V_3 and $\hat{L}$ in accordance with the least-squares principle. It may be readily shown that $\hat{u}_*$ is given by

$$\hat{u}_* = k_V \frac{I_V(z_1,\ z_2;\ \hat{L})(V_2 - V_1) + I_V(z_2,\ z_3;\ \hat{L})(V_3 - V_2)}{I_V^2(z_1,\ z_2;\ \hat{L}) + I_V^2(z_2,\ z_3;\ \hat{L})}$$

Step 4: Estimate θ_* from θ_1 and θ_2 and $\hat{L}$ with identity

$$\theta_* = \frac{\theta_2 - \theta_1}{I_\theta(z_1, z_2; \hat{L})}$$

where I_θ is the integral of the vertical gradient for potential temperature between z_1 and z_2.

Step 5: Estimate z_o from V_1 and $\hat{u}_*$ with identity

$$k_V V_1 = \hat{u}_* I_V(\hat{z}_o, z_1; \hat{L})$$

Under stable stratification, since both integrals I_V and I_θ are linear functions of L, the equation in step 2 may be rewritten as an explicit equation for $\hat{L}$ and the values of I_V and I_θ can be readily determined with the knowledge of $\hat{L}$. The only transcendental relation arises in Step 5.

Under lapse stratification, however, either tabular or graphical representations of I_V as a function of L with z_1 and z_2 as parameters are required to obtain $\hat{L}$. We have found the tabular representation with variable increment in L serves the purpose quite adequately.

It is readily shown that the proposed vertical gradient of wind restricts the value of R_1 within certain ranges that depend on the levels of measurements, regardless of values of the universal constants. For example, with the choice of wind measurements at z = 2, 4 and 8m, it is expected that

$.8409 < R_1 \leqq 1$ under lapse stratification

and

$1 < R_1 < 2$ under stable stratification

Consequently, whenever the observed winds give rise to values of R_1 outside the prescribed ranges, the scheme fails to yield logically satisfactory estimates.

The conflicts between estimate and observation may be conveniently divided into two kinds. A conflict of the first kind occurs when the observed value of R_1 is either less than the lower limit under lapse stratification or greater than the upper limit under stable stratification. In either case the nearest possible estimate calls for $\hat{L} = 0$ which invalidates the proposed gradient equation. On the other hand, a conflict of the second kind obtains when the observed value of R_1 is either greater than the upper limit under lapse stratification or less than the lower limit under stable stratification. In either case the closest estimate calls for $\hat{L} \to \infty$, a situation which is likely to cause inconsistencies among $\hat{u}_*$, $\hat{\theta}_*$ and $\hat{L}$.

When we applied this scheme to the measurements in the lowest levels of the Report, we found that 29 and 7 out of the 68 cases under lapse stratification had conflicts of the first and second kinds, respectively. The discovery was so discouraging as to make us look for Scheme II which is described below.

(b) Scheme II - This method assumes that the roughness length z_o is known and requires measurements of both wind and temperature at two levels.

Step 1: Obtain ratio R_2 defined by

$$R_2 = \frac{V_2}{V_1}$$

Step 2: Estimate L from R_2 with

$$R_2 = \frac{I_V(z_o,\ z_2;\ \hat{L})}{I_V(z_o,\ z_1;\ \hat{L})}$$

Step 3: Estimate u_* according to

$$u_* = k_V \frac{I_V(z_o, z_1; \hat{L})V_1 + I_V(z_o, z_2; \hat{L})V_2}{I_V^2(z_o, z_1; \hat{L}) + I_V^2(z_o, z_2; \hat{L})}$$

Step 4: Estimate θ_* according to

$$\theta_* = \frac{\Theta_2 - \Theta_1}{I_\theta(z_1, z_2; \hat{L})}$$

As in Scheme I, the proposed gradient equations of wind limit the value of R_2 within certain ranges. With the choice of z = 2 and 4m and z_o = 2cm for instance, it may be shown that

$1.0736 < R_2 \leq 1.1505$ under lapse stratification

$1.1505 < R_2 < 2.0101$ under stable stratification

Similar conflicts as those of R_1 may be shown to exist between estimated and observed values of R_2.

When we applied this scheme to the data of the Report in the lowest levels, we found 4 conflicts of the second kind in the 68 cases of lapse stratification and 10 conflicts of the second kind in the 42 cases of stable stratification. There was not a case of conflict of the first kind under either stratification. In the results presented below, we opted to ignore the inconsistencies associated with the conflict of the second kind and obtained both $\hat{u}_*$ and $\hat{\theta}_*$ with estimate $\hat{L} \to \infty$. This assured us of finite values of estimated momentum and heat fluxes.

Figures 1.1 - 1.4 present the scatter diagrams of u_* and θ_* in which the values estimated with Scheme II are plotted in ordinates against those calculated from the measurements of $\overline{uw}$ and $\overline{w\theta}$. The roughness length $z_o = 2.44$cm was mentioned by Businger et al. and is believed to be representative of the site of the measurements. The scatter diagrams obtained with two other values of z_o, 2.00 and 5.00cm are included to show the sensitivity of the estimates to changes in the value of z_o. The influence of the accuracy of z_o on that of the estimates on u_* and θ_* with Scheme II is quite obvious from these figures.

1.1.4.3 Estimation of wind and temperature with the aid of micrometeorological estimates.

The two tables in Table 1.8 present the root-mean-square errors of estimate obtained when the vertical gradients are integrated to estimate wind speed and potential temperature. Each table lists the errors obtained with the set of the universal constants found optimal or recommended in this study and those with the set proposed by Businger et al. Along with each set of the constants are two sets of values of the micrometeorological parameters: one measured in the lowest levels and the other estimated from the wind- and temperature-measurements at $z = 2$m and 4m. The integration of a vertical gradient starts at $z = 4$m and the roughness length $z_o = 2.44$cm is used throughout.

We see in the results under lapse stratification what we have anticipated. In the first place the errors with measured values of the parameters are smaller than the errors with estimated values, with a few exceptions of small differences. All categories show an increase with height of the magnitude of the error. There is little difference, as we found earlier in Section 1.1.3, between the two sets of the universal constants, either with measured or with estimated values of the parameters.

The results under stable stratification, on the other hand, seem to defy our expectations and to elude our rationalization on one important count. On the one hand, they are consistent with those under lapse stratification in showing that the errors increase with height in all categories. They are also consistent with the results found in Section 1.1.3 in that the errors with the use of the recommended set of the constants are smaller than the errors with the use of the set of Businger et al. But, they also show that, at all levels and in all sets of the constants, the errors produced with the use of estimated values of the parameters are significantly smaller than those resulting when measured values of the parameters are used. Since these universal constants have been obtained by optimization of the vertical gradients or vertical differences with the aid of the measured values of the parameters, such a showing raises a doubt as to whether the optimization procedure was appropriate for the purpose of the estimation on hand. It may also be due to the simple fact that there is a component of considerable magnitude in these measurements that has not been accounted for at all by the proposed form of the vertical gradients.

1.1.5 Conclusions

We have carried out a number of exercises using the data collected in the Kansas 1968 Field Program Data Report to explore the flux-profile relationships in the atmospheric surface layer.

The experiment on optimization (Section 1.1.3) shows that the use of an equivalent but slightly different objective function of optimization and less complete data for the micrometeorological parameters result in a set of the universal constants different from that proposed by Businger et al. There is, however, no significant difference in root-mean-square errors between these sets under lapse stratification. The only serious discrepancy arises in the case of potential temperature under stable stratification.

The comparison of accuracy between the micrometeorological method and purely statistical methods (Section 1.1.4.1) fails to exhibit the advantage of the micrometeorological measurements so far as estimation of wind and temperature at other levels within the surface layer is concerned.

In designing a scheme of estimating micrometeorological parameters from wind and temperature measurements we have found the two-fold importance of the roughness length z_o. (Section 1.1.4.2). In the first place, the assumption of its knowledge allows a scheme which requires one fewer observation on wind speed and yet is more tolerant of the observations that cannot be accounted for by the proposed form of the vertical gradient. Secondly, the accuracy of estimates on friction velocity u_* and scaling temperature θ_* is found to be sensitively affected by the accuracy of z_o.

We find it difficult to understand what we observe in the estimation of wind and temperature at upper levels from those at lower levels with the aid of estimated micrometeorological parameters under stable stratification (Section 1.1.4.3). We speculate that the results are due to the fact that the top of the surface layer under stable stratification is on many occasions lower than some of the upper levels, say 16m or 32m.

1.1 Appendix

Integral $\int_{z_1}^{z_2} z^{-1}(1 + az)^{-1/n}\,dz$

The integral

$$I_n\,(z_1,\ z_2;\ a) = \int_{z_1}^{z_2} z^{-1}(1 + az)^{-1/n}\,dz$$

where $z_1,\ z_2 > 0$, $a \geqq 0$ and n a positive integer may be transformed into

$$I_n\,(y_1,\ y_2) = \int_{y_1}^{y_2} \frac{ny^{n-2}}{(y^n - 1)}\,dy$$

in which $y_1 = (1 + az_1)^{1/n}$, $y_2 = (1 + az_2)^{1/n}$

For $n = 1, 2, 3$ and 4, the integral may be expressed in terms of elementary functions.

$$I_1(z_1,\ z_2;\ a) = \ln \frac{z_2}{z_1} - \ln \frac{1 + az_2}{1 + az_1}$$

$$I_2(z_1,\ z_2;\ a) = \ln \frac{(1 + az_2)^{\frac{1}{2}} - 1}{(1 + az_1)^{\frac{1}{2}} - 1} - \ln \frac{(1 + az_2)^{\frac{1}{2}} + 1}{(1 + az_1)^{\frac{1}{2}} + 1}$$

$$I_3(z_1,\ z_2;\ a) = \ln \frac{(1 + az_2)^{1/3} - 1}{(1 + az_1)^{1/3} - 1} - \ln \frac{\{(1 + az_2)^{2/3} + (1 + az_2)^{1/3} + 1\}^{\frac{1}{2}}}{\{(1 + az_1)^{2/3} + (1 + az_1)^{1/3} + 1\}^{\frac{1}{2}}}$$

$$+ \sqrt{3}\,\tan^{-1}\left[\frac{2(1 + az_2)^{1/3} + 1}{\sqrt{3}}\right] - \sqrt{3}\,\tan^{-1}\left[\frac{2(1 + az_1)^{1/3} + 1}{\sqrt{3}}\right]$$

$$I_4(z_1, z_2; a) = \ln \frac{(1 + az_2)^{\frac{1}{4}} - 1}{(1 + az_1)^{\frac{1}{4}} - 1} - \ln \frac{(1 + az_2)^{\frac{1}{4}} + 1}{(1 + az_1)^{\frac{1}{4}} + 1}$$

$$+ 2 \tan^{-1} (1 + az_2)^{\frac{1}{4}} - 2 \tan^{-1} (1 + az_1)^{\frac{1}{4}}$$

REFERENCES

1. Businger, J. A., Wyngaard, J. C., Izumi, Y. and E. F. Bradley, 1971: Flux-Profile Relationships in the Atmospheric Boundary Layer, J. Atmos. Sci., 28, pp 181-189.

2. Haugen, D. A., Kaimal, J. C. and E. F. Bradley, 1971: An Experimental Study of Reynold Stress and Heat Flux in the Atmospheric Surface Layer, Quart. J. R. Met. Soc., 97, pp 168-180.

3. Izumi, Y., 1971: Kansas 1968 Field Program Data Report, AFCRL-72-0041, Air Force Cambridge Research Laboratories.

4. Panofsky, H. A., 1974: The Atmospheric Boundary Layer Below 150 Meters, Annual Review of Fluid Mechanics, Vol. 6, pp 147-176.

TABLE 1.1 - The root-mean-square errors of estimate wind speed difference, lapse condition (m/sec)

a) $n_V = 3$

		Layer				
k_V	γ_V	(2,4)	(4,8)	(8,16)	(16,32)	(2,32)
.32	14	.067	.060	.093	.097	.081
.33	11	.064	.058	.089	.093	.078
.34	10	.065	.058	.086	.092	.076
.35	8	.066	.059	.082	.089	.075
.36	7	.071	.061	.080	.088	.075
.37	6	.076	.063	.077	.087	.076
.38	5	.082	.067	.075	.086	.078
.39	4	.087	.070	.074	.086	.080
.40	3	.092	.075	.074	.089	.083
.41	3	.105	.080	.071	.086	.086
.42	2	.108	.084	.074	.093	.091
.43	2	.120	.090	.071	.089	.094
.44	2	.132	.098	.071	.087	.100

TABLE 1.1 (continued)

b) $n_v = 4$

k_v	γ_v	Layer (2,4)	(4,8)	(8,16)	(16,32)	$\overline{(2,32)}$
.32	25	.066	.057	.084	.092	.076
.33	20	.065	.057	.082	.091	.075
.34	17	.067	.058	.079	.089	.074
.35	14	.070	.059	.077	.088	.074
.36	11	.072	.061	.076	.088	.075
.37	10	.080	.065	.073	.087	.077
.38	8	.085	.068	.072	.087	.078
.39	6	.089	.071	.073	.089	.081
.40	5	.096	.076	.072	.090	.084
.41	4	.103	.080	.072	.092	.087
.42	4	.116	.087	.070	.088	.092
.43	3	.122	.091	.071	.091	.095
.44	2	.126	.096	.074	.099	.100

TABLE 1.1 (continued)

c) n = 5

		Layer				
k_V	γ_V	(2,4)	(4,8)	(8,16)	(16,32)	$\overline{\text{2,32)}}$
.32	42	.067	.057	.079	.092	.075
.33	34	.068	.057	.077	.091	.074
.34	27	.069	.058	.075	.091	.074
.35	22	.073	.060	.074	.090	.075
.36	17	.075	.062	.073	.091	.076
.37	14	.081	.065	.072	.091	.078
.38	11	.085	.069	.072	.092	.080
.39	9	.092	.073	.071	.092	.082
.40	8	.101	.078	.069	.092	.086
.41	6	.106	.082	.070	.093	.089
.42	5	.114	.087	.070	.094	.093
.43	4	.122	.092	.071	.096	.097
.44	3	.129	.096	.072	.099	.101

TABLE 1.2 - The mean square error of estimate wind speed difference, lapse condition
(10^{-6} m^2/sec^2)

$n_v = 4$

	k_v .33	.34	.35
γ 13	7523	6063	5770
14	6954	5786	5523
15	6511	5613	5592
16	6175	5528	5730
17	5928	5515	5926
18	5759	5564	6170
19	5655	5665	6453
20	5608	5810	6770

TABLE 1.3a - Optimal sets of the universal constants, lapse stratification

Wind Speed				Temperature			
k_v	n_v	γ_v	RMSE (m/sec)	n_h	k_h	γ_h	RMSE (°K)
.34	4	17	.074	2	1.00	20	.084
.35	4	14	.074	2	1.00	18	.084

TABLE 1.3b - Recommended sets of the universal constants lapse stratification

Wind Speed				Temperature			
			RMSE				RMSE
k_v	n_v	γ_v	(m/sec)	n_h	k_h	γ_h	(^{o}K)
.34	4	18	.075	2	1.00	18	.085
.35	4	16	.076	2	1.00	16	.086

TABLE 1.4a - Optimal sets of the universal constants stable stratification

Wind Speed				Temperature			
			RMSE				RMSE
k_v	β_v	δ_v	(m/sec)	k_h	β_h	δ_h	(^{o}K)
.34	1.1	3.0	.200	1.00	1.3	1.1	.184
.35	1.1	3.0	.199	1.00	1.4	1.1	.184

TABLE 1.4b - Recommended sets of the universal constants stable stratification

Wind Speed				Temperature			
			RMSE				RMSE
k_v	β_v	δ_v	(m/sec)	k_h	β_h	δ_h	(^{o}K)
.34	1.0	3.1	.203	1.00	1.0	1.2	.192
.35	1.0	3.2	.206	1.00	1.0	1.2	.193

TABLE 1.5a - The root-mean square errors of estimate (m/sec) wind speed differences, lapse stratification

$n_v = 4$

		Layer				
k_v	γ_v	(2,4)	(4,8)	(8,16)	(16,32)	$\overline{(2,32)}$
.34	17°	.067	.058	.079	.089	.074
	18^{r}	.069	.058	.079	.089	.075
.35	14°	.070	.060	.077	.088	.074
	15^{b}	.072	.060	.076	.088	.075
	16^{r}	.075	.061	.076	.088	.076

TABLE 1.5b - The root-mean square errors of estimate (^{o}K), potential temperature differences, lapse stratification

$n_h = 2$

			Layer				
k_v	k_h	γ_h	(2,4)	(4,8)	(8,16)	(16,32)	$\overline{(2,32)}$
.34	1.00	18^{r}	.130	.099	.037	.035	.085
		20°	.134	.086	.037	.038	.084
.35	1/.74	9^{b}	.158	.066	.045	.037	.090
	1.00	16^{r}	.130	.100	.038	.035	.086
		18°	.135	.085	.037	.038	.084

TABLE 1.6a - The root-mean-square errors of estimate (m/sec) wind speed differences, stable stratification

k_v	(β_v, δ_v)	Layer				
		(2,4)	(4,8)	(8,16)	(16,32)	$\overline{(2,32)}$
.34	$(1.1, 3.0)^{o}$	.112	.087	.166	.334	.200
	$(1.0, 3.1)^{r}$	.079	.063	.178	.351	.203
.35	$(1.1, 3.0)^{o}$	.100	.076	.170	.338	.199
	$(1.0, 3.2)^{r}$	.073	.062	.181	.359	.206
	$(1.0, 4.7)^{b}$	.069	.127	.257	.622	.344

TABLE 1.6b - The root-mean-square errors of estimate (^{o}K) potential temperature differences, stable stratification

$k_h = 1.00$

k_v	(β_h, δ_h)	Layer				
		(2,4)	(4,8)	(8,16)	(16,32)	$\overline{(2,32)}$
.34	$(1.0, 1.2)^{r}$	.089	.105	.189	.306	.192
	$(1.3, 1.1)^{o}$	.107	.114	.171	.286	.184
.35	$(1.0, 1.2)^{r}$	.089	.106	.189	.308	.193
	$(1.4, 1.1)^{o}$	.113	.119	.169	.283	.184
	$(.74, 4.7)^{b}$	.152	.321	.677	1.447	.818

TABLE 1.7 - The root-mean-square errors of estimate

a) Wind speed (m/sec)

Stratification	Method	Level (m) 2	4	8	16	32
	Micromet	0	.067	.104	.148	.178
Lapse	Lin. Reg.	"	.059	.125	.186	.250
	Pol. Log.	"	.158	.318	.445	.583
	Micromet	"	.217	.676	1.563	3.475
Stable	Lin. Reg.	"	.049	.112	.181	.303
	Pol. Log.	"	.132	.261	.359	.442

b) Potential temperature (°K)

Stratification	Method	Level (m) 2	4	8	16	32
	Micromet	0	.253	.345	.465	.565
Lapse	Lin. Reg.	"	.226	.346	.429	.490
	Pol. Log.	"	.210	.311	.395	.448
	Micromet	"	.128	.359	.823	1.825
Stable	Lin. Reg.	"	.131	.312	.592	1.016
	Pol. Log.	"	.213	.292	.349	.383

TABLE 1.8 - The root-mean-square errors of estimate (micrometeorological method)

a) Wind (m/sec)

stratification	universal constants	micro-parameters	Level (m) 8	16	32
lapse	$n_V = 4$ $k_V = .34$ $\gamma_V = 17$	measured	.058	.107	.151
		estimated	.134	.288	.466
	$n_V = 4$ $k_V = .35$ $\gamma_V = 15$	measured	.060	.105	.146
		estimated	.122	.262	.431
stable	$k_V = .34$ $\beta_V = 1.0$ $\delta_V = 3.1$	measured	.465	1.356	3.270
		estimated	.097	.287	.774
	$k_V = .35$ $\beta_V = 1.0$ $\delta_V = 4.7$	measured	.787	2.331	5.557
		estimated	.229	.663	1.654

TABLE 1.8 (continued)

b) Potential temperature (^{o}K)

stratification	universal constants	micro parameters	Level (m)		
			8	16	32
lapse	$n_v = 2$ $k_v = .34$ $k_h = 1.00$ $\gamma_h = 20$	measured	.105	.226	.332
		estimated	.143	.218	.289
	$n_v = 2$ $k_v = .35$ $k_h = 1/.74$ $\gamma_h = 9$	measured	.195	.280	.421
		estimated	.253	.426	.572
stable	$k_v = .34$ $\beta_h = 1.0$ $\delta_h = 1.2$	measured	.236	.707	1.713
		estimated	.039	.156	.393
	$k_v = .35$ $\beta_h = .74$ $\delta_h = 4.7$	measured	1.185	3.594	8.526
		estimated	.460	1.414	3.430

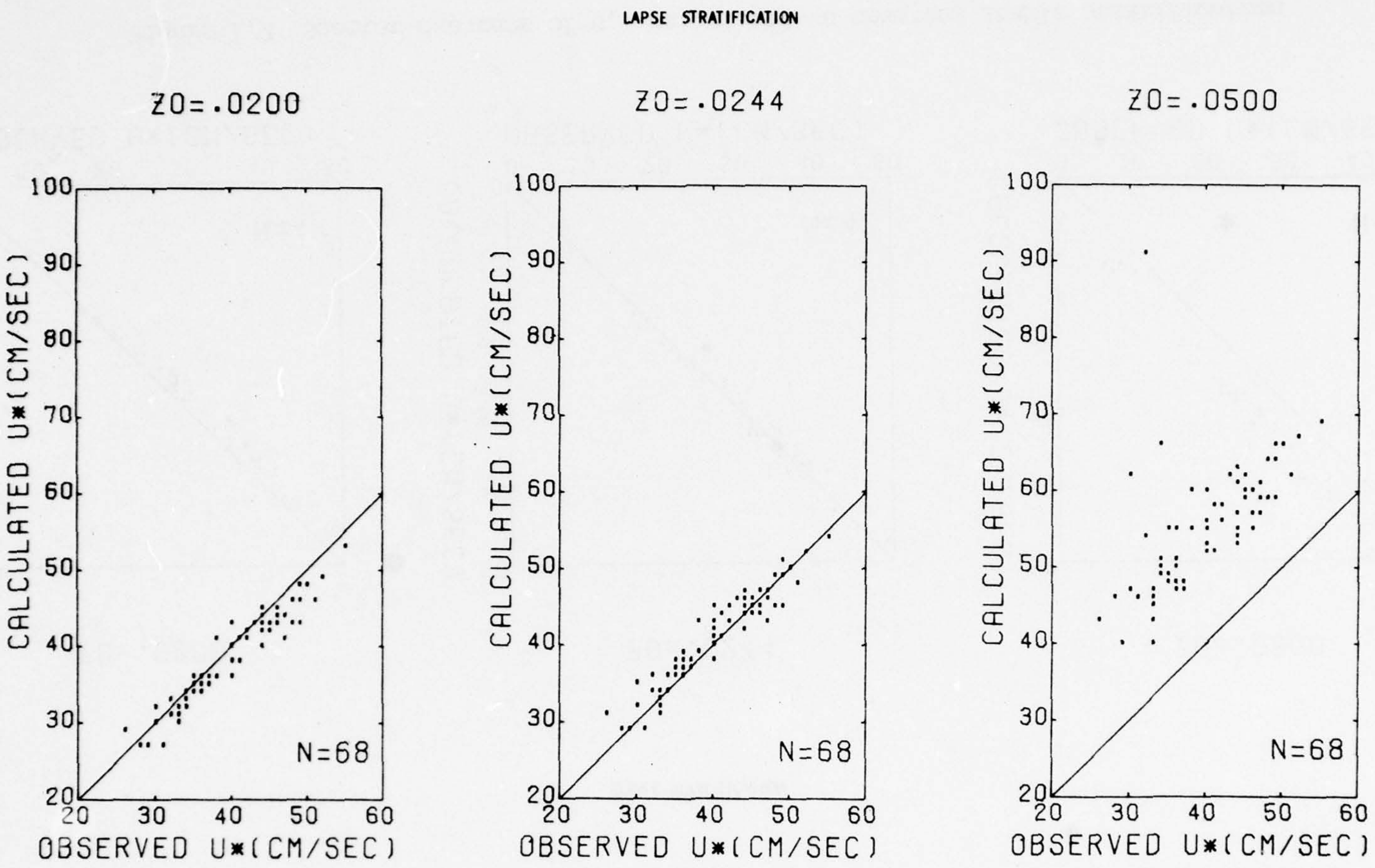

Figure 1.1 Scatter diagrams of u_*, calculated vs observed lapse stratification

STABLE STRATIFICATION

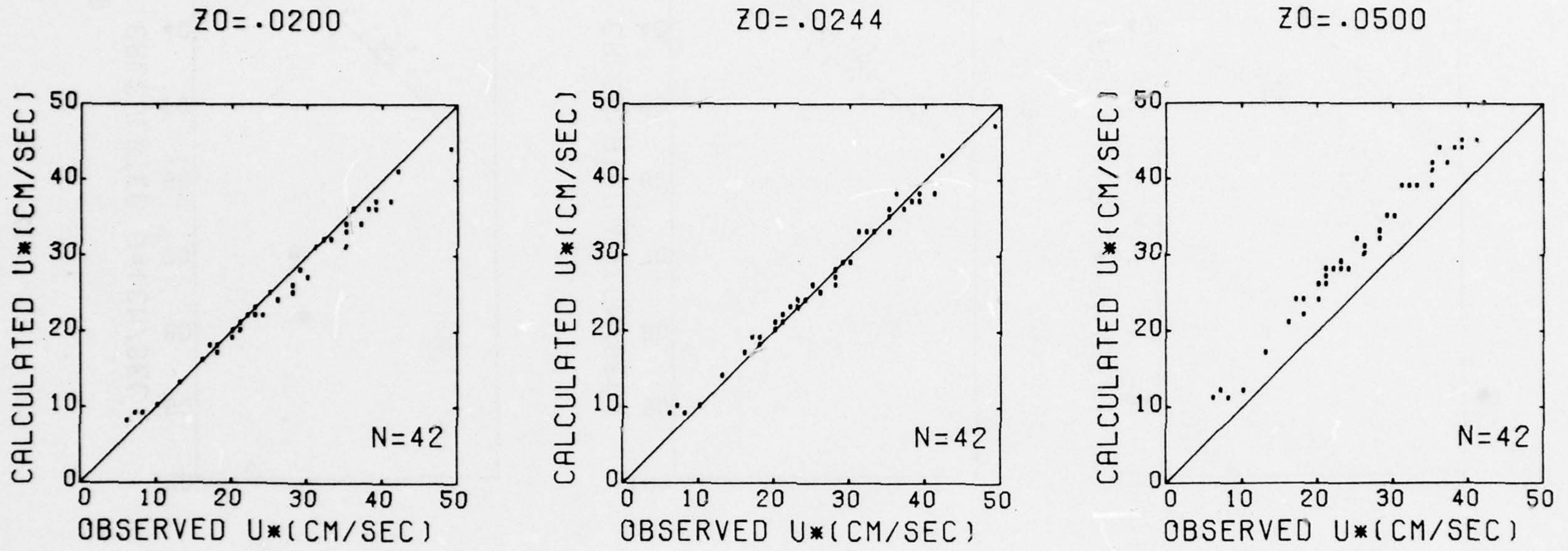

Figure 1.2 Scatter diagrams of u_*, calculated vs observed stable stratification

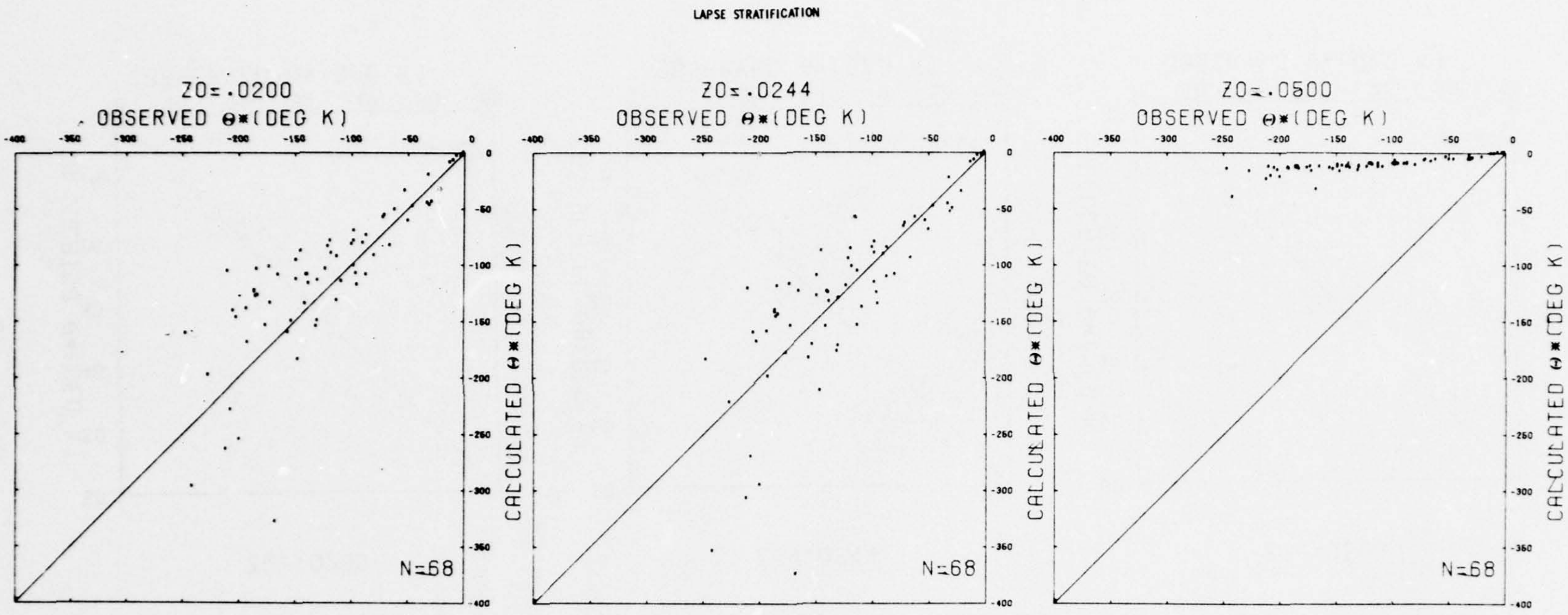

Figure 1.3 Scatter diagrams of θ_*, calculated vs observed lapse stratification

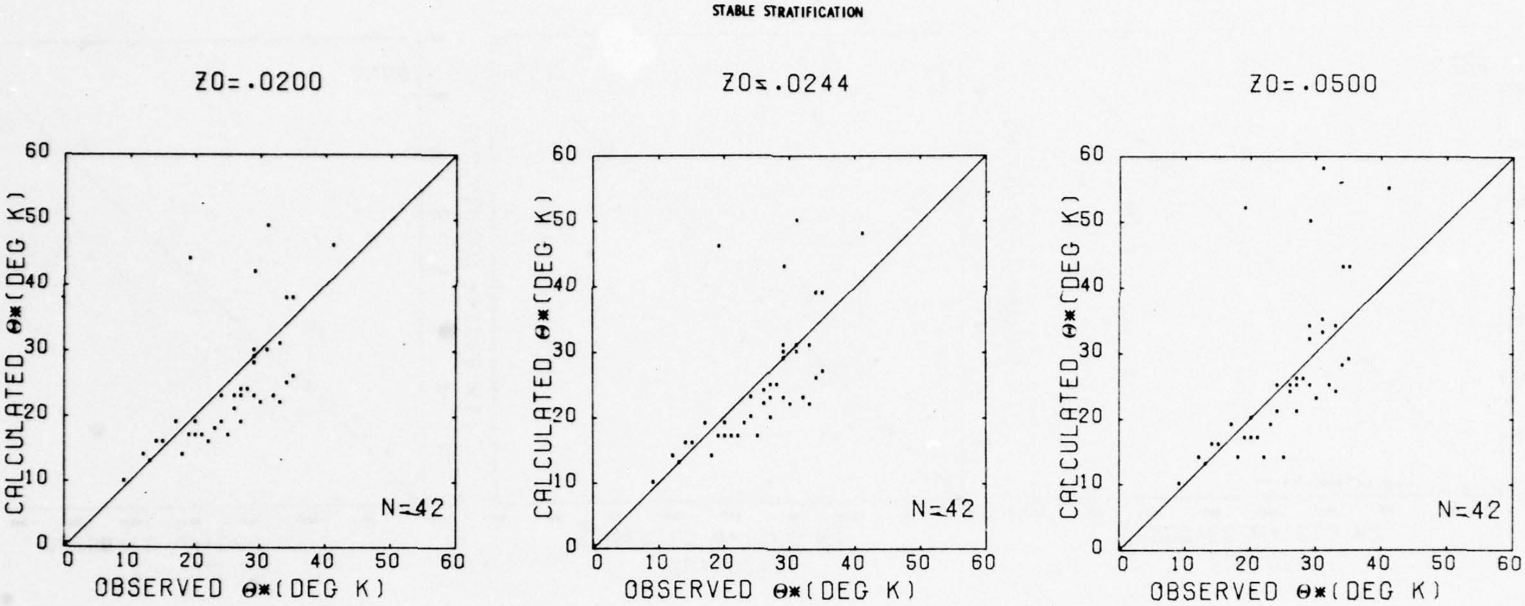

Figure 1.4 Scatter diagrams of θ_*, calculated vs observed stable stratification

1.2 A Contour Analysis of the Temperature Forecast Errors in the Boundary Layer Model

1.2.1 Introduction

Contour maps of forecast errors are produced to exhibit the geographical distribution of the difference between prediction and observation in the course of studying the AFGWC boundary layer model. The maps are used primarily to help us detect any extraordinary feature or consistent pattern which may be associated with any of the parameters (such as time, position, forecast category, model, etc.) used to identify the forecasts. They serve this purpose very well either individually or in small groups by permitting easy visual comparisons.

As the number of the maps increased with increases in both the number of synoptic cases and the number of models, however, it became obvious to us that some systematic method for categorization and registration had to be devised in order that we could retain correctly and use properly the information contained in the individual maps. What is needed are measures of those attributes in the maps that can be efficiently employed to characterize the individual maps and to discriminate their various properties. As such, the task of meeting these objectives falls under the category of pattern recognition.

To put the work reported here in proper perspective it must be pointed out that in designing the intervals and symbols of the contour maps we did not anticipate the undertaking of this study and, as a result, we did not have in the contour maps all the qualities that are desired for the purpose of this study. We have simply taken whatever were available to us and tried to see how well we could do with them.

For the purpose of understanding the rationale and technique of the methods developed, it is not necessary to know what constitutes each of the models or what distinction there are among different levels mentioned in the presentation below. Nevertheless, for the purpose of balance and reference, we present a brief description of the models considered and the nature of the contour maps analyzed.

Six prediction models of the planetary boundary layer are considered. They are:

(1) Model "O": the AFGWC operational model,

(2) Model "6": the AFGWC model adopted for use at the AFGL computing facilities,

(3) Model "C": Model "6" with a new method of estimating eddy diffusivity,

(4) Model "H": Model "C" with virtual temperature used in the hydrostatic relation,

(5) Model "V": Model "C" with a new vertical differencing, and

(6) Model "R": the persistence forecast in which the value observed 24 hours ago is taken as the predicted value.

All models predict the value of air temperature at each of the 27x29 grid points on each of the 8 levels in the domain of prediction. The forecast error at each grid point is defined to be the difference between the predicted and the observed values. The latter is obtained by the objective analysis and is common to all models.

The contour lines are drawn using bilinear interpolation on the 27x29 grid-point values of the forecast error on each level. The interval of $5^{O}C$ for temperature is chosen for convenience and economy in the production and inspection of the maps.

Figures 1.1 and 1.2 are samples of the contour plots of errors of temperature.

They are self-explanatory once it is known what information they contain. Each contains the model number and three statistics for the entire grid in the right hand column. Below that are the values and locations of the maximum and minimum. Next are the contour symbols and below that the contour increments. The symbols and increments are the same for all the plots in each variable. The range of forecast, the hour and date of the forecast, and the level in the vertical appear on the top of the plot under the header.

1.2.2 Technique of analysis

1.2.2.1 General contour features and qualities

Concentric positive or negative contours do not necessarily indicate contours of different absolute value. In some cases the inner contour is of the same absolute value (as measured from the zero level contour) as the adjacent outer contour. This occurrence was labeled with the term "volcano", while the more conventional occurrence of a higher value for the inner contour was labeled as a "peak" or "hill".

Comparative estimates of relative height were determined primarily by counting concentric contours. This was known to be not entirely accurate, but in the few cases checked from the table-printout, the correlation was sufficiently high to enable meaningful conclusions to be drawn.

Relative gradients were also determined by counting concentric contours, as well as examining contour spacing. Thus,if two first-increment contours were nearly the same, and each had a second inner contour, but one had also a third inner contour, then this latter structure would be described as having a higher relative gradient. Again, the lack of proper contour symbol identification caused a certain degree of uncertainty.

1.2.2.2 Measures

The analysis was separated into two modes. The first was a measure of deviation of the individual model forecasts from the observation. The second was a comparison of patterns among the several models.

The deviation measure was defined so as to indicate the presence of a specified range of error in a particular region of the domain. The range which was selected corresponded to values such that no second increment contour would be evident. A quadrant was selected as the unit region. Since such a measure corresponded to the absence of the second concentric contour, initial recordings reflected this. Each quadrant was later compared with the tabular printout to verify the presence of "volcanoes" (See preceding for term definition). Their frequency of occurrence was subsequently recorded.

This measure of deviation (D-S) was intended to provide an overall indication of "goodness" of prediction in a given quadrant because it measures directly the amount of error present in the measured quantity.

The discrimination of patterns is accomplished by first comparing specific contours or contour groupings as to similarity of location. Next, the peaks are compared as to height, quantity, location, and gradient. Different categories describe each of these attributes. Thirdly, included in each category is an allowance for certain of these qualities to vary, and a notation is provided for recording this.

Thus the categorization scheme consists of three parts. The first is a contour similarity comparison primarily as to location. Second is a peak similarity comparison as to height, quantity, location, and gradient. Third is the gray scale comparison that delineates which category has more of a given contour level or higher peaks (larger gradients). This categorization scheme is summarized in Similarity Comparison Categorization Table 1.1.

1.2.3 Results of analysis

Table 1.2 presents the fraction of the so-called "good" forecasts of each of the six models. A "good" forecast is one that has no second contour on either side of the zero contour, that is, one with no error greater than or equal to 10°C in magnitude. The fraction is the ratio of the number of quadrants with good forecasts to the total number of quadrants analyzed. The figures in the table were obtained after volcanoes and hills in the contour maps had been distinguished by referring them to the corresponding tabular printouts of the grid-point values of the error.

Analysis of the comparative structures of the contour plots among the various model groupings was carried out utilizing the categorization detailed earlier in Section 1.2.2.2. The number and distribution of forecasts and quadrants analyzed were those listed in Table 1.2. Various qualities were examined and the results are discussed below.

1.2.3.1 Models "C", "H" and "V"

The comparisons among models "C", "H", and "V" showed a significant lack of differences. In only four quadrants at one level, specifically a 12 hour night forecast at 300 meters, it was not possible to assign the S-NI descriptor to the full grouping. Combining this information with the closeness of the fractions of "good" forecasts obtained in Table 1.2, we conclude that the three models are insignificantly different.

It is also clear from Table 1.2 that this group out-performed any other model in all but one category, the 24-hour night forecast. In the latter model "R" is seen to be best of all and, model "7" is as good as the group.

1.2.3.2 Model 6

The contours of model "6" were found to show a bias toward positive for both 12-hour night forecast and the 24-hour day forecast when compared with the group of "C", "H", and "V". Comparisons with model "O" for these forecasts also showed the same bias. The bias is found primarily at levels above the surface. At the surface, the bias was sometimes discernible, but only infrequently. In order to observe the bias properly it was generally necessary to have the (S-G) descriptor applicable. However, the comparisons at surface were often made with the (S-C) or (S-NI) descriptors.

No bias was observed in the 12-hour day forecast. The bias in the 24-hour night forecast was at best erratic, none discernible at surface and most found at 900 and 1600 meters. However, the usage of the (S-G) comparison was quite widespread in this forecast category.

Presence or absence of the bias appears to correspond well with the values of the fraction of "good" forecasts in Table 1.2. Only in the 12-hour day forecast is it found that the performance of model "6" is as good as the other models, while it is significantly inferior to them in all of the other categories.

1.2.3.3 Similarity comparisons

Comparisons of models "O" and "6" with the group of "C", "H", and "V" were made on the basis of contour pattern by counting the number of quadrants in which comparison S-C or better was applicable. The results are summarized in Table 1.3. Distinctions are drawn among the cases if an entire forecast containing 16 quadrants falls in the category (forecasts), if an entire level with 4 quadrants on it is in the category or, if neither of the above is true (quadrants).

It is obvious that the contrast in the counts between models "0" and "6" amplifies what has been found in the deviation analysis. Except for the 12 hour day forecast in which model "6" exhibits no bias, all categories show that model "0" is a great deal similar in contour pattern to model "6".

When the statistics on the two different attributes are in agreement, they reinforce our confidence on the visual impressions. On the other hand, as in the comparisons of models "7" and "R", it was quite often that no unanimous inference could be drawn from the two analyses.

TABLE 1.1

SIMILARITY COMPARISON CATEGORIZATION

SIMILARITY		CONTOURS				PEAKS				
category	symbol	All	first and lower	first and higher	second and higher	All	Height second contour and higher	Quantity* (same, more, or less	Location second contour and higher	Gradient** (marks higher peaks only, all else the same)
Identical	S-1	same				same				
Nearly Identical	S-N1	nearly	nearly			nearly				
Similar	S-S			same			same	same	same	(applicable) (**)
Close	S-C			nearly	same		same	more first contours (*)	same	(applicable) (**)
Gross	S-G			nearly			nearly	more at or above second contour (*)	nearly	(applicable) (**)

Notes: * Designate for model A as ";E-P:A" ** Designate for model A as ";E-G:A"

TABLE 1.2

FRACTIONS OF "GOOD" FORECASTS

(Per Cent)

Forecast Category	No. Fcsts	No. Quads	Fraction (per cent) Models						
			0	6	C	H	V	R	7
12h/night	8	128	68.8	47.7	78.9	78.1	77.3	45.3	77.3
12h/day	9	144	43.8	43.8	45.8	47.2	46.5	38.9	45.8
24h/night	4	64	25.0	18.8	37.5	35.9	31.3	56.3	34.4
24h/day	9	144	45.8	19.4	56.3	54.9	56.3	51.4	50.7

THIS PAGE IS BEST QUALITY PRACTICABLE
FROM COPY FURNISHED TO DDC

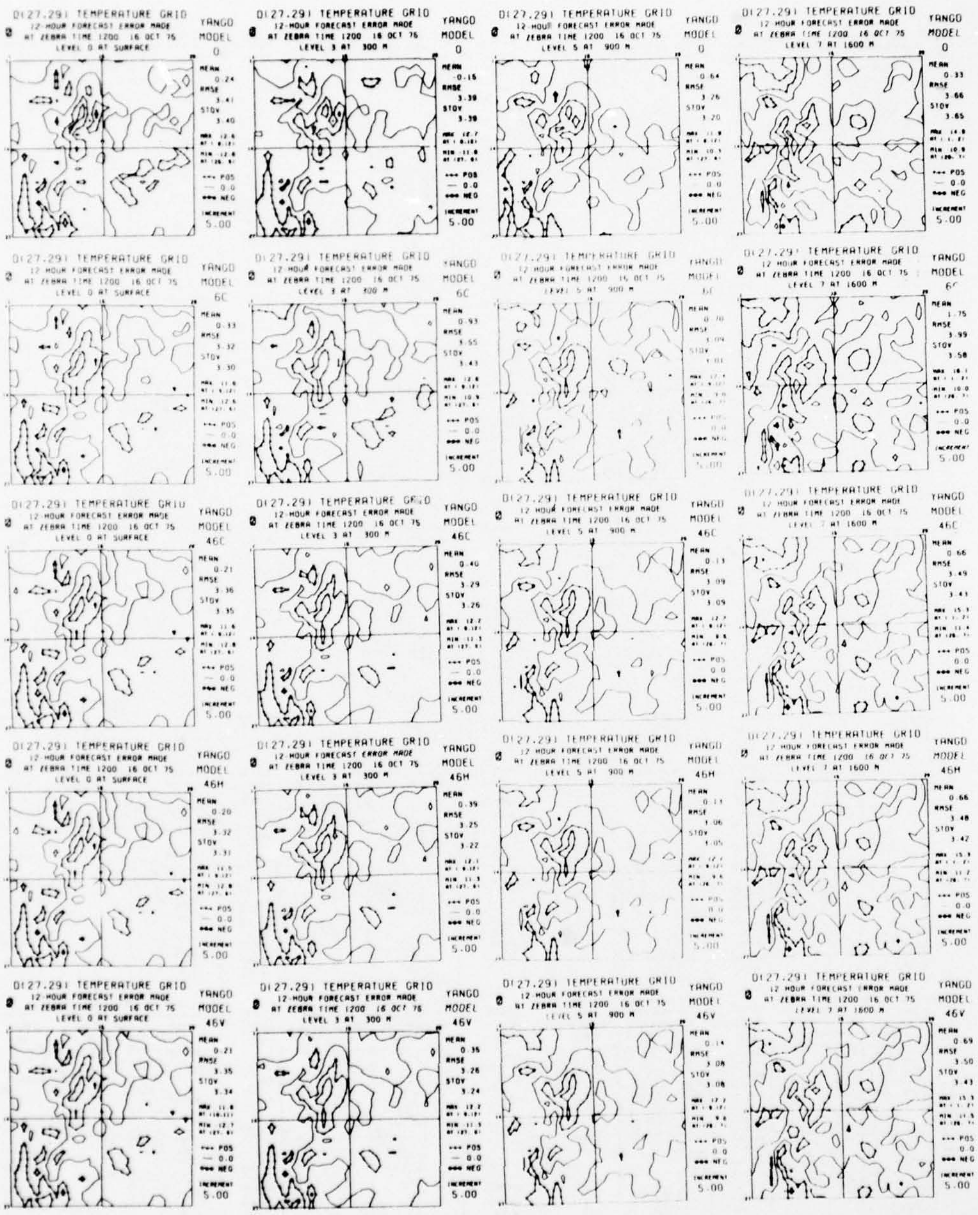
D(27.29) TEMPERATURE GRID
12-HOUR FORECAST ERROR MADE
AT ZEBRA TIME 1200 16 OCT 75
LEVEL 0 AT SURFACE
LEVEL 3 AT 300 M
LEVEL 5 AT 900 M
LEVEL 7 AT 1600 M
YANGO MODEL 0
YANGO MODEL 6C
YANGO MODEL 46C
YANGO MODEL 46H
YANGO MODEL 46V
MEAN 0.24 RMSE 3.41 STDV 3.40
MEAN -0.15 RMSE 3.39 STDV 3.39
MEAN 0.64 RMSE 3.26 STDV 3.20
MEAN 0.33 RMSE 3.66 STDV 3.65
MEAN 0.33 RMSE 3.32 STDV 3.30
MEAN 0.93 RMSE 3.55 STDV 3.43
MEAN 0.70 RMSE 3.04 STDV 3.01
MEAN 1.75 RMSE 3.99 STDV 3.58
MEAN 0.21 RMSE 3.36 STDV 3.35
MEAN 0.40 RMSE 3.29 STDV 3.26
MEAN 0.13 RMSE 3.09 STDV 3.09
MEAN 0.66 RMSE 3.49 STDV 3.43
MEAN 0.20 RMSE 3.32 STDV 3.31
MEAN 0.39 RMSE 3.25 STDV 3.22
MEAN 0.11 RMSE 3.06 STDV 3.05
MEAN 0.66 RMSE 3.48 STDV 3.42
MEAN 0.21 RMSE 3.35 STDV 3.34
MEAN 0.35 RMSE 3.28 STDV 3.24
MEAN 0.14 RMSE 3.08 STDV 3.08
MEAN 0.69 RMSE 3.50 STDV 3.43
POS
0.0
NEG
INCREMENT 5.00

Figure 1.1 Contour maps of temperature forecast errors, 12 hr forecasts

PRECEDING PAGE NOT FILMED
BLANK

THIS PAGE IS BEST QUALITY PRACTICABLE
FROM COPY FURNISHED TO DDC

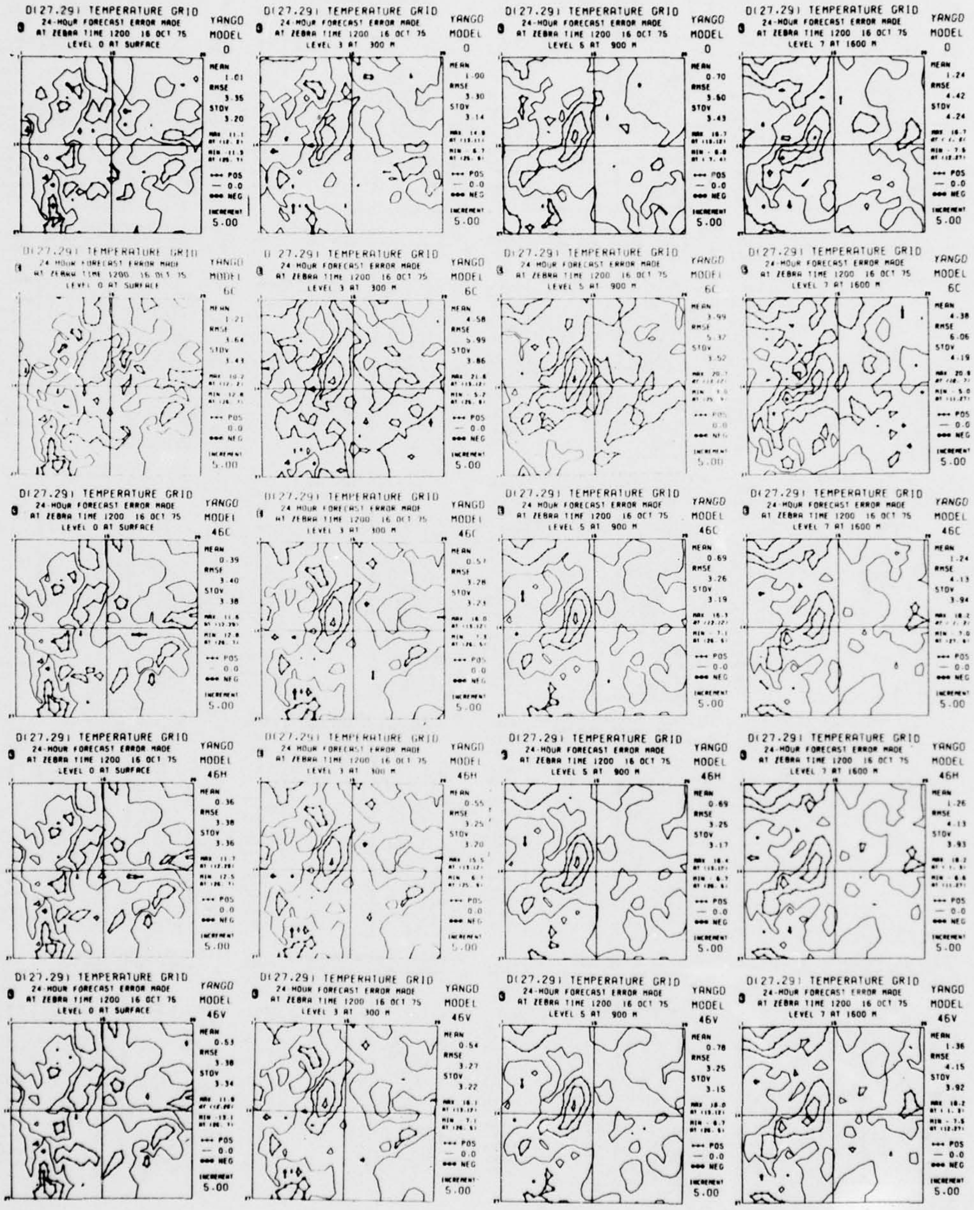
D(27,29) TEMPERATURE GRID
24-HOUR FORECAST ERROR MADE
AT ZEBRA TIME 1200 16 OCT 75
LEVEL 0 AT SURFACE
LEVEL 3 AT 300 M
LEVEL 5 AT 900 M
LEVEL 7 AT 1600 M
YANGO MODEL
0
6C
46C
46H
46V
MEAN
RMSE
STDV
MAX
MIN
POS
0.0
NEG
INCREMENT
5.00

Figure 1.2 Contour maps of temperature forecast errors, 24 hr forecasts

2.0 AUTOMATED WEATHER SYSTEM DEVELOPMENT

2.1 Introduction

The advent of low-cost, reliable microprocessing technology coupled with the pressing need within the U.S. Air Force for a modernized operational weather support capability has spawned a major program of research and development. The overall goal of the program is the development of a fully-automated airfield weather observation and forecasting system which will fulfill the weather support requirements of today's and tomorrow's Air Force while utilizing considerably fewer people than does the present system. Integral to this goal is the solution of several difficult and heretofore unsolved automated atmospheric sensing problems; namely, present weather determination, cloud ceiling height, cloud cover and glidescope slant visual range. Additionally, the future needs of the Air Force include objective and automated methodologies (algorithms, models, etc.) to generate terminal area weather predictions of aviation-critical elements (cloud ceiling, runway and slant visual range and landing zone wind conditions) for forecast intervals ranging from a few minutes to 2-3 hours. Within the period of performance of this contract effort, particular attention has been paid to the development of automated procedures to specify the type and intensity of surface weather phenomena (i.e., present weather determination) and to the development of indirect methods to specify and predict landing zone slant visual range. These studies will be described in subsequent sections of this Chapter.

An R&D undertaking of this type required the collection of atmospheric data representing widely varying weather conditions. A Weather Test Facility (WTF) was established by the Air Force Geophysics Laboratory on Otis AFB, Cape Cod, Massachusetts, for this purpose in late 1975. It is ideally situated, being in an area frequented by considerable low cloudiness, coastal fog and a full range of precipitation forms and is located on an open and flat area well removed from the airfield's runways. It is described in detail in the next section.

2.2 Weather Test Facility Site Description

The Weather Test Facility (WTF) at Otis AFB, MA, consists of an array of instrumented meteorological towers and ground stations distributed in the manner shown in Figure 2.0. While there are several one-of-a-kind sensors deployed in the WTF, there are certain other sensors which are deployed at multiple locations. These include Climatronics Mark I wind sensors, EG&G forward scatter meters (FSM) and EG&G temperature-dewpoint sensors which are placed on the towers at levels approximately 50 ft apart. The central tower complex consists of three towers extending to 20 ft, 100 ft, 200 ft (denoted by C, B, and A in Figure 2.0). They are configured to simulate an aircraft approach zone and to provide continuous weather observations at Category I and II decision height levels (200 ft and 100 ft respectively) essential to the evaluation of glidescope slant visual range and low-level wind shear techniques. Two additional 100 ft towers (labelled P and Q in Figure 2.0) are placed about 1500 ft either side of the simulated approach zone complex for the purpose of providing predictor data for the offset tower techniques for glidescope slant visual range specification and prediction.

Table 2.1 lists the various sensors deployed in the WTF, the atmospheric variable they are designed to sense, their respective location(s) and the number of sensors at each location. The placement of weather sensors at location X (the ground instrumentation site in Figure 2.0) is for the purpose

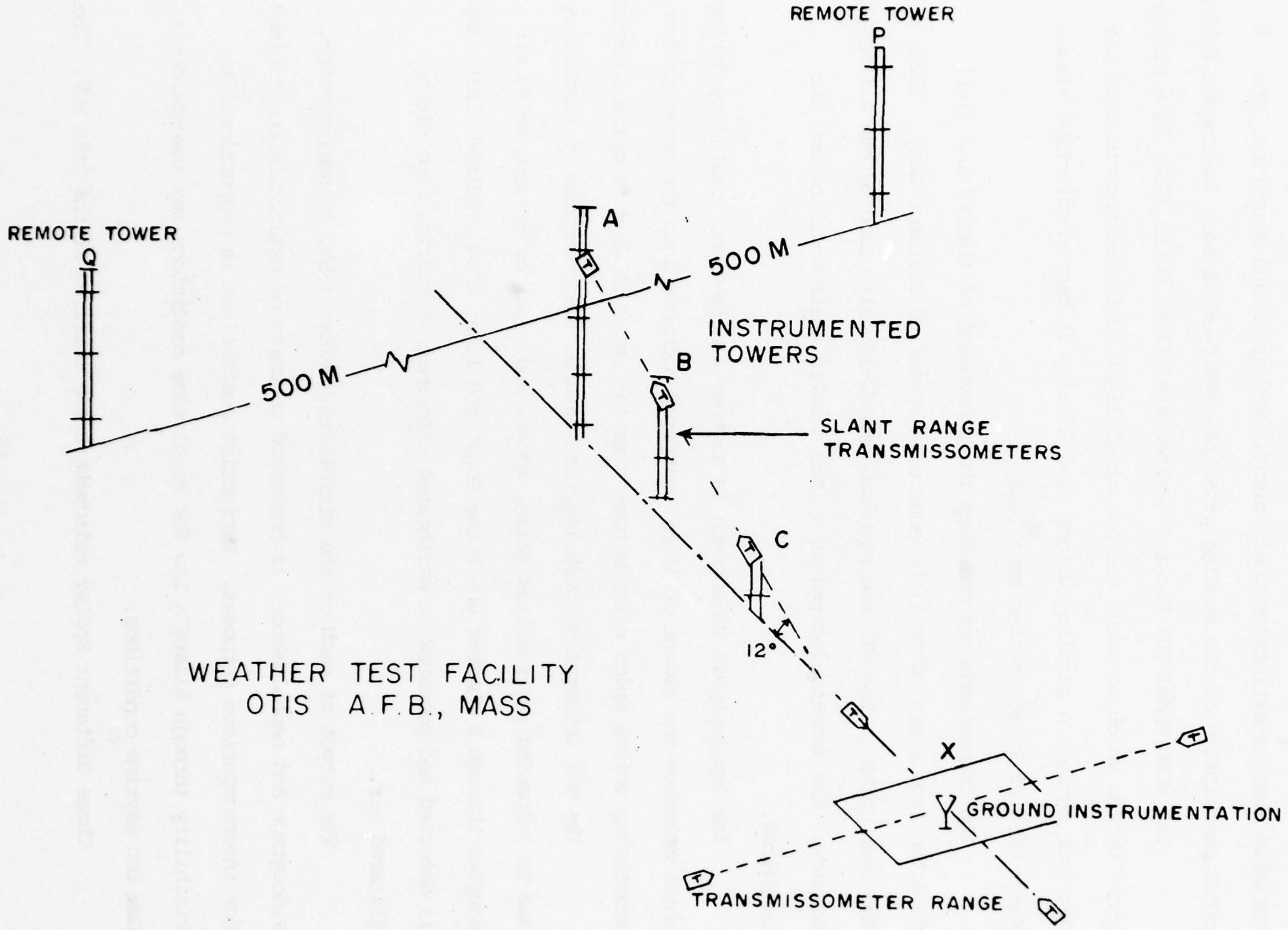
REMOTE TOWER
P
REMOTE TOWER
Q
A
500 M
500 M
INSTRUMENTED TOWERS
B
SLANT RANGE TRANSMISSOMETERS
C
T
12°
WEATHER TEST FACILITY
OTIS A.F.B., MASS
X
GROUND INSTRUMENTATION
TRANSMISSOMETER RANGE

FIGURE 2.0

THE AFGL/LYU WEATHER TEST FACILITY LOCATED AT OTIS AFB MA of intercomparisons among sensors designed to measure the same atmospheric variable such as extinction coefficient, wind speed and direction, etc. A short description of the sensing principle employed in each instrument follows.

The EG&G Model 207 Forward Scatter Visibility Meter (FSM) is a single-ended device which measures the amount of light scattered forward into the detector through a sampling volume of 0.05 m^3. It has an effective visual range of 0.06 km to greater than 16km.

The transmissometer measures the percentage of transmitted light detected from a projector light source, a specified distance away. Three of the four units in the WTF are standard AN/GMQ-10 units used by the Air Weather Service. The fourth, located at X, has a solid state modification kit installed.

The Impulsphysik Videograph is another single-ended visibility device which measures the amount of light scattered backward into the detector from a scattering volume which extends over a range from 3 to 25 m from the detector.

The MRI Integrating Nephelometer measures the reduction to visibility due to suspended particulates (haze, smoke, and dust) by drawing dried air samples through a chamber where the scattered light from a pulsed flash lamp is detected and compared to calibrated reference scattering from clean, filtered air.

The output of each of the visibility devices (FSM, transmissometer, videograph and nephelometer) is converted to units of extinction coefficient for intercomparison purposes. Extinction coefficient is proportional to visibility through Allard's Law for night time conditions and Koschmieder's Law for daytime conditions.

Three different Eppley radiometers are utilized at the Otis WTF. The pyranometer consists of a wire-wound thermopile which measures total sun and sky incoming radiation. The normal incidence pyrheliometer, mounted on an equatorial mount to track the sun, measures direct solar intensity. The so-called infrared radiometer (pyrgeometer) measures unidirectional terrestrial long-wave radiation.

The luminance meter is a laboratory version of a simple light meter which measures background luminance in a narrow field of view. As deployed at Otis, it is mounted at the 100 ft level of tower A and pointed towards the horizon along the simulated glide scope.

The Climatronics Mark I cup and vane wind set measures wind speed by a light chopping principle and wind direction using a non-contacting transducer. It features a light weight construction, low power consumption and has a very low threshold speed (0.43 knots).

The J-Tec vortex anemometer measures wind speed by measuring the spacing between vortices formed by the movement of air past an obstruction by means of an ultrasonic beam. Wind direction is obtained from a moving vane using a potentiometer.

The Rosemount orthogonal airspeed sensor measures airspeed vectors by developing differential pressures after air flow through pressure sensings ports located along the cylindrical body of the device. It has a no-moving-parts design and has a heating element built into the sensing head to insure an all-weather capability.

The Gill propvane is an instrument which records azimuth angle for wind direction and the rotational speed of the propellor for wind speed.

The EG&G temperature set utilizes platinum resistance thermometers to an accuracy of ± 0.3C. The dewpoint set uses a thermo-electrically-cooled

TABLE 2.1

Otis WTF Weather Sensor Inventory

Sensor Type	Variable	Location (Number)
EG&G FSM	Extinction Coeff.	A(5), B(3), C(2), P(3), Q(3), X(1)
Transmissometer	Atm. Transmission	A(1), B(1), X(2)
Videograph	Extinction Coeff.	X(1)
Nephelometer	Extinction Coeff.	X(1)
Pyranometer	Solar radiation	X(2)
Pyrheliometer	Direct sun radiation	X(1)
Pyrgeometer	Terrestrial radiation	X(1)
Luminance meter	Background luminance	X(1)
Climatronics Cup and Vane	Wind Speed + Direction	A(4), P(2), X(1)
J-Tec Vortex	Wind Speed + Direction	X(1)
Rosemount Orthogonal Airspeed	Wind Speed + Direction	X(1)
Gill Propvane	Wind Speed + Direction	X(1)
EG&G Thermistor	Dry bulb temperature	A(3), X(1)
EG&G Cooled Mirror	Dewpoint temperature	A(3), X(1)
Tipping bucket raingage	Precipitation Amount	X(1)

detection mirror held at the dewpoint (or frost point) and a condensate-detecting optical system to precisely determine the dewpoint temperature.

The Belfort tipping-bucket rain guage records precipitation rate and amount using a 0.005 inch bucket. The accumulation of bucket tips over a specified period corresponds, therefore, to the precipitation amount.

The weather data which are continuously and automatically gathered at the Otis WTF is done so by means of a Doric 200-channel data logger system. Each sensor is polled in the system 5 times per minute (ten times in the case of winds) and records on 7-track magnetic tape the voltage output received from each device. One magnetic tape is written per day;thus weekend recordings are paced at one scan per minute to ensure the tape lasting from Friday afternoon until Monday morning. The tapes are routinely transmitted, by mail, to AFGL at Hanscom AFB where detailed processing is conducted on the CDC 6600 to monitor the daily performance of the various sensors, to prepare data for subsequent analysis and to assist in the analysis of significant weather events.

2.3 Data Reduction and Analysis

A lengthy CDC 6600 computer program called "REQUOTE" was developed to convert raw signal voltages from the numerous weather sensing instruments to useful meteorological data. The program has evolved through several stages and has recently achieved expansion to include its sixteenth instrument group addition.

A major revision of the original logic was made necessary in early 1977 when a new data recording system replaced the original design. Repeatedly since its inception, additions and revisions have been necessary as new instruments have been added to the experiments or problems developed in existing components.

Each voltage received from the various sensors is converted into meteorological form and averaged over the minute's sampling. These one minute averages are printed out in sequenced pages as shown in Figure 2.1 to Figure 2.11. One page represents one hour's worth of data and the groupings of sensors per page are arranged for ease in evaluating sensor performance, technique development and evaluation and in the analysis of significant weather events. Printed sensor output is returned to the Otis WTF site personnel for additional sensor evaluation and monitoring.

Figure 2.1 shows the day-of-year and time of day (GMT) and the voltages recorded (-99.99 indicates no voltage present from that sensor). Letters refer to the specific towers or ground locations shown in Figure 2.0 and the numbers, the height above ground except for numbers 46 to 55 which are other identification numbers.

Figure 2.2 contains the time span covered by the input data tape, the sunrise-sunset times for the days involved and the forward scatter meters used for the slant visual range algorithm discussed in Section 2.5. Also included are the start and end times of reduced visibility episodes which occurred during this tape's time frame and a table of the units referred to in subsequent pages.

Figure 2.3 contains the extinction coefficients calculated from the 18 forward scatter meters and the four transmissometers plus the observed and estimated averages of certain scatter meters used in slant visual range and in the determination of the most probable extinction coefficient calculated from a Markov prediction model being evaluated for short range visibility prediction.

159   813

```
  P100 SP     P100 DIR    P50 SP      P50 DIR     A200 SP     A200 DIR    A150 SP     A150 DIR    A100 SP     A100 DIR
  .95   1.10  2.78  3.00   .87  1.06  2.75  2.82  1.18  1.48  3.55  2.32  1.42  1.27  1.27  2.50  1.19  1.25  3.55  3.96
 1.27   1.22  2.62  2.93  1.15  1.16  2.65  2.93  1.28  1.11  3.93  2.11  1.10   .88  3.23  4.17   .77   .97  3.93  4.06
 1.08   1.22  2.94  2.86  1.10  1.04  2.91  3.08  1.42  1.34  4.11  2.58  1.16  1.59  2.64  1.62   .80   .82  4.11  4.11
  .72   1.02  2.05  2.81  1.05   .91  2.          2.89  1.30  1.65  4.01  1.77  1.49  1.45  2.11  1.39  1.23  1.20  4.01  4.11
  .91    .90  2.75  3.00   .63   .95  2.74  2.82  1.47  1.39  3.59  2.87  1.43  1.34  3.20  2.46  1.26  1.12  3.59  4.12

  A 50 SP     A 50 DIR     X  SP       X  DIR     VRTX SP     VRTX DIR    GILL SP     GILL DIR    RSE U       RSE V
  .89   1.01   .57   .65  1.12  1.01   .57  4.05   .72   .74  1.97  2.03   .73   .65  1.39  2.05-99.99-99.99-99.99-99.99
  .93    .90   .54   .58   .94  1.15  3.71  2.94   .62   .75  2.09  2.12   .57   .66  2.09  2.01-99.99-99.99-99.99-99.99
  .87    .76   .65   .70   .93  1.16  3.98  3.76   .74   .80  2.20  2.13   .67   .58  2.03  2.10-99.99-99.99-99.99-99.99
  .80   1.07   .67   .65   .96   .99  3.95   .74   .63   .73  1.96  2.11   .56   .62  1.98  2.06-99.99-99.99-99.99-99.99
 1.20   1.19   .62   .69   .80  1.02   .47   .73   .57   .61  2.01  2.03   .57   .56  1.87  1.94-99.99-99.99-99.99-99.99

 FSM A200     A150        A100        A50         A10         B100        B50         B10         C10         P100
 -.57    .72  -.64   .94  -.59   .88  -.58   .94  -.60  1.09   .98  -.64  -.57   .85  -.57   .82  -.58   .93  -.51   .76
 -.56    .69  -.64   .92  -.59   .87  -.58   .93  -.60  1.06   .99  -.65  -.57   .83  -.57   .79  -.58   .91  -.53   .70
 -.56    .67  -.64   .91  -.59   .86  -.58   .92  -.60  1.04   .99  -.65  -.57   .82  -.57   .79  -.58   .90  -.52   .67
 -.56    .67  -.64   .92  -.59   .87  -.59   .91  -.60  1.02   .99  -.65  -.57   .82  -.57   .77  -.58   .90  -.51   .64
 -.55    .64  -.64   .95  -.59   .87  -.58   .89  -.60  1.02  1.01  -.65  -.57   .80  -.56   .75  -.58   .87  -.51   .64

  P50         P10         Q100        Q50         Q10          X           Y           Z           MRI   AB    BC    KL
 -.60    .84  -.59  1.18  1.44  -.62  -.62   .86  -.57  1.06  -.52   .94  -.57  1.02-99.99-99.99   .07  3.59  4.11  4.17
 -.59    .80  -.58  1.14  1.45  -.62  -.62   .84  -.57  1.06  -.48   .67  -.57  1.01-99.99-99.99   .07  3.66  4.11  4.16
 -.58    .77  -.58  1.12  1.45  -.62  -.62   .86  -.57  1.04  -.53  1.04  -.57  1.00-99.99-99.99   .06  3.72  4.11  4.18
 -.58    .73  -.58  1.10  1.44  -.62  -.62   .86  -.57  1.02  -.53   .95  -.57  1.00-99.99-99.99   .05  3.73  4.14  4.19
 -.58    .73  -.56  1.07  1.42  -.62  -.62   .87  -.57  1.02  -.54  1.15  -.57   .99-99.99-99.99   .05  3.67  4.16  4.15

  MN   A200T   DP   A150T   DP   A100T   DP   A50 T   DP    X T    DP   RAD1  RAD2  RAD3  RAD4  RAD5  RAIN  NEFF VIDEO  LUMI
 4.52   3.37  3.39  3.39  3.34  3.36  3.37  3.39  3.33  3.40  3.35  -.00-99.99  -.00   .00-99.99  4.56   .13   .93   .12
 4.52   3.37  3.39  3.40  3.35  3.36  3.37  3.39  3.33  3.41  3.35  -.00-99.99  -.00   .00-99.99  4.56   .13   .89   .12
 4.52   3.37  3.39  3.40  3.35  3.36  3.37  3.39  3.33  3.41  3.36  -.01-99.99  -.00   .00-99.99  4.56   .13   .91   .12
 4.53   3.37  3.39  3.40  3.35  3.36  3.37  3.39  3.33  3.41  3.35  -.00-99.99  -.00   .00-99.99  4.56   .12   .88   .12
 4.52   3.37  3.39  3.40  3.35  3.36  3.37  3.39  3.33  3.41  3.35  -.00-99.99  -.00   .00-99.99  4.56   .12   .97   .12

 FUMO           46    47    55    49    50    51    52    53    54    LQ   CHEK        E200        E150        E100  PHOTO
 1.18-99.99   4.38 -1.02  1.71  2.10   .52  -.03  -.03   .02  -.03   .14   .95  -.55   .91  4.16  -.75  -.59  1.02 -4.03
 1.19-99.99   4.37 -1.05  1.71  2.17   .53  -.03  -.03   .02  -.03   .13   .95  -.55   .89  4.16  -.75  -.59  1.02 -4.03
 1.20-99.99   4.37 -1.04  1.72  2.20   .55  -.03  -.03   .02  -.03   .13   .95  -.55   .88  4.18  -.72  -.56   .99 -4.03
 1.22-99.99   4.33 -1.04  1.71  2.19   .56  -.03  -.03   .02  -.03   .13   .95  -.52   .91  4.18  -.72  -.56   .99 -4.03
 1.19-99.99   4.34 -1.04  1.72  2.18   .56  -.03  -.03   .02  -.03   .13   .95  -.52   .99  4.16  -.72  -.56   .97 -4.03

  FSM POLE 4    POLE 5    POLE 6
-99.99-99.99-99.99-99.99-99.99-99.99-99.99-99.99-99.99-99.99-99.99-99.99-99.99-99.99-99.99-99.99-99.99-99.99-99.99-99.99-99.99
-99.99-99.99-99.99-99.99-99.99-99.99-99.99-99.99-99.99-99.99-99.99-99.99-99.99-99.99-99.99-99.99-99.99-99.99-99.99-99.99-99.99
-99.99-99.99-99.99-99.99-99.99-99.99-99.99-99.99-99.99-99.99-99.99-99.99-99.99-99.99-99.99-99.99-99.99-99.99-99.99-99.99-99.99
-99.99-99.99-99.99-99.99-99.99-99.99-99.99-99.99-99.99-99.99-99.99-99.99-99.99-99.99-99.99-99.99-99.99-99.99-99.99-99.99-99.99
-99.99-99.99-99.99-99.99-99.99-99.99-99.99-99.99-99.99-99.99-99.99-99.99-99.99-99.99-99.99-99.99-99.99-99.99-99.99-99.99-99.99
```

FIGURE 2.1

THIS PAGE IS BEST QUALITY PRACTICABLE
FROM COPY FURNISHED TO DDC

```
                SUMMARY FOR TAPE BEGINNING AT 8JN07/1313 AND ENDING AT 8JN08/1127.     1 EPISODES WERE DEFINED.

SUNRISE= 8JN07/0909SUNSET= 8JN08/0014

SUNRISE= 8JN08/0909SUNSET= 8JN09/0015

FSMS USED FOR OBS SVR: A100  A50  A10
FSMS USED FOR ES1 SVR: Q100  Q50  Q10
FSMS USED FOR ES2 SVR:  Q50  A10
WHERE: OBS SVR =(A100+2( A50)+ A10)/4.
       ES1 SVR =(Q100+2( Q50)+ Q10)/4.
       ES2 SVR = .85( Q50)+.31( A10)

EPISODE BEGAN      ENDED      LENGTH

 8JN08/0659    8JN08/1127     4HRS 28MINS

                          - TABLE OF UNITS -

        SYMBOL                       UNITS                              RANGE
        ------                       -----                              -----

         R      ACCUMULATED NUMBER OF 0.005" RAIN BUCKET TIPS          (0 TO 9999)
         T      NUMBER OF INDIVIDUAL 0.005" BUCKET TIPS PER SCAN       (0 TO 9)
         L      LANGLEYS/MINUTE * 100                                  (0 TO 200)
         S      METERS/SECOND                                          (0 TO 45)
         D      ANGULAR DEGREES                                        (0 TO 360)
         C      DEGREES CELSIUS * 10.                                  (-580 TO 580)
         EXCO   E*-4/M                                                 (-0 TO 700)
         V1     VOLTS * 100                                            (-500 TO 1010)
         V2     VOLTS                                                  (-11.0 TO 11.0)
         P      PERCENT PROBABILITY                                    (0 TO 100%)
```

FIGURE 2.2

```
METRIC UNITS
HOUR BEGINNING:   3JN08/0800

                 EXTINCTION COEFFIEICINTS (EXCO)                                                   (EXCO)            SVR 100 PROB (P)
.200.200.150.150.          100       .       50       .          10        .    FIELD    .  AB   BC   KL   MN.
. A . E . A . E . A   B   E   P   Q . A   B   P   Q . A   B   C   P   Q . X   Y   Z .       TRANS         . CES  ES1  ES2  F1   P2   F3     EXCO

   9  12  12   0  11   2  13  10   2  12  11  11  13  12  11  12  15  14  11  14       34   21   12   12   12   11   15    0    0    0    10.55
  11  13  14   0  13   2  14  11   2  14  13  12  15  15  12  14  16  17  14  15       35   21   12   12   14   12   17    0    0    0    11.85
  15  21  21   0  19   3  21  16   2  19  19  16  18  21  18  19  23  20  26  23       46   25   17   16   20   15   22    0    0    0    14.36
  10  14  14   0  13   2  14  11   2  14  13  12  14  16  12  12  16  15   6  12       35   20   10   12   14   11   16    0    0    0    10.74
   7  11  10   0   9   2  11   7   2   9   9   8  12  10   8   9  10  14   8  11       34   20   10   10   10   10   14    0    0    0     9.97
   9  12  11   0  10   2  12   8   2  11  10   9  15  12  10  11  11  15  15  13       42   20   11   12   11   12   16    0    0    0    11.42
  12  17  16   0  14   3  16  10   2  15  14  11  19  16  13  15  14  20  19  18       42   23   14   14   15   15   21    0    0    0    14.85
  14  21  19   0  17   3  20  16   2  18  17  16  18  20  16  19  24  19  23  22       39   25   16   16   16   14   22    0    0    0    14.26
  15  19  20   0  18   3  19  17   2  19  19  18  16  22  17  19  27  16  15  21       39   24   15   15   19   13   20    0    0    0    12.7
  12  15  16   0  15   3  16  16   2  16  16  17  13  19  14  16  24  14  15  15       40   23   13   13   16   10   16    0    0    0    10.21
  12  15  16   0  14   3  16  13   2  15  14  14  14  17  13  15  19  17  13  17       41   22   14   13   15   12   18    0    0    0    11.74
  10  13  14   0  12   2  14  11   2  13  13  12  13  16  12  13  16  15  13  14       49   22   13   12   14   10   16    0    0    0    10.21
  10  12  12   0  11   2  13  10   1  12  11  11  12  14  10  12  13  13  10  14       42   22   14   13   12    9   14    0    0    0     9.32
   9  11  12   0  11   2  12   9   1  11  11  10  11  13  10  11  14  13  12  12       35   22   12   11   12    9   13    0    0    0     8.80
   9  11  11   0  10   2  11   9   1  10  10  10  10  12  10  11  13  12  10  12       54   20   11   11   11    8   12    0    0    0     8.30
   8  11  11   0  10   2  11   9   1  10  10  10  10  12  10  11  12  12  13  13       41   21   12   12   11    8   12    0    0    0     8.4
  13  18  17   0  15   3  17  13   2  16  15  14  20  18  14  16  19  24  16  20       40   25   16   15   16   16   22    0    0    0    16.23
  17  24  22   0  20   4  24  17   2  21  20  19  23  25  20  23  26  27  27  26       56   26   20   16   22   19   27    0    0    0    18.52
  17  25  21   0  20   4  24  16   2  21  20  20  22  25  19  23  27  26  30  26       49   27   21   16   22   18   27    0    0    0    17.83
  15  19  18   0  17   3  20  14   2  18  17  16  18  22  16  18  23  22  12  16       47   22   14   12   19   15   22    0    0    0    15.04
   8   9   9   0   9   2  13  10   1  10   9  11   8  11   8   9  13  10   5   9       43   21   10    9   10    7   10    0    0    0     6.52
   7   8   7   0   8   1   8   8   1   7   7   8   6   8   7   6   9   9   7   8       39   22   10   10    8    5    8    0    0    0     5.26
   7  11   8   0   8   2  11   9   1   8   8   8   9   9   7   9   9  10  13  10       49   22   11   11    7    7   10    0    0    0     7.02
  16  20  19   0  16   3  25   9   2  17  16   9  21  16  14  16  11  26  32  19       51   29   20   17   17   18   23    0    0    0    17.31
  26  37  30   0  32   5  34  21   3  30  29  23  29  34  27  35  32  35  38  35       60   32   27   22   32   24   35    1    0    0    23.73
  18  24  24   0  25   4  26  21   2  25  23  23  19  31  22  25  30  23  10  23       40   24   15   13   26   16   25    0    0    0    15.35
   7   8   9   0   9   2  10  10   1  10   9  11   6  12   6   9  13   9   5   9       42   20   10    9   10    7   11    0    0    0     6.5
   5   6   6   0   6   1   6   5   1   6   6   6   5   7   5   6   7   6   5   6       33   22    9    9    6    4    7    0    0    0     4.45
   6   8   7   0   7   1   8   6   1   7   7   6   7   7   6   7   6   8  12  10       45   21   11   11    7    6    8    0    0    0     5.93
  15  26  20   0  19   4  23  14   3  18  18  15  26  20   7  20  20  31  28  25       54   29   21   18   19   22   29    0    0    0    21.34
  23  37  31   0  29   5  33  20   4  29  28  24  33  34  27  34  31  41  51  43       59   34   30   20   30   23   39    2    0    0    27.41
  27  39  36   0  38   6  39  25   4  30  37  30  37  46  33  38  43  40  45  44       53   35   29   24   40   31   46    4    0    0    30.31
  37  61  53   0  47   8  53  32   6  50  49  36  57  59  44  54  56  69  59  60       96   40   41   35   52   43   67   33    0    0    46.61
  31  40  43   0  43   7  48  34   4  45  46  40  42  57  40  50  56  51  69  64       03   39   42   32   48   35   53    9    0    0    34.11
  55  93  72   0  82  12  88  52   7  80  76  61  72 100  70  84  88  81  91 100       90   50   59   47   85   58   92   56    1    0    56.88
  48  69  68   0  69  10  72  47   6  68  67  55  59  90  63  70  02  71  35  63       04   40   36   20   74   49   73   36    0    0    47.72
  17  24  26   0  24   4  27  22   2  25  25  26  20  32  23  24  33  24  11  22       06   26   19   13   26   17   27    0    0    0    16.4
   9  12  12   0  12   2  13  11   1  12  12  12  10  14  11  12  14  12  11  13       47   28   16   12   12    8   13    0    0    0     8.21
   9  12  12   0  13   2  13  12   1  13  13  13   9  15  12  13  16  10  12  14       58   26   17   13   14    7   12    0    0    0     7.21
   7   8   9   0   9   2   9   9   1   9   9  10   7  11   8   9  12   7   5   9       59   26   13   10   10    5    9    0    0    0     5.36
   5   6   7   1   7   1   7   7   1   7   6   7   5   8   6   7   8   6   5   7       55   27   11    9    7    4    7    0    0    0     4.3
   5   7   6   4   6   1   7   6   1   5   5   6   5   6   5   6   6   5   7   7       55   25   10    9    8    4    6    0    0    0     4.2
   9  13  11  11  11   2  12   8   1  10  10   8  12  11   8  11   8  14  15  11       52   30   15   13   11   10   14    0    0    0     9.79
   8  12  11  10  10   2  11   8   1  10   9   8   8  11   8   9   9  10   5   7       64   25   11   10   10    6   10    0    0    0     6.41
   5   6   6   6   5   1   7   6   1   5   5   6   5   6   5   6   6   6   4   5       57   23    9    9    6    4    6    0    0    0     3.9
   5   7   5   5   5   1   6   5   1   5   5   5   4   5   4   5   5   5   4   5       60   23    8    9    5    3    5    0    0    0     3.41
   4   6   5   4   5   1   6   4   1   4   4   4   4   5   4   5   5   5   3   5       54   22    8    8    5    3    5    0    0    0     3.42
   4   6   5   4   5   1   5   4   1   5   5   4   4   5   4   5   5   5   4   5       40   22    7    9    4    3    5    0    0    0     3.37
   4   5   5   4   5   1   5   4   1   4   5   4   4   5   4   5   5   5   4   5       47   22    7    8    5    3    5    0    0    0     3.4
   4   6   5   4   5   1   5   4   1   4   4   4   5   5   4   5   5   6   4   5       50   20    7    8    5    4    6    0    0    0     4.34
   5   6   5   4   5   1   6   4   1   5   5   4   6   5   4   5   5   6   4   6       47   21    7    9    5    5    6    0    0    0     4.46
   9  16  11   3  11   2  14   7   1  10  11   6  12  11   9  14   7  14  45  32       72   25   25   21   10   10   14    0    0    0     9.58
  34  53  40   1  47   6  49  37   3  46  44  39  51  55  39  56  63  68  83  75       81   41   50   42   49   44   61   25    0    0    42.75
  27  38  35   0  41   6  39  40   2  40  40  47  27  49  35  45  71  33  23  41       56   33   27   21   42   22   38    0    0    0    21.02
  13  19  17   0  16   3  21  22   1  18  20  27  14  23  17  21  36  16  15  21       71   23   15   14   19   11   19    0    0    0    10.90
   9  12  12   0  12   2  14  13   1  12  12  16  10  14  10  12  19  12   6  12       40   22   13   11   12    6   13    0    0    0     7.98
   9  11  10   0  10   2  11   9   1   9   9  10   8  10   8   9  11   9  13  13       48   23   14   12    9    7   10    0    0    0     6.47
  13  19  16   0  17   3  17  15   1  16  16  16  11  20  15  17  23  13  12  17       55   23   15   13   17    9   16    0    0    0     8.87
  14  21  18  10  18   3  21  13   1  17  16  13  19  21  16  19  20  22  15  17       56   27   17   14   18   15   22    0    0    0    14.32
   9  13  11  10  11   2  13  10   1  11  11  11  12  13  10  12  15  15  10  13       57   23   13   11   11   10   14    0    0    0     9.77
```

FIGURE 2.3

THIS PAGE IS BEST QUALITY PRACTICABLE
FROM COPY FURNISHED TO DDC

```
METRIC UNITS
HOUR BEGINNING:    8JN06/0800

. A200     A150     A100     P100     P50      A50      X        .   A200      A150      A100      A50       X      .       RAIN CODE
. SP DIR   SP DIR   SP DIR   SP DIR   SP DIR   SP DIR   SP DIR   . TEMP DPS  TEMP DPS  TEMP DPS  TEMP DPS  TEMP DPS.
   S  D     S  D     S  D     S  D     S  D     S  D     S  D       C    C     C    C     C    C     C    C     C    C          R  T

   9  23    5   6    9 214   10 210   11 210    7 206    5 205     174   0   181  14   173   1   179  14   180   9       32.00000
  12  20    2  52    8 214   12 196   10 203    9 205    6 199     174   0   181  14   174   1   179  14   180  10       33.10000
   9  20    3  70    9 217   12 200   10 204    9 206    9 215     175   0   181  13   174   1   179  14   180  10       34.10000
   8  38    5  44   11 221   13 198   11 206   10 207    7 216     175   0   181  13   174   1   179  14   181  11       35.10000
   9  24    3  66    9 211   10 199    9 203    8 204    5 212     175   0   181  14   174   1   180  14   181  11       35.00000
   9  33    8  81   10 202   11 199   10 206   10 209    6 213     175   0   182  14   174   0   180  14   182  11       35.00000
   3 173    5  59   10 214   11 203    9 208    9 209    7 213     175   0   182  14   174   0   180  14   182  11       36.10000
   4  12    6  53   10 216   11 199   10 203    8 213    7 216     175   0   180  12   173   0   179  13   181  10       38.10010
  10  34    6  38   10 227   11 206   10 209   10 206    6 206     174   0   180  11   173   0   179  13   181  10       39.01000
   8  27    7  56    8 205    9 227   10 204   10 201    7 206     174   0   179  10   173   0   179  13   181   9       40.00010
  13  21    5 141   11 226   10 239   11 201   10 210    7 208     174   0   180  11   173   0   179  13   180   9       40.00000
  10  32    4   8   11 229   10 242    9 212   10 208    9 212     175   0   180  11   173   0   179  13   182  10       41.10000
   7  26    5  91   10 216    9 216    8 203    8 211    7 212     174   0   180  11   172   0   178  12   181  10       42.00001
  10  16    4  15    9 202   10 210    9 211    9 206    6 184     174   0   180  11   172   0   178  11   181  11       42.00000
  10  30    2 247    9 210   11 200   10 206   10 213    5 216     174   0   180  10   173   0   179  12   181  11       43.10000
  13  11    6  34   10 223   11 208   10 207   10 196    7 213     174   0   180  11   172   0   178  12   181  12       43.00000
   2 253    6  25    9 216   10 199    8 204   10 207    7 208     175   0   180  11   173   0   179  12   181   9       44.10000
  10  27    5   5    8 205   10 204    9 198    9 204    6 210     174   0   179  10   173   0   179  12   179   4       46.11000
   7 210    5  17    7 156   13 194   11 197   11 201    9 205     174   0   178   9   172   0   178  11   179   6       48.10010
  11 202    4  84   10 215   11 200   11 209   11 204    8 197     174   0   178   9   172   0   178  11   179   6       49.10000
  11 206    1 270   10 214   10 201   11 198    8 209    9 208     174   0   178   8   172   0   178  11   180   5       50.00010
  11 203    5  75    9 201    9 198    8 196    8 204    7 202     174   0   178   9   172   0   178  10   180   5       50.00000
  11 203    5  50    9 214    9 199    8 196   10 206    7 204     174   0   180  10   172   0   178  11   181   5       50.00000
   5 204    5  77   10 209   10 191    8 197    9 201    9 197     173   0   179   9   172   0   178  10   181   6       52.10001
   7 187    6  23    9 199   10 190    9 196    9 200    9 202     174   0   178   8   172   0   178  10   179   5       54.11000
  11  35   10  66    7 214    9 196    9 202   10 200    7 192     173   0   177   7   171   0   177  10   178   5       56.20000
  12  23   10  54    7 207   12 189   11 197   10 203    8 199     174   0   177   7   171   0   177  10   179   6       56.00000
  11   9    6   2    9 195   11 190    9 203    9 196    6 196     173   0   177   6   171   0   177  10   180   6       56.00000
   7 204    1   6    8 209   12 196   11 197   10 213    6 215     174   0   177   6   171   0   178  11   180   6       56.00000
  12 203    7  40   10 204   12 194   11 205   10 205    8 204     174   0   177   8   172   0   178  10   180   6       57.10000
  12 209    9 104    8 221   12 186   11 197   10 209   10 211     174   0   177   7   171   0   178  10   179   6       61.20101
  11 202    8   8   10 209   12 194   10 202    9 199    8 200     174   0   177   7   171   0   178  10   178   5       65.20011
  14 207   10  84    8 204   13 192   13 197   12 207   11 212     173   0   177   7   171   0   177   9   178   4       70.31001
  10 189    6  59   11 219   13 191   10 199   10 200   10 201     174   0   178   7   171   0   177   9   178   4       75.21011
  14 200    3  55    1   4   13 194   11 201   12 194    8 201     173   0   177   6   171   0   177   9   178   5       79.01111
  10 193    8  47    6 253   14 188   13 192   11 199    8 194     173   0   178   6   171   0   177   8   178   4       80.01100
   9 175    8  87    9 174   12 192   11 199   12 196    7 198     174   0   178   6   171   0   178   9   178   3       81.10000
   4 192    5  69   11 207   14 190   13 193   11 196    9 198     174   0   178   6   171   0   178   9   178   2       81.00000
   7   9    6  49    8 214   11 191   11 196   10 195    8 194     174   0   178   6   171   0   178   9   178   3       82.01000
  13  11    9  83    7 227   14 196   13 202   12 204    9 196     174   0   178   6   171   0   178   9   178   6       82.00000
  11  11    9 101   10 209   13 197   11 199    9 199   10 205     174   0   178   6   172   0   179   9   178   7       82.00000
   9 213    4  50    7 252   12 190   11 199   10 205    7 208     174   0   178   6   172   0   179   9   178   7       82.00000
  11 190    5  56    9 213   11 195   10 203    9 200   10 193     174   0   178   6   172   0   178   9   178   5       83.00100
  14 201    8  59    9 223   14 192   12 201   12 208    8 207     174   0   178   6   172   0   178   9   178   3       83.00000
  13 198    7  44   12 207   10 194   10 202   10 201    7 200     173   0   177   6   171   0   178   9   178   3       83.00000
  14 195    5  61    8 212   12 191   11 193   13 197   10 196     173   0   177   6   171   0   178   8   178   4       83.00000
  14 196   10   2    3 220   13 164   11 193   11 204    9 195     173   0   177   6   171   0   178   9   177   4       83.00000
  14 202    9  82   10 207   11 187   10 195   11 199    8 198     173   0   177   6   171   0   178   9   177   3       83.00000
   9 191    5   9   10 205   12 192   10 202    9 198   11 200     173   0   177   6   171   0   178   9   177   2       83.00000
  13 199    6  28   10 214   13 188   11 191   11 205    7 203     173   0   177   6   171   0   178  10   177   3       83.00000
  11 194    7  36   10 199   10 192   11 206    9 194    9 196     173   0   176   6   170   0   178   9   177   3       83.00000
  12 201    3  94   12 220   11 166    9 192   11 207   11 192     173   0   176   6   171   0   178  10   177   3       85.10001
   9 197    6  50    8 208   10 191   11 192   10 196   10 192     172   0   176   6   170   0   177   9   176   4       92.41110
  12 191   10  41   10 189   12 189    9 198   10 198    8 192     172   0   176   6   169   0   178   8   176   4       95.21000
  15 198    7  72    5 224   14 184   12 192   12 196    8 202     172   0   176   6   170   0   177   9   176   5       96.00100
  12 198    4  56    9 213   12 185   11 194   10 201    9 199     172   0   176   6   170   0   177   9   176   5       96.00000
  10  55    7  83   11 195   10 196    8 199   10 192    9 196     171   0   175   6   169   0   176   8   176   5       96.00000
   7  11   10  83    9 205   12 182   12 194   10 199    9 200     171   0   175   6   169   0   176   8   176   5       98.20000
  12  32   12  43    6 223   11 195   11 193    9 202    9 200     172   0   176   6   169   0   176   9   176   6      100.10100
  10   7   10  74    5 193   11 169    9 197   11 203    8 206     171   0   175   6   169   0   176   9   176   6      100.00000
```

FIGURE 2.4

THIS PAGE IS BEST QUALITY PRACTICABLE
FROM COPY FURNISHED TO DDC

```
METRIC UNITS
HOUR BEGINNING:  8JN08/0600

  .A150 A150  RSE  RSE    X           VRTX      GI-L  MRI FUMO    X NEPH VIDE       RADIOMETERS        LUMI LQ1C  Q1C   FHC
     SP  DIR   SP  DIR   SP  DIR   SP  DIR   SP  DIR                               PYG  PYA  PYA  PYH  FYH
      S    D    S    D    S    D    S    D    S    D   V1   V1 EXCO EXCO EXCO    L    L    L    L    L   V1   V1 EXCO    V1

 0    5    6              5  205    8  206    3  201    6  115   11    1   17    0         0    0        12   15   14  -403
 1    2   52              6  199    8  195    4  192    5  116   14    1   17    0         0    0        12   17   17  -403
 2    3   70              9  215   11  213    5  200   12  122   26    1   23    0         0    0        12   20   20  -403
 3    5   44              7  216    9  213    4  205    5  116    8    1   12    0         0    0        12   15   15  -403
 4    3   86              5  212    8  204    4  197    3  114    8    1   13    0         0    0        12   14   14  -403
 5    8   81              6  213    9  211    4  202    3  113   15    1   14    0         0    0        12   16   15  -403
 6    5   59              7  213   10  210    5  210    4  114   19    1   19    0         0    0        12   20   20  -403
 7    6   53              7  216    9  216    4  206    7  114   23    1   23    0         0    0        12   20   19  -403
 8    6   38              6  208    9  205    4  204    5  121   15    1   20    0         0    0        12   18   18  -403
 9    7   56              7  208    9  202    4  200    6  118   15    1   19    0         0    0        12   15   14  -403
10    5  141              7  208   12  202    6  197    4  116   13    1   16    0         0    0        12   17   17  -403
11    4    6              9  212   12  202    5  201    4  118   13    1   14    0         0    0        12   15   15  -403
12    5   91              7  212   11  204    5  201    7  114   18    1   18    0         0    0        12   14   13  -403
13    4   15              8  184   13  196    6  191    0  119   12    1   13    0         0    0        12   12   12  -403
14    2  247              8  218   12  206    5  202    4  115   10    1   11    0         0    0        12   12   12  -403
15    6   34              7  213   10  205    5  196    7  115   13    1   15    0         0    0        12   12   12  -403
16    6   25              7  208   10  201    5  201   10  115   16    1   22    0         0    0        12   24   24  -403
17    5    5              6  210    9  201    4  199    9  120   27    1   25    0         0    0        12   28   27  -403
18    9   17              9  205   11  204    5  199    7  122   30    1   27    0         0    0        12   26   26  -403
19    4   84              9  197   11  190    5  195    5  119   12    1   16    0         0    0        12   23   22  -403
20    1  270              9  200   13  203    5  197    3  115    5    1    6    0         0    0        12   10   10  -403
21    5   75              7  202   10  194    5  194    3  112    7    1   10    0         0    0        12    8    8  -403
22    9   50              7  204   11  202    5  204    4  113   13    1   12    0         0    0        12   10   10  -403
23    5   77              9  197   11  197    5  197    7  116   32    1   27    0         0    0        12   27   26  -403
24    6   23              9  202   11  199    5  195   12  145   38    1   37    0         0    0        12   37   35  -403
25   10   66              7  192   10  196    6  180    7  122   10    1   14    0         0    0        12   23   23  -407
26   10   54              8  199   12  194    4  197    3  114    5    1    8    0         0    0        12   10    9  -405
27    6    2              6  196    9  196    5  190    2  116    5    1   10    0         0    0        12    7    6  -404
28    1    6              8  215   11  210    6  204    2  114   12    1   13    0         0    0        12    3    6  -405
29    7   40              8  204   10  202    5  190    5  122   26    1   26    0         0    0        12   32   31  [illegible]
30    9  104             10  211   13  201    7  203   10  156   51    1   39    0         0    0        12   43   41  -413
31    8    8              8  208   11  204    5  199   22  140   45    1   38    0         0    0        12   48   46  -415
32   10   84             11  212   14  206    6  206   30  225   59    1   50    0         0    0        12   72   65  -416
33    6   59             10  201   12  199    5  193   23  181   69    1   46    0         0    0        12   52   51  -416
34    3   55              6  201   11  190    5  195   40  233   61    1   66    0         0    0        12   55   61    **
35    8   47              7  194   11  192    6  194   34  184   35    1   40    0         0    0        12   73   71    **
36    8   87              9  198   11  193    5  194   13  123   11    1   16    0         0    0        12   24   24
37    5   69              3  198   10  198    5  188    5  112   11    1   13    0         0    0        12   12   12
38    6   49              9  194   13  195    6  191    6  114   12    1   15    0         0    0        12   10   10
39    9   63              9  196   11  201    5  193    3  112    5    1    6    0         0    0        12    7    7
40    9  101             10  205   12  204    6  195    1  106    5    1    7    0         0    0        12    6    6
41    4   50              7  208   14  190    4  198    2  112    7    1    8    0         0    0        12    6    6
42    5   56             10  193   13  205    7  195    2  115   15    1   16    0         0    0        12   15   14
43    8   59              8  207   11  200    5  185    2  115    5    1    6    0         0    0        12   10   10
44    7   44              7  200   11  195    4  200    1  112    4    1    7    0         0    0        12    6    6
45    5   61             10  196   14  194    7  193    1  113    4    1    7    0         0    0        12    5    5
46   10    2              9  195   13  201    5  191    1  113    3    1    6    0         0    0        12    5    5
47    9   82              8  190   11  192    5  191    1  109    4    1    9    0         0    0        12    5    5    **
48    5    9             11  200   15  206    6  197    1  112    4    1    9    0         0    0        12    5    5    **
49    6   26              7  203   10  190    5  193    1  112    4    1    9    0         0    0        12    6    6    **
50    7   36              9  196   12  192    5  191    1  108    4    1   10    0         0    0        12    6    6    **
51    3   94             11  192   13  192    7  185    3  129   45    1   25    0         0    0        12   14   14    **
52    6   50             10  192   12  191    6  157   35  134   63    1   52    0         0    0        12   71   65    **
53   10   41              8  192   11  196    6  139   20  147   23    1   30    0         0    0        12   34   33    **
54    7   72              8  202   11  196    5  192   12  116   15    1   16    0         0    0        12   10   16    **
55    4   56              9  199   12  195    6  194    7  112    8    1   12    0         0    0        12   12   12    **
56    7   83              9  196   11  192    5  191    3  111   13    1   17    0         0    0        12   10 [illegible]  -495
57   10   83              9  200   13  197    7  191    6  119   12    1   15    0         0    0        12   13   13  -475
58   12   43              9  200   13  194    6  193    7  125   15    1   23    0         0    0        12   22   22  -468
59   10   74              8  206   11  203    5  200    4  111   10    1   16    0         0    0        12   15   15  -457
```

FIGURE 2.5

THIS PAGE IS BEST QUALITY PRACTICABLE
FROM COPY FURNISHED TO DDC

```
          HOURLY WIND SPEED AVERAGES

60 MIN. WIND DATA FOR  8JN07BEGINNING AT     1400Z
              F100    P 50    A200    A150    A100    A 50     X      VRTX    GILL   ROSE

CORRECTION-100.   -100.    136.    136.    136.    133.    126.    -11.    -10.
HOUR

1400          5.5     5.3     5.2     5.3     5.0     4.6     4.3     6.7     2.7   *****
1500          6.8     6.5     6.5     6.6     6.2     6.0     5.2     7.9     3.3   *****
1600          7.4     7.0     7.4     7.4     7.1     6.7     5.7     8.4     3.7   *****
1700          7.3     6.9     7.7     7.7     7.4     7.0     6.0     8.8     4.0   *****
1800          8.0     7.5     8.5     8.5     8.0     7.7     6.2     9.0     4.1   *****
1900          8.5     7.9     8.5     8.5     8.1     7.7     6.4     9.4     4.1   *****
2000          7.9     7.8     7.8     7.8     7.4     6.9     5.9     8.7     3.9   *****
2100          6.7     6.3     7.3     7.2     6.7     6.3     5.1     7.7     3.3   *****
2200          6.5     6.0     7.0     6.9     6.3     5.9     5.1     7.7     3.2   *****
2300          6.1     5.7     6.6     6.5     6.0     5.6     4.6     7.0     2.9   *****
0000          6.4     5.8     7.5     7.3     6.7     6.2     5.0     7.5     3.2   *****
0100          7.3     6.5     8.3     8.0     7.3     6.8     5.4     8.1     3.5   *****
0200          7.0     6.2     7.9     7.7     7.0     6.4     5.0     7.5     3.2   *****
0300          7.1     6.3     8.0     7.8     7.0     6.4     5.3     7.9     3.4   *****
0400          7.6     6.8     8.5     8.3     7.6     7.0     5.4     8.1     3.5   *****
0500          9.7     8.6    10.6    10.4     9.5     8.7     6.5     9.4     4.3   *****
0600         10.5     9.5    11.1    10.7     9.9     9.0     7.6    10.7     5.0   *****
0700         10.5     9.7    11.5    11.1    10.2     9.4     7.8    10.9     5.0   *****
0800         10.6     9.4    11.7    11.3    10.3     9.3     7.4    10.5     4.8   *****
0900         11.5    10.2    12.1    11.7    10.6     9.5     8.3    11.2     5.3   *****
1000          8.8     7.9    10.2     9.9     9.0     8.1     6.8    10.1     4.3   *****
1100         10.0     9.2    10.4    10.1     9.5     8.7     7.0    10.2     4.4   *****
```

FIGURE 2.6

```
                 HOURLY WIND DIRECTION AVERAGES

60 MIN. WIND DATA FOR  3JN07BEGINNING AT      1400Z
             P100    P 50    A200    A150    A100    A 50     X      VRTX    GILL    ROSE
CORRECTION-100.    -100.    138.    138.    136.    133.    128.    -11.    -10.
HOUR

1400         210.6   214.8   211.6   222.5   220.4   210.3   214.8   209.6   225.7   0.0
1500         206.7   211.0   216.6   227.7   224.8   214.9   223.4   218.0   213.3   0.0
1600         211.7   216.8   211.3   222.6   221.4   212.1   216.4   210.9   207.2   0.0
1700         198.5   204.6   208.2   219.0   217.9   208.9   210.7   206.6   201.3   0.0
1800         201.2   207.4   200.9   210.9   209.1   201.2   202.1   200.3   194.6   0.0
1900         195.6   201.9   203.0   212.1   211.9   204.5   207.3   204.7   199.6   0.0
2000         166.6   193.9   193.4   202.4   202.0   195.4   195.6   194.0   189.0   0.0
2100         180.7   188.1   185.3   192.8   192.9   187.0   182.8   181.2   177.1   0.0
2200         179.8   187.5   187.5   194.6   194.0   167.0   166.4   164.7   170.6   0.0
2300         179.1   184.3   167.6   194.0   195.4   168.0   166.9   164.6   160.3   0.0
0000         187.0   192.3   194.7   202.5   202.3   195.7   195.7   192.5   187.0   0.0
0100         192.1   197.2   198.9   207.1   207.3   200.3   199.5   196.5   192.0   0.0
0200         188.4   194.5   196.1   203.9   203.2   196.1   195.7   193.3   188.9   0.0
0300         192.1   197.4   200.2   208.1   206.9   199.3   199.6   197.8   192.6   0.0
0400         189.0   194.9   197.1   205.0   203.2   197.2   196.5   194.4   189.4   0.0
0500         197.3   203.3   203.7   220.0   212.4   204.7   205.0   201.9   197.0   0.0
0600         197.3   202.7   204.6   223.4   213.4   205.8   207.2   203.5   198.8   0.0
0700         197.7   201.5   208.7    40.7   214.0   204.6   204.7   201.5   196.4   0.0
0800         198.6   201.9   198.8    50.9   211.6   204.2   205.3   201.9   196.3   0.0
0900         199.0   202.0   159.6    53.5   214.9   204.6   204.7   202.9   196.4   0.0
1000         224.7   224.6   227.2   221.5   234.2   225.7   232.1   224.6   220.6   0.0
1100         213.4   218.5   219.6   131.9   226.5   219.1   225.9   218.7   213.9   0.0
```

FIGURE 2.7

```
                 HOURLY STANDARD DEVIATICNS OF U AND V

60 MIN. WIND DATA FOR  6JN07BEGINNING AT     1400Z
              P100    P 50    A200    A150    A100    A 50     X      VRTX    GILL   ROSE
CORRECTION-10.   -20.    135.    138.    135.    133.    126.    -11.    -10.
HOU

1400           1.5     1.5     1.3     1.4     1.2     1.3     1.4     2.1      .9   *****
1500           1.7     1.7     1.9     2.1     1.9     2.0     1.9     2.8     1.2   *****
1600           1.9     1.6     1.5     1.8     1.7     1.5     1.5     2.4     1.2   *****
1700           2.0     1.9     1.6     1.9     1.6     1.7     1.9     2.6     1.2   *****
1800           2.4     2.3     1.6     2.6     2.4     1.8     1.9     2.7     1.2   *****
1900           2.0     1.9     1.8     2.5     2.5     1.9     2.0     2.7     1.3   *****
2000           1.7     1.7     1.7     2.5     2.2     1.8     1.6     2.6     1.2   *****
2100           1.4     1.5     1.3     1.4     1.4     1.4     1.3     2.1      .9   *****
2200           1.6     1.6     1.5     1.4     1.4     1.3     1.5     2.3     1.0   *****
2300           1.2     1.3     1.4     1.3     1.3     1.2     1.3     1.9      .9   *****
0000           1.6     1.5     1.7     1.7     1.7     1.6     1.4     2.0      .9   *****
0100           1.4     1.4     1.6     1.8     1.6     1.5     1.4     2.1      .9   *****
0200           1.4     1.3     1.9     1.6     1.5     1.4     1.3     2.0      .9   *****
0300           1.5     1.5     1.5     1.9     1.3     1.4     1.4     2.0      .9   *****
0400           1.7     1.6     1.8     2.5     2.4     1.6     1.5     2.2     1.0   *****
0500           2.2     1.9     2.5     9.6     5.3     2.0     1.6     2.5     1.2   *****
0600           2.3     2.2     2.7    10.7     6.2     1.9     2.1     2.6     1.3   *****
0700           2.6     2.2    10.6    10.9     4.6     2.1     2.2     2.5     1.4   *****
0800           3.4     2.2    11.5    10.8     5.1     2.1     2.5     2.8     1.4   *****
0900           4.2     3.1    12.1    11.1     7.8     3.0     4.0     3.7     1.7   *****
1000           2.8     2.2    10.0     9.6     3.6     2.0     2.3     2.7     1.3   *****
1100           2.0     2.7     2.6    10.1     3.6     2.4     2.2     3.1     1.5   *****
```

FIGURE 2.8

THIS PAGE IS BEST QUALITY PRACTICABLE
FROM COPY FURNISHED TO DDC

```
          TOTAL SPEED AND DIRECTION PAIRS CONTRIBUTING TO HOURLY AVERAGES

60 MIN. WIND DATA FOR  8JN07BEGINNING AT     1400Z
            P100     P 50     A200     A150     A100     A 50      X      VRTX     GILL     ROSE
CORRECTION-100.     -100.     136.     136.     136.     135.     126.     -11.     -10.
HOUR

1400        600.     600.     600.     600.     600.     600.     600.     600.     600.      0.
1500        600.     600.     600.     600.     600.     600.     600.     600.     600.      0.
1600        600.     600.     600.     600.     600.     600.     600.     600.     600.      0.
1700        600.     600.     600.     600.     600.     600.     600.     600.     600.      0.
1800        600.     600.     600.     600.     600.     600.     600.     600.     600.      0.
1900        600.     600.     600.     600.     600.     600.     600.     600.     600.      0.
2000        600.     600.     600.     600.     600.     600.     600.     600.     600.      0.
2100        600.     600.     600.     600.     600.     600.     600.     600.     600.      0.
2200        600.     600.     600.     600.     600.     600.     600.     600.     600.      0.
2300        600.     600.     600.     600.     600.     600.     600.     600.     600.      0.
[illegible] [illegible] [illegible] [illegible] 600. [illegible] [illegible] [illegible] [illegible] [illegible] [illegible]
0100        [illegible] [illegible] [illegible] [illegible] [illegible] [illegible] [illegible] [illegible] [illegible] [illegible]
0200        [illegible] [illegible] [illegible] [illegible] [illegible] [illegible] [illegible] [illegible] [illegible] [illegible]
[illegible] [illegible] [illegible] [illegible] [illegible] [illegible] [illegible] [illegible] [illegible] [illegible] [illegible]
0400        600.     600.     600.     600.     600.     600.     600.     600.     600.      0.
0500        600.     600.     600.     600.     600.     600.     600.     600.     600.      0.
0600        600.     600.     600.     600.     600.     600.     600.     600.     600.      0.
0700        600.     600.     600.     600.     600.     600.     600.     600.     600.      0.
0800        600.     600.     600.     600.     600.     600.     600.     600.     600.      0.
0900        600.     600.     600.     600.     600.     600.     600.     600.     600.      0.
1000        600.     600.     600.     600.     600.     600.     600.     600.     600.      0.
1100        570.     570.     570.     570.     570.     570.     570.     570.     570.      0.
```

THIS PAGE IS BEST QUALITY PRACTICABLE
FROM COPY FURNISHED TO DDC

FIGURE 2.9

```
              HOURLY WIND AVERAGE DIRECTION DEVIATIONS FROM X

60 MIN. WIND DATA FOR  8JN078EGINNING AT     1400Z

               P100    P 50    A200    A150    A100    A 50     X       VRTX     GILL    ROSE
CORRECTION-100.  -100.   138.    138.    136.    139.    128.     -11.     -10.
HOUR

1400            4.2      .0     3.1    -7.7    -5.7     4.0  ******     5.2      9.1    214.0
1500           16.7    12.3     6.0    -4.3    -1.4     3.5  ******     5.4     10.1    223.4
1600            4.7     -.4     5.1    -6.2    -5.0     4.3  ******     5.7      9.3    216.4
1700           12.2     6.1     2.5    -8.3    -7.2     1.7  ******     4.1      9.3    210.7
1800             .9    -5.3     1.2    -8.8    -7.0      .9  ******     1.8      7.3    202.1
1900           11.7     5.4     4.4    -4.0    -4.5     2.6  ******     2.7      7.7    207.3
2000            8.9     1.7     2.2    -6.8    -6.4      .2  ******     1.6      6.6    195.6
2100            2.2    -5.3    -2.5    -9.9   -10.1    -4.2  ******     1.6      5.7    182.8
2200            6.5    -1.1    -1.1    -8.2    -7.6     -.6  ******     1.7      7.0    166.4
2300            7.6     2.1    -1.0    -8.0    -8.5    -1.2  ******     2.3      6.5    186.9
0000            8.7     3.4     1.1    -6.7    -6.6      .6  ******     3.3      8.8    195.7
0100            7.4     2.3      .6    -7.6    -7.8     -.8  ******     3.0      7.5    199.5
0200            7.4     1.2     -.4    -8.2    -7.5     -.4  ******     2.4      6.0    195.7
0300            7.5     2.2     -.6    -8.5    -7.3      .3  ******     1.0      7.0    199.6
0400            7.5     1.7     -.5    -8.5    -6.6     -.7  ******     2.1      7.1    196.5
0500            7.7     1.7     1.2   -15.1    -7.5      .3  ******     3.1      8.0    205.0
0600            9.9     4.6     2.6   -16.2    -6.1     1.4  ******     3.7      8.4    207.2
0700            6.9     3.1    -4.0   164.0    -9.[illegible]      .0  ******     3.1      8.3    204.7
0800            6.7     3.5     6.5   154.4    -6.3     1.1  ******     3.4      7.0    205.3
0900            5.7     2.7    45.1   146.2   -10.3      .1  ******     1.7      6.3    204.7
1000            7.3     7.5     4.9    10.5    -2.2     5.3  ******     7.4     11.5    232.1
1100           12.5     7.3     6.3    94.0     -.6     5.7  ******     7.2     12.0    225.9
```

FIGURE 2.10

```
FSM SELECTION FOR HOUR  8JN78/0600

     0         5         10        15        20        25        30        35        40        45        50        55
A10  1 1 1 1 1 1 1 1 1 1 1 1 1 1 1 1 1 1 1 1 1 1 1 1 1 1 1 1 1 1 1 1 1 1 1 1 1 1 1 1 1 1 1 1 1 1 1 1 1 1 1 1 1 1 1 1 1 1 1 1   A10
B10  0 0 0 0 0 0 0 0 0 0 0 0 0 0 0 0 0 0 0 0 0 0 0 0 0 0 0 0 0 0 0 0 0 0 0 0 0 0 0 0 0 0 0 0 0 0 0 0 0 0 0 0 0 0 0 0 0 0 0 0   B10
C10  0 0 0 0 0 0 0 0 0 0 0 0 0 0 0 0 0 0 0 0 0 0 0 0 0 0 0 0 0 0 0 0 0 0 0 0 0 0 0 0 0 0 0 0 0 0 0 0 0 0 0 0 0 0 0 0 0 0 0 0   C10
 X   0 0 0 0 0 0 0 0 0 0 0 0 0 0 0 0 0 0 0 0 0 0 0 0 0 0 0 0 0 0 0 0 0 0 0 0 0 0 0 0 0 0 0 0 0 0 0 0 0 0 0 0 0 0 0 0 0 0 0 0    X
A50  1 1 1 1 1 1 1 1 1 1 1 1 1 1 1 1 1 1 1 1 1 1 1 1 1 1 1 1 1 1 1 1 1 1 1 1 1 1 1 1 1 1 1 1 1 1 1 1 1 1 1 1 1 1 1 1 1 1 1 1   A50
B50  0 0 0 0 0 0 0 0 0 0 0 0 0 0 0 0 0 0 0 0 0 0 0 0 0 0 0 0 0 0 0 0 0 0 0 0 0 0 0 0 0 0 0 0 0 0 0 0 0 0 0 0 0 0 0 0 0 0 0 0   B50
A100 1 1 1 1 1 1 1 1 1 1 1 1 1 1 1 1 1 1 1 1 1 1 1 1 1 1 1 1 1 1 1 1 1 1 1 1 1 1 1 1 1 1 1 1 1 1 1 1 1 1 1 1 1 1 1 1 1 1 1 1   A100
B100 0 0 0 0 0 0 0 0 0 0 0 0 0 0 0 0 0 0 0 0 0 0 0 0 0 0 0 0 0 0 0 0 0 0 0 0 0 0 0 0 0 0 0 0 0 0 0 0 0 0 0 0 0 0 0 0 0 0 0 0   B100
 Q   1 1 1 1 1 1 1 1 1 1 1 1 1 1 1 1 1 1 1 1 1 1 1 1 1 1 1 1 1 1 1 1 1 1 1 1 1 1 1 1 1 1 1 1 1 1 1 1 1 1 1 1 1 1 1 1 1 1 1 1    Q
 P   0 0 0 0 0 0 0 0 0 0 0 0 0 0 0 0 0 0 0 0 0 0 0 0 0 0 0 0 0 0 0 0 0 0 0 0 0 0 0 0 0 0 0 0 0 0 0 0 0 0 0 0 0 0 0 0 0 0 0 0    P

FSM SELECTION FOR HOUR  8JN78/0700

     0         5         10        15        20        25        30        35        40        45        50        55
A10  1 1 1 1 1 1 1 1 1 1 1 1 1 1 1 1 1 1 1 1 1 1 1 1 1 1 1 1 1 1 1 1 1 1 1 1 1 1 1 1 1 1 1 1 1 1 1 1 1 1 1 1 1 1 1 1 1 1 1 1   A10
B10  0 0 0 0 0 0 0 0 0 0 0 0 0 0 0 0 0 0 0 0 0 0 0 0 0 0 0 0 0 0 0 0 0 0 0 0 0 0 0 0 0 0 0 0 0 0 0 0 0 0 0 0 0 0 0 0 0 0 0 0   B10
C10  0 0 0 0 0 0 0 0 0 0 0 0 0 0 0 0 0 0 0 0 0 0 0 0 0 0 0 0 0 0 0 0 0 0 0 0 0 0 0 0 0 0 0 0 0 0 0 0 0 0 0 0 0 0 0 0 0 0 0 0   C10
 X   0 0 0 0 0 0 0 0 0 0 0 0 0 0 0 0 0 0 0 0 0 0 0 0 0 0 0 0 0 0 0 0 0 0 0 0 0 0 0 0 0 0 0 0 0 0 0 0 0 0 0 0 0 0 0 0 0 0 0 0    X
A50  1 1 1 1 1 1 1 1 1 1 1 1 1 1 1 1 1 1 1 1 1 1 1 1 1 1 1 1 1 1 1 1 1 1 1 1 1 1 1 1 1 1 1 1 1 1 1 1 1 1 1 1 1 1 1 1 1 1 1 1   A50
B50  0 0 0 0 0 0 0 0 0 0 0 0 0 0 0 0 0 0 0 0 0 0 0 0 0 0 0 0 0 0 0 0 0 0 0 0 0 0 0 0 0 0 0 0 0 0 0 0 0 0 0 0 0 0 0 0 0 0 0 0   B50
A100 1 1 1 1 1 1 1 1 1 1 1 1 1 1 1 1 1 1 1 1 1 1 1 1 1 1 1 1 1 1 1 1 1 1 1 1 1 1 1 1 1 1 1 1 1 1 1 1 1 1 1 1 1 1 1 1 1 1 1 1   A100
B100 0 0 0 0 0 0 0 0 0 0 0 0 0 0 0 0 0 0 0 0 0 0 0 0 0 0 0 0 0 0 0 0 0 0 0 0 0 0 0 0 0 0 0 0 0 0 0 0 0 0 0 0 0 0 0 0 0 0 0 0   B100
 Q   1 1 1 1 1 1 1 1 1 1 1 1 1 1 1 1 1 1 1 1 1 1 1 1 1 1 1 1 1 1 1 1 1 1 1 1 1 1 1 1 1 1 1 1 1 1 1 1 1 1 1 1 1 1 1 1 1 1 1 1    Q
 P   0 0 0 0 0 0 0 0 0 0 0 0 0 0 0 0 0 0 0 0 0 0 0 0 0 0 0 0 0 0 0 0 0 0 0 0 0 0 0 0 0 0 0 0 0 0 0 0 0 0 0 0 0 0 0 0 0 0 0 0    P

FSM SELECTION FOR HOUR  8JN78/0800

     0         5         10        15        20        25        30        35        40        45        50        55
A10  1 1 1 1 1 1 1 1 1 1 1 1 1 1 1 1 1 1 1 1 1 1 1 1 1 1 1 1 1 1 1 1 1 1 1 1 1 1 1 1 1 1 1 1 1 1 1 1 1 1 1 1 1 1 1 1 1 1 1 1   A10
B10  0 0 0 0 0 0 0 0 0 0 0 0 0 0 0 0 0 0 0 0 0 0 0 0 0 0 0 0 0 0 0 0 0 0 0 0 0 0 0 0 0 0 0 0 0 0 0 0 0 0 0 0 0 0 0 0 0 0 0 0   B10
C10  0 0 0 0 0 0 0 0 0 0 0 0 0 0 0 0 0 0 0 0 0 0 0 0 0 0 0 0 0 0 0 0 0 0 0 0 0 0 0 0 0 0 0 0 0 0 0 0 0 0 0 0 0 0 0 0 0 0 0 0   C10
 X   0 0 0 0 0 0 0 0 0 0 0 0 0 0 0 0 0 0 0 0 0 0 0 0 0 0 0 0 0 0 0 0 0 0 0 0 0 0 0 0 0 0 0 0 0 0 0 0 0 0 0 0 0 0 0 0 0 0 0 0    X
A50  1 1 1 1 1 1 1 1 1 1 1 1 1 1 1 1 1 1 1 1 1 1 1 1 1 1 1 1 1 1 1 1 1 1 1 1 1 1 1 1 1 1 1 1 1 1 1 1 1 1 1 1 1 1 1 1 1 1 1 1   A50
B50  0 0 0 0 0 0 0 0 0 0 0 0 0 0 0 0 0 0 0 0 0 0 0 0 0 0 0 0 0 0 0 0 0 0 0 0 0 0 0 0 0 0 0 0 0 0 0 0 0 0 0 0 0 0 0 0 0 0 0 0   B50
A100 1 1 1 1 1 1 1 1 1 1 1 1 1 1 1 1 1 1 1 1 1 1 1 1 1 1 1 1 1 1 1 1 1 1 1 1 1 1 1 1 1 1 1 1 1 1 1 1 1 1 1 1 1 1 1 1 1 1 1 1   A100
B100 0 0 0 0 0 0 0 0 0 0 0 0 0 0 0 0 0 0 0 0 0 0 0 0 0 0 0 0 0 0 0 0 0 0 0 0 0 0 0 0 0 0 0 0 0 0 0 0 0 0 0 0 0 0 0 0 0 0 0 0   B100
 Q   1 1 1 1 1 1 1 1 1 1 1 1 1 1 1 1 1 1 1 1 1 1 1 1 1 1 1 1 1 1 1 1 1 1 1 1 1 1 1 1 1 1 1 1 1 1 1 1 1 1 1 1 1 1 1 1 1 1 1 1    Q
 P   0 0 0 0 0 0 0 0 0 0 0 0 0 0 0 0 0 0 0 0 0 0 0 0 0 0 0 0 0 0 0 0 0 0 0 0 0 0 0 0 0 0 0 0 0 0 0 0 0 0 0 0 0 0 0 0 0 0 0 0    P

FSM SELECTION FOR HOUR  8JN78/0900

     0         5         10        15        20        25        30        35        40        45        50        55
A10  1 1 1 1 1 1 1 1 1 1 1 1 1 1 1 1 1 1 1 1 1 1 1 1 1 1 1 1 1 1 1 1 1 1 1 1 1 1 1 1 1 1 1 1 1 1 1 1 1 1 1 1 1 1 1 1 1 1 1 1   A10
B10  0 0 0 0 0 0 0 0 0 0 0 0 0 0 0 0 0 0 0 0 0 0 0 0 0 0 0 0 0 0 0 0 0 0 0 0 0 0 0 0 0 0 0 0 0 0 0 0 0 0 0 0 0 0 0 0 0 0 0 0   B10
C10  0 0 0 0 0 0 0 0 0 0 0 0 0 0 0 0 0 0 0 0 0 0 0 0 0 0 0 0 0 0 0 0 0 0 0 0 0 0 0 0 0 0 0 0 0 0 0 0 0 0 0 0 0 0 0 0 0 0 0 0   C10
 X   0 0 0 0 0 0 0 0 0 0 0 0 0 0 0 0 0 0 0 0 0 0 0 0 0 0 0 0 0 0 0 0 0 0 0 0 0 0 0 0 0 0 0 0 0 0 0 0 0 0 0 0 0 0 0 0 0 0 0 0    X
A50  1 1 1 1 1 1 1 1 1 1 1 1 1 1 1 1 1 1 1 1 1 1 1 1 1 1 1 1 1 1 1 1 1 1 1 1 1 1 1 1 1 1 1 1 1 1 1 1 1 1 1 1 1 1 1 1 1 1 1 1   A50
B50  0 0 0 0 0 0 0 0 0 0 0 0 0 0 0 0 0 0 0 0 0 0 0 0 0 0 0 0 0 0 0 0 0 0 0 0 0 0 0 0 0 0 0 0 0 0 0 0 0 0 0 0 0 0 0 0 0 0 0 0   B50
A100 1 1 1 1 1 1 1 1 1 1 1 1 1 1 1 1 1 1 1 1 1 1 1 1 1 1 1 1 1 1 1 1 1 1 1 1 1 1 1 1 1 1 1 1 1 1 1 1 1 1 1 1 1 1 1 1 1 1 1 1   A100
B100 0 0 0 0 0 0 0 0 0 0 0 0 0 0 0 0 0 0 0 0 0 0 0 0 0 0 0 0 0 0 0 0 0 0 0 0 0 0 0 0 0 0 0 0 0 0 0 0 0 0 0 0 0 0 0 0 0 0 0 0   B100
 Q   1 1 1 1 1 1 1 1 1 1 1 1 1 1 1 1 1 1 1 1 1 1 1 1 1 1 1 1 1 1 1 1 1 1 1 1 1 1 1 1 1 1 1 1 1 1 1 1 1 1 1 1 1 1 1 1 1 1 1 1    Q
 P   0 0 0 0 0 0 0 0 0 0 0 0 0 0 0 0 0 0 0 0 0 0 0 0 0 0 0 0 0 0 0 0 0 0 0 0 0 0 0 0 0 0 0 0 0 0 0 0 0 0 0 0 0 0 0 0 0 0 0 0    P
```

THIS PAGE IS BEST QUALITY PRACTICABLE
FROM COPY FURNISHED TO DDC

FIGURE 2.11

Figure 2.4 details the wind speed in meters per second and the wind direction of seven wind sets, the temperature and the dewpoint spread in degrees Celsius and the rainfall amount indicator. The rain code contains the accumulated number of .005-inch rain bucket tips from the beginning of the tape to the left of the decimal point. The number of tips per scan for a given minute is depicted in the five positions to the right of the decimal point.

Figure 2.5 contains the data from the remaining wind sets and the observations from the remaining visibility sensors and radiation meters.

Figure 2.6 through Figure 2.10 contain intercomparison data of the hourly averaged wind output. Horizontal and vertical profiles of wind conditions can be analyzed from these data as well as the relative performance characteristics of the various wind sensors at location X.

Figure 2.11 depicts the output of the scatter meters used each minute to calculate the observed and estimated values of slant visual range using the methods discussed in Section 2.5.

The REQUOTE program also evaluates the FSM data to identify episodes of reduced visibility according to prescribed criteria. In addition to developing specialized data listings for these periods, correction factors for the transmissometers are calculated and printed out to aid in evaluating the instrument drift during reduced visibility episodes. This is a common problem with transmissometers which must be accounted for prior to their utilization in analysis and prediction studies.

A separate subroutine was added to REQUOTE in mid-1978 to evaluate the slant visual range estimation and short range prediction procedures previously developed. A control forecast technique which computes the most probable extinction coefficient using a well-tested Markov model is part of the evaluation. Both techniques assume normality in converting the deterministic predictions to exceedance probabilities.

Recently, routines have been added to include scatter plots of the Rosemount, Gill and J-Tec wind direction and speed output against the Climatronics wind set. Finally, REQUOTE generates a specialized data file (stored on permanent file in the CDC 6600 system) containing the sensor outputs required by the computer program being used in the present weather automation studies discussed in Section 2.4.

The evolving nature of the research requirements and sensor configurations of the Otis WTF put heavy demands on and add to the complexity of a basic data processing program like REQUOTE. The resulting problems have been further complicated by some major setbacks in the data logging system at Otis. Special data editing routines had to be developed to monitor each sensor's output voltage to ensure its validity before inclusion in subsequent averaging and conversion routines. Criteria for data acceptability underwent evolution as experience was gained with the data logging system. Other routines had to be developed to filter excessive noise from the useful data stream. Data loss rates became excessive in mid-1977 when the 6600 system could not successfully read magnetic tapes being generated at Otis. After numerous attempts to circumvent the problem with software modifications to REQUOTE, the problem was traced to the tape drive at the Otis WTF which was replaced. Subsequent routine processing of the collected data has generally been without incidence and timely.

2.4 Automation of Visual Present Weather Observations

The automated array of weather instruments described previously provides an ideal setting for the evaluation of techniques for discrimination of present weather elements. A decision-tree approach was chosen to determine the extent to which an objective solution to the problem could be made. Primary consideration was given to extracting present-weather information from a selected subset of the weather instruments cited in Section 2.2.

The decision tree developed under this contract is shown in generalized form in Figure 2.12. It consists of two basic programs, (a), an obstruction to visibility determination and, (b), a present weather determination. One of the more obvious decision points in the first of these programs is the test to determine if a restriction to visibility exists. The forward-scatter-meter provides this information. The next test determines the humidity of the air. If low, then the program branches to the "dry" obstructions and with input from the nephelometer, snow conditions and wind gustiness discriminates between smoke (K), haze (H), dust (D), or blowing snow, sand or dust (BS, BN, or BD). If the humidity is high, then the program leads to the fog branch and determines ground fog (GF), fog (F) or ice fog (IF) through examinations of the vertical variations of visibility and temperature.

The present weather determination is triggered by a positive report from the tipping-bucket rain guage. The frequency of tips is related to intensity and is used to separate the precipitation into three classes, light (-), moderate ( ), and heavy (+). Temperature tests separate freezing precipitation from liquid and differences between the backscatter meter and forward-scatter-meter discriminate snow (S) from rain (R), freezing rain (ZR) and freezing drizzle (ZL). Empirical evidence which shows that the

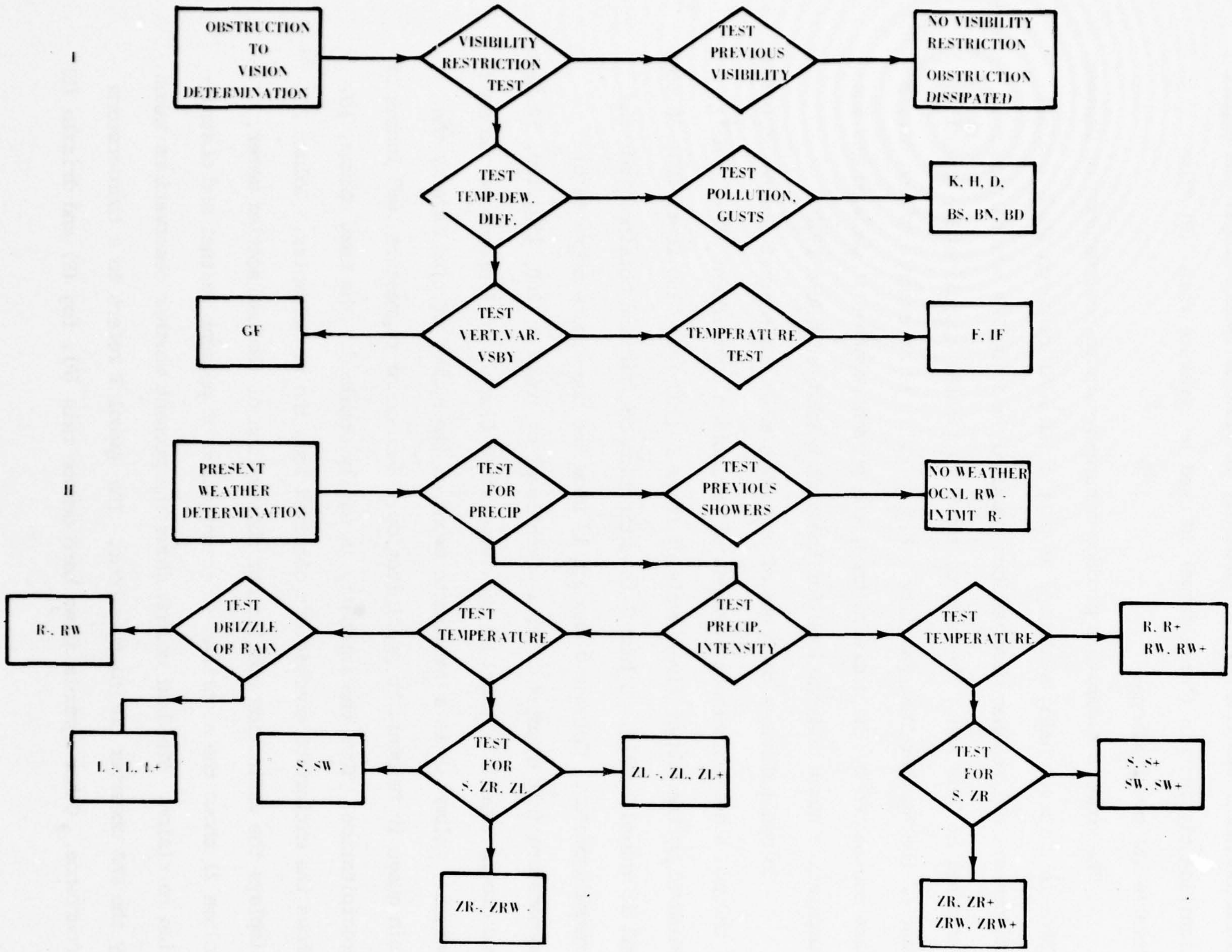
I
OBSTRUCTION TO VISION DETERMINATION
VISIBILITY RESTRICTION TEST
TEST PREVIOUS VISIBILITY
NO VISIBILITY RESTRICTION
OBSTRUCTION DISSIPATED
TEST TEMP-DEW. DIFF.
TEST POLLUTION, GUSTS
K, H, D, BS, BN, BD
GF
TEST VERT.VAR. VSBY
TEMPERATURE TEST
F, IF
II
PRESENT WEATHER DETERMINATION
TEST FOR PRECIP
TEST PREVIOUS SHOWERS
NO WEATHER OCNL RW- INTMT R-
R-, RW
TEST DRIZZLE OR RAIN
TEST TEMPERATURE
TEST PRECIP. INTENSITY
TEST TEMPERATURE
R, R+ RW, RW+
L-, L, L+
S-, SW-
TEST FOR S, ZR, ZL
ZL-, ZL, ZL+
TEST FOR S, ZR
S, S+ SW, SW+
ZR-, ZRW-
ZR, ZR+ ZRW, ZRW+

Figure 2.12 Generalized flow diagram of present weather decision tree model

]

transmissometer and FSM respond similarly in drizzle (small drops) but depart significantly in rain (large drops) is used to separate rain (R) from drizzle (L) observations.

The model's algorithms produce minute-by-minute observations of weather. These in turn are being evaluated as part of an AFGL research study against the operational weather observations routinely made by FAA control tower personnel at Otis AFB. The control tower is located approximately one mile east of the Weather Test Facility. Figure 2.13 is an example of one hour's data considered by the decision tree, the present weather it deduced and the comparative human observations for the same period on 8 June 1978.

Column 1 denotes the time of observation to the nearest minute, Columns 2 through 6 are one-minute averages of extinction coefficient ($x\ 10^{-4}\ m^{-1}$) measured by the FSM at five levels of tower A (200 feet, 150 feet, 100, 50 feet and at ground level). Column 7 is extinction coefficient obtained from the transmissometer. Columns 8 through 17 show the one-minute averages of temperature (x10 degrees C) at a given level of tower A (200, 150, 100, 50 feet and ground level) followed by the temperature-dewpoint difference at the same height. Column 18 is a one-minute count of the number of tips made by the rain guage in response to precipitation. Each count represents .005 inches of precipitation. Thus the intensity is easily obtained. The next column, 19, shows the extinction coefficient obtained from the nephelometer. Column 20 displays the extinction coefficient observation of the backscatter meter. Column 21 shows the algorithm's determination of present weather and obstruction to vision. The last column shows the present weather observations taken by the FAA observer during this hour. The symbol T refers to a thunderstorm occurrence. Other symbols shown here denote rain (R), fog (F) and drizzle (L)

```
METRIC UNITS
HOUR BEGINNING:  8JN08/0900

     A200  A150  A100   A50     Y    MN      A200     A150     A100      A50       X     RAIN NEFH VIDE  WEATHER     FAA
      FSM   FSM   FSM   FSM   FSM   TRN     TMP DPS  TMP DPS  TMP DPS  TMP DPS  TMF DPS

 0    9.3  12.0  12.1  11.0   9.4     8     171  -6  175   6  169  -5  176   9  175   6   101   1   15           R,F

 1    7.3  10.1   9.3   8.9   9.6     7     172  -6  176   5  169  -5  177   9  176   5   102   1   13           R,F
 2   10.0  14.2  12.3  11.3  11.7     6     171  -6  175   6  169  -6  176   9  176   5   103   1   18           R,F
 3    9.4  14.9  12.0  11.5   9.6     7     172  -6  176   6  169  -6  176   9  176   4   104   1   13           R,F
 4    7.4  10.5   8.9   8.4   7.9     6     171  -7  175   6  169  -6  176   9  176   4   104   1   13           R,F
 5    7.1   9.7   8.3   7.6   8.0     6     171  -7  175   6  169  -6  176   9  176   1   105   1   13           R,F
 6    7.6   9.9   8.5   8.0   9.2     7     171  -7  175   6  169  -6  176   6  176   2   105   1   14           R,F
 7   10.1  14.4  11.0  10.3  11.5     6     171  -7  175   6  168  -6  176   9  176   2   106   1   16           R,F
 8   17.9  24.6  18.8  18.3  28.3    12     171  -7  175   5  168  -6  176   8  175   2   109   1   25          R+,F
 9   27.5  39.9  30.7  32.3  49.1    20     171  -7  175   6  168  -6  176   6  175   2   115   1   41          R+,F
10   42.7  61.1  43.1  46.6  76.3    28     171  -7  175   5  168  -6  175   6  176   3   118   1   45          R+,F
11   42.7  55.7  47.9  51.6  30.0    17     171  -7  175   6  168  -7  175   6  175   4   121   1   42          R+,F
12   30.3  47.1  33.8  38.5  47.0    17     172  -7  176   6  169  -6  177   9  176   4   127   1   37          R+,F
13   42.1  58.4  46.3  51.6  60.3    23     171  -7  175   5  168  -7  176   8  176   4   131   1   45          R+,F
14   52.1  66.2  61.9  64.6  67.6    31     171  -6  175   5  168  -7  176   6  176   4   135   1   53          R+,F
15   62.9  76.3  73.3  77.9  93.2    39     171  -7  175   5  168  -7  175   7  176   4   140   1   60          R+,F
16   73.4  90.2  90.3  96.2  99.3    47     171  -8  175   5  166  -8  175   7  176   4   145   1   72          R+,F
17   63.4  77.9  81.4  83.6  95.8    43     172  -7  176   5  168  -7  176   7  176   3   151   1   62          R+,F     RF
18   48.2  66.7  65.5  70.3  51.3    28     172  -7  176   5  168  -7  176   7  176   7   156   1   47          R+,F
19   45.6  67.3  59.7  63.6  67.1    34     172  -6  176   5  168  -6  176   7  176  10   159   1   50          R+,F
20   43.2  59.4  57.3  59.0  63.0    30     172  -6  176   5  168  -8  176   7  176   6   165   1   46          R+,F
21   64.6  82.8  80.8  81.4  93.1    44     171  -8  176   5  168  -8  176   7  176   7   169   1   67          R+,F
22   57.0  73.1  73.2  80.1  80.8    43     172  -8  176   5  168  -8  176   7  176   7   172   1   53          R+,F
23   45.2  65.7  66.5  65.8  60.0    37     173  -7  177   5  169  -6  176   7  177   6   175   1   51          R+,F     TRF
24   32.3  56.3  53.3  54.3  51.6    30     173  -7  177   5  170  -6  177   6  177   5   185   1   50          R+,F
25   15.9  27.6  24.9  27.1  14.5    11     174  -7  178   5  170  -7  179   9  178   5   187   1   16          R+,F
26    9.6  15.6  14.0  14.9  11.8     9     174  -6  178   5  171  -7  179   9  178   5   187   1   14           R,F
27    6.7  10.5   9.8  10.0   7.5     7     174  -7  178   5  171  -7  180   9  176   4   187   1   12           R,F
28    5.9   8.5   8.2   7.9   7.9     7     174  -7  178   5  171  -7  180   9  177   4   187   1   12        L-, F
29    6.5   9.6   9.3   9.0   9.4     8     175  -6  178   5  171  -7  179   9  178   3   188   1   12        R-, F
30    7.9  10.8  10.4  10.0  13.9     8     174  -7  178   5  170  -7  179   9  178   3   189   1   15        R-, F
31    9.6  14.4  13.2  12.7  12.9     9     174  -7  178   5  170  -7  179   6  178   2   189   1   15        R-, F
32    8.5  12.1  11.5  11.2  11.4     8     174  -7  177   5  170  -6  179   6  178   3   189   1   14        R-, F
33    9.1  13.0  12.1  11.7  12.3     9     174  -7  178   5  171  -7  179   6  178   2   190   1   13        R-, F
34    8.8  11.6  11.2  11.0   8.3     7     174  -7  178   5  170  -7  179   8  178   3   190   1   11        L-, F
35    8.3  10.8  10.7  10.4   8.1     7     174  -7  178   5  170  -7  179   6  178   2   190   1   12        L-, F
36    6.0   8.9   8.3   8.6   6.6     6     175  -7  178   5  171  -7  179   6  178   3   190   1    8        L-, F
37    5.9   7.6   7.5   7.2   7.6     6     175  -7  178   5  171  -7  180   9  178   3   190   1    9        R-, F
38    5.1   6.4   6.4   6.5   4.2     5     175  -7  178   5  171  -7  180   8  179   3   190   1    7        L-, F
39    5.6   6.8   6.7   6.5   7.3     6     174  -7  178   5  171  -7  180   9  178   2   190   1    9        L-, F
40    6.3   7.2   7.3   7.4   5.2     5     174  -7  178   5  171  -7  179   6  178   2   191   1    8        L-, F
41    6.2   7.5   7.1   7.0  10.2     7     175  -7  178   5  171  -7  179   8  178   2   191   1   11        R-, F     TR-F
42    7.0   9.2   9.9   9.2   9.4     7     175  -7  178   5  171  -7  180   8  178   1   191   1   10        R-, F
43    6.5   8.3   8.1   8.1   9.2     6     175  -7  178   5  171  -7  180   9  178   1   191   1   11        R-, F
44    8.8  10.3   9.7   9.5  12.9     8     174  -7  177   5  171  -7  179   6  178   2   191   1   13        R-, F
45   12.7  19.5  16.2  16.9  25.6    13     175  -7  178   5  171  -7  180   9  179   2   193   1   22          R+,F
46   13.0  16.3  16.5  17.7  22.1    11     175  -7  178   5  172  -7  180   9  179   2   194   1   10           R,F
47   13.3  19.1  16.8  17.3  23.1    11     176  -6  179   6  172  -7  180   9  179   2   195   1   18           R,F
48   13.1  18.1  16.2  16.9  13.4     9     176  -7  179   5  172  -7  181   9  179   2   196   1   15           R,F
49   12.5  15.8  15.2  15.2  14.6     9     176  -7  179   5  172  -7  180   6  179   1   197   1   17           R,F
50   12.2  14.9  14.7  14.9  13.9     9     175  -7  179   5  172  -7  180   6  180   2   197   1   15           R,F
51    8.9  10.7  10.7  10.7  10.8     7     175  -7  179   5  172  -7  180   8  180   3   198   1   10           R,F
52    7.8   9.9   9.7   9.6  10.6     7     175  -7  179   5  172  -7  181   9  180   1   198   1   11        R-, F
53    7.3   9.2   9.3   9.6   8.2     6     175  -7  178   5  172  -7  181   9  179   1   198   1    9        R-, F
54    7.9   9.5   9.3   9.0  11.9     8     174  -6  177   5  171  -7  180   6  178   1   198   1   13        R-, F
55    9.3  11.5  11.4  11.3  12.7     8     173  -8  176   5  170  -7  179   6  177  -1   199   1   13        R-, F
56    9.1  12.5  11.9  11.9  14.8     9     173  -8  176   5  170  -7  178   8  177  -1   199   1   13        R-, F
57   10.9  15.4  13.6  13.7  22.6    12     171  -9  174   4  166  -7  177   6  175  -2   200   1   16           R,F
58   11.4  17.5  14.9  15.7  13.6    10     171  -6  174   5  166  -6  176   6  174  -1   201   1   15           R,F
59    6.9  13.5  11.7  12.3  10.0     7     171  -6  174   5  165  -6  175   9  173  -1   202   1   11           R,F
```

Figure 2.13 An example of one hour of weather observations determined by the present weather algorithm

THIS PAGE IS BEST QUALITY PRACTICABL
FROM COPY FURNISHED TO DDC

with the intensity variations mentioned above.

Preliminary results of the comparisons between the present weather program and the FAA observations have been very encouraging. The technique has proved to be very responsive to rapidly changing weather events as illustrated by the variations of precipitation during this particular hour. Visibility variations are as quickly observed. The importance of quickly determining significant changes in weather for aviation needs cannot be overemphasized.

2.5 Remote Tower Slant Visual Range Studies

2.5.1 Background

As the operational minima for low visibility approaches and landings are reduced at certain airfields due to improved automated landing systems being installed, the requirements for accurate and timely measurements of airfield visibility are becoming more urgent. Currently, information supplied to the pilot consists of human observer estimates of prevailing visibility and instrumented measurements of runway visual range (RVR) at one or more locations adjacent to the runway. Although these observations supply essential information, experience has shown that the surface RVR measurements and general-area visibility observations are often not representative of the conditions encountered by the pilot as he proceeds along the glide path through the decision height (DH) to touchdown.

The development of an effective technique for the measurement of slant visual range (SVR) ahead of the aircraft along and below the glide slope path has been the primary objective of this research. Field experiments at the Otis Weather Test Facility (WTF) have been conducted using an instrumented tower approach. Summarizing, the study seeks to determine the accuracy with which SVR in a simulated approach zone could be specified at selected time intervals from time zero to plus ten (10) minutes using various combinations of forward scatter meter (FSM) measurements made at time zero at a tower 1500 ft offset from the simulated approach zone.

2.5.2 Initial data analysis

Five episodes of reduced visibility, totalling 9480 minutes, were selected to serve as a data base for this study. The March 1976 episode was used as a dependent set with the other four episodes comprising the independent set. Coastal advection fog occurred in the March 1976, May 1976 and July 1976 episodes. The August 1977 episode was a radiation fog episode.

The dependent data set was exhaustively examined in order to define the approach to be taken. A program SCATTER was developed to evaluate the linear relationships among those FSMs positioned at identical heights on towers A and Q above ground. The examination of the statistics from SCATTER revealed systematic errors among the FSMs, the result of a gradual accumulation of a residual film on the lens of the FSMs. Correction factors were calculated and applied to the dependent data set thereby minimizing this systematic error. A similar process was applied to the independent data set.

A tool which proved very helpful in editing and validating the basic data sets was the Interactive Graphics device available through the AFGL CDC 6600 system. The graphics software package, provides options to display and edit, on a CRT, user selected subsets of sensor measurements collected at WTF. The software can display up to 360 data points (typically 6 hr of data in our case) of one to four sensors at any one time. As simple instructions are displayed in the CRT, the user interacts with the CDC 6600 system using either a light pen or keyboard. A hard copy pen plot option is also available.

The data generated at the Otis WTF was frequently examined using the interactive graphics device. In particular, portions of the five data sets were edited and hard copies made through this device. An indepth description of the procedures which comprise the software package can be found in Appendix 2A.

As illustrated in Figure 2.0 (Section 2.2), the Otis WTF includes transmissometers mounted along a slant path of about 12 degrees from the horizontal between towers A and C. They were so positioned to provide SVR measurements appropriate to a 100 ft decision height. The initial formulation for these studies was to incorporate the slant transmissometer measurements into the predictand definition. Unfortunately, the slanted position of the transmissometers often resulted in extinction coefficient values which were non-representative of actual conditions during periods of precipitation. Liquid water on the detector surface and that which accumulated at the base of the detector hood undoubtedly contaminated the measurements. A program was written, called TRANSCOR, to evaluate the transmissometer data against the tower-mounted FSM output during selected episodes. An analysis of its output confirmed the bias towards high extinction coefficient values from the transmissometers.

2.5.3 Analysis technique formulation

An alternative, and equally valid, approach to defining the predictand for the study was then formulated. An unweighted average of the FSM measurements at tower A up to the 100 ft level was computed to represent the SVR in the simulated approach zone:

$$\bar{A} = (A_{100} + A_{50} + A_{10})/3$$

where subscripts 100, 50, and 10 refer to the height of the FSM in feet.

Specific combinations of Q_{100}, Q_{50}, Q_{10} and A_{10} were selected as predictors of $\bar{A}$. The series of predictors were chosen to investigate specification accuracy based on the number and spacing of the instruments as follows:

1) $\bar{A} = (Q_{100} + Q_{50} + Q_{10})/3. + \delta$

2) $\bar{A} = K_1 Q_{50} + K_2 A_{10} + \delta$

3) $\bar{A} = A_{10} + \delta$

Some simplifying assumptions were made to establish, in advance, the specification algorithms. Method (1) assumes horizontal homogeneity of fog density over the 1500 ft distance between towers A and Q. Method (2) is a prediction algorithm with estimates of coefficients K_1 and K_2 obtained through multiple linear regression techniques using the dependent data set. Method (3) is merely a representation of the current operational methodology which uses the runway visual range (RVR) to aid the pilot in his landing decision. For the purposes of this study, it represents a control technique against which the two offset tower methods (1 and 2) will be evaluated. Methods (1) through (3) provide deterministic solutions for SVR specification and short range prediction. Transformation to exceedance probability form was pursued through two approaches. The first model was defined as follows:

$$-p = \frac{SVR_T - SVR_\phi}{RMSE}$$

where p = equivalent normal variate

SVR_T = SVR threshold (daytime: ½ mile : $SVR_T = 46$)

SVR_ϕ = SVR at $t = \phi$

RMSE = Root Mean Square Error

RMSE was empirically determined to be a value of 20 in extinction coefficient units. The second model was defined as follows:

$$-p = \frac{f_t - Rf_o}{(1 - R^2)^{\frac{1}{2}}}$$

where p = equivalent normal variate

f_t = SVR_T equivalent normal variate

f_o = SVR_ϕ equivalent normal variate

R = hour-to-hour correlation coefficient of equivalent normal variates

Note that the denominator is the standard error of estimate (SE). A set of mutually exclusive and exhaustive equations, fined tuned for time of day and season, are used to relate SVR_T (extinction coefficient) to f_t (equivalent normal variate).

2.5.4 Results

The three specification/prediction methods were applied to each of the four independent data episodes on a minute-by-minute basis. Since fog density tends to be horizontally uniform over distances of several kilometers, comparisons of the specified SVR, by the two tower methods, with the observed SVR ($\bar{A}$) reveal nearly a one-to-one correspondence. Even though the time variations of SVR are significant over periods as short as several minutes, the offset tower estimates closely track the observed conditions 1500 ft away.

Method 2 which uses data from the 50 ft level of tower Q in combination with the RVR value (A_{10}) yields results equally as good as Method 1 which draws on data to the 100 ft level of tower Q. The information content in the layer, surface to 50 ft, sufficiently identifies the intensity of the vertical gradient of extinction coefficient such that the increment from 50 to 100 ft is superfluous. Meanwhile both methods improve upon the control forecast technique (Method 3) by a significant amount.

A convenient way to compare the deterministic solutions of the three methods is to evaluate their skill relative to preselected thresholds of extinction coefficient which have operational significance. The threshold used was 12 km^{-1} which corresponds to daytime visibilities of one-quarter mile and nighttime of one-half mile respectively. By summarizing the results into 2x2 contingency tables, for each threshold separately, one can compute the Probability of Detection (PoD) for each method and for each independent episode. Table 2.2 summarizes the PoD's for SVR specification (0 lag) and predictions ranging from 2 to 10 min. With the exception of the August 1977 radiation fog episode, the PoD exceeds 90% for both Method 1 and Method 2 for the 0 lag and 2 min prediction. The high temporal variability of extinction coefficient becomes clearly evident by 10 minutes after observation time. By contrast, however, the control forecast technique (Method 3) has considerably less skill in the advection episodes. Since it relies exclusively on the surface RVR, it consistently overestimates SVR in radiation fog episodes which explains its high PoD.

Comparison of the two methods of transforming the deterministic solutions to exceedance probabilities was achieved through the use of the p-score statistic which calculates the mean-squared-probability error. It has the characteristic that a value of zero relates to perfect estimation and a value of 1 to totally imperfect estimation. Based on the independent episodes summarized in Table 2.3, the second method, which considers the equivalent normal variates of SVR, generally resulted in lower (i.e., better) p-scores, especially for prediction times of 15 minutes or greater.

TABLE 2.2

THRESHOLD = 12 km^{-1}

		PROBABILITY OF DETECTION (%)			
		LAG (MINUTES)			
METHOD	EPISODE	0	2	5	10
1	1 APR 76 AD FOG	94	90	83	71
	JULY 76 RAIN/AD Fog	97	96	91	83
	MAY 76 AD FOG	97	97	97	94
	AUG 77 RAD FOG	80	80	80	79
2	1 APR 76 AD FOG	91	88	80	69
	JULY 76 RAIN/AD Fog	91	90	86	79
	MAY 76 AD FOG	97	96	96	94
	AUG 77 RAD FOG	78	78	78	78
3	1 APR 76 AD FOG	13	13	13	12
	JULY 76 RAIN/AD Fog	56	56	56	54
	MAY 76 AD FOG	87	87	87	87
	AUG 77 RAD FOG	100	100	100	98

TABLE 2.3

THRESHOLD: 5 km^{-1} (day) P SCORE

12 km^{-1} (night) LAG (MINUTES)

METHOD	EPISODE	2	5	15	30	60
1	APRIL 76	.065	.105	.211	.259	.439
	MAY 76	.006	.010	.031	.058	.111
	JULY 76	.014	.024	.052	.071	.115
	AUGUST 77	.049	.053	.071	.106	.187
2	APRIL 76	.066	.108	.175	.225	.315
	MAY 76	.007	.010	.031	.056	.108
	JULY 76	.013	.023	.048	.063	.091
	AUGUST 77	.049	.053	.068	.095	.150

2A APPENDIX: Interactive Graphics Program Description

2A-1 Introduction

Graphics is an interactive capability available at Terminal #2 (Bldg 1105B, Room 156) of the AFGL CDC 6600 System. Section 17 of the AFGL User's Guide (revised Jun 1977) provides detailed description of program setup, terminology and internal display control routine description.

The graphics system is used for LYU purposes to display a maximum of 360 points - six hours of data - of one to four sensors. This system is primarily used to edit the data collected at Otis Weather Test Facility according to the user's specification. The operator can change many of the values of the variables in the program. The user can do this either by punching data in on the available typewriter, or activating a series of instructions by means of the light pen - a pen placed to the right of the console.

2A-1.1 There are four program decks that are used in conjunction with graphics - Files, Ready, Two Graphics decks. All of the data for the Otis Project is either stored on an archived tape or processed directly off a Cap Tape. In either case, each record contains a one minute average of a maximum of 150 weather parameters (Exco, Speed, Temp, Neph, etc.) and the time. Files is a program that converts the data you wish to edit into six hour blocks of one sensor to be input to graphics. Three permanent files are created in this program - two random - mass storage files arranged in six-hour blocks (edited and unedited) and a file with the start date of the data, start date of the first block and the number of blocks.

2A-1.2 Ready is a program that converts the six hour block data of one sensor into one minute averages of one hundred fifty sensors with time. This new edited file can now be used as input to any statistical analysis program.

2A-1.3 The two graphics programs are used to put the graphics overlays into the system. The first program created a permanent file with any changes the user might want to add to the program. Sometimes labels might be changed or default values may be altered. This is done by the delete and insert statements. The second program attaches all four files necessary for running graphics. These are the edited and unedited files of data, the ident file containing time and number of blocs, and the graphics file containing the user changes and the original graphics overlays.

2A-2 Overlay (0,0)

The graphics program operates on a system of overlays. Each overlay deals with a specific area of the program. There are 10 overlays labelled from 0 to 9. The Overlay (0,0) contains all the logical, common, dimension and subroutines that open, read, write, and close mass storage, set the origin for the screen, and set the labelling for the hard copy. This overlay immediately goes into the next overlay without the help of a light button. A light button is an instruction on the screen that can be activated by the light pen.

2A-3 Overlay (1,0)

Overlay (1,0) is only used at the beginning of the graphics program. In this overlay, the start of the data, the first block time, and the number of blocks for a specific case are read into the program from a card. The beginning of the data is put up on the screen. A cross always appears on the screen where the origin is set. The origins (x, y values) of the four possible graphs are placed in two arrays. The screen is approximately

17" x 17" using the lower left hand corner as the origin. Four graphs must be fitted into this frame of reference.

In the block data statements, max and min (default values) are given for temp, direction, speed and exco. At this point in the program, they can be altered. Several statements will flash on the screen. The instructions are self-evident. Type XXX.XXX. This tells you to type in two numbers with a maximum of three whole numbers before the decimal point. This is the instruction for the temp, direction and the exco values. The instruction for speed is XX.XX. - 2 numbers for the max and min values of 2 whole numbers before the decimal point.

There is only one safeguard in typing in instructions. If wrong numbers are punched in the correct format, the program accepts the incorrect data. However, if either more or less than the correct number of characters are punched in, the program will reject it and you will be allowed to type in again. This overlay also specifies whether you wish to plot the Exco values on a log or linear scale. This is actually semi-log because the X-axis is always linear (time every minute up to six hours).

2A-4 Overlay (2,0)

Overlay (1,0) immediately goes to the third Overlay (2,0), DATN (DATA). This overlay sets up the data used for the first block and all subsequent blocks. There are four possible options. These options are activated by placing the light pen on the instruction at the bottom of the screen that says one, two, three or four.

In Option One, you type in 8 digits to specify 4 sensors you wish to work with. In the program, the numerical values are translated into sensor names. The data for 6 hours of each of four sensors specified is read off of a random access file that was created before the program was executed. The index of the file must be computed in the program by the block number. If the index is missing, the data are filled with missing data 9999. The labels of increments for plotting are computed by subtracting the minimum value from the maximum value and dividing by seventeen. The time window for the current time is put on the screen. The time array is computed with a time associated with every 360 minutes.

The random access file is arranged in the following manner. Each record contains 360 minutes of data of one sensor. There is an overlap of 60 minutes on each record. The first hour of one record and the last hour of the previous record are the same. Therefore you really only get five new hours of the data on the screen.

In subsequent uses, any of the four options can be used depending on the user's needs. Option One can be activated if the user wants to advance a six hour period with the same four sensors. The time array is advanced 5 hours because one hour is overlapped from previous frame. The new data are read from the random access file first updating the block by one.

2A-4.1 Option Two can be activated if the user wants to look at four different sensors at the same time as was used previously. The number of sensors are typed in. There is added instruction of U or E. The program is given two identical random mass storage files created to be input to graphics. One of these files U remains untouched through graphics. The other file E can be edited, in the course of using graphics, according to the user's specifications. In this option the scale for plotting can be changed from linear to logarithmic or vice versa.

2A-4.2 Option Three is activated if, at any time, the user wants to reset the time frame to any block of data in the random access file. If the time that is typed in is not the beginning of a block, the program cycles to the nearest block. The user types in the 8 digits, e.g., 02034147 (2 for each sensor), he wishes to look at. Then he types in 10 digits to specify the start time he is interested in, 2 each for month, day, year, hour, and minute, (e.g., 1027770830). The program computes the nearest block index and reads the appropriate data. Then it sets the correct time array based on the current time.

2A-4.3 Option Four is activated if the user wants to display data (maximum six hours) within two blocks. The user again specifies the four sensors (8 digits) he wishes to use. He types in whether he wishes to use the unedited or edited file. He then types in the initial time (10 characters) and the final time (10 characters). The maximum span of time from initial to final time is six hours. Any time span less than this would be acceptable. The data and time arrays are appropriately set. When this overlay is completed, the program goes immediately into the Eras Overlay described below. Two light buttons are set in the Datn Overlay - (1) Eras, (2) End. Since the Datn Overlay goes immediately to the Eras Overlay, these light buttons are superfluous.

2A-5 Overlay (3,0)

The Eras Overlay erases the screen. The program puts up several light buttons. A light button activates an overlay. You can activate a light button by means of the light pen. Hitting one of the names of the overlays on the side of the screen puts the operator into that overlay. The light buttons for the Eras Overlay are Quad, Datn, Zoom, End, and Draw. Eras also puts up the time for the beginning of the data and either the current time or initial and final time.

2A-6 Overlay (4,0)

Quad is an overlay that sets up the sensors to be plotted. There are four light buttons displayed on the right hand side of the screen - Draw, End, Zoom, and Delt. On the left hand side of the screen is a message - "Which Quadrant". Underneath, there are two columns, the left hand column has four rows, each row containing the name of one of the four sensors. The right hand column contains the same four rows with a + beside each name. The fifth row on this side contains the word "GO". Each of these words in both columns is activated by a light pen. There is a distinct difference between the two columns. When the message, "Pick Quad", is flashed at the bottom of the screen, the user must make a decision as to which column to activate. If he only wants to plot the six-hour block of one, two, three, or four sensors he has picked in data, he may pick the sensors from the right hand column and then hit go. This will immediately erase the screen and plot the sensor (s) the user has selected (go to Draw Overlay).

However, if he wants to do something else, he uses the left hand column. He activates the sensors he wishes to use. Then he uses the light pen to activate the overlay on the right hand side of the screen. He has three real choices. He may activate Zoom which will blow up vertically and horizontally a small scale of time. He may activate Delt which will allow the user to edit the data he is plotting. His third choice is Draw which just plots the sensor he picks. He can also end the program at this point with the End Overlay.

2A-7 Overlay (5,0)

Draw is the overlay that plots the six hour block (360 points) of from one to four sensors, log or linearly. Several light buttons are put up on the right hand side of the screen. They are Quad, Datn, Zoom, Delt, Stor, Hard, Eras, and End. He may decide to go to any of these overlays from Draw. Draw puts on the screen whatever is in the data array.

2A-8 Overlay (6,0)

Zoom is the overlay that sets up the sensor that is specified for a zooming routine. The y - axis - in units of the sensor is expanded to fill the entire screen. The x - axis - time scale - is typed in during the execution of the Zoom Overlay. The instructions are shown at the bottom of the screen. Type in XX.XX (format) to specify hour to zoom (beginning of hour to zoom). Type in XX.XX (end hour). There is a line to type in beginning and ending hours. The time array and data array will be set up for plotting in the zooming array. After all the instructions have been satisfied, this overlay will go immediately to the Draw Overlay. From here the user can go to the editing overlay (Delt). Many times it is easier to edit a sensor in the Zoom Overlay because it is blown up in such a way that the bad data are easily seen and accurately deleted.

2A-9 Overlay (7,0)

Delt is the overlay which edits the data. Seven light buttons are put up on the right hand side of the screen. From this overlay, the user can go to

AD-A067 937 REGIS COLL WESTON MASS F/G 4/2
METEOROLOGICAL STUDIES--ATMOSPHERIC ANALYSIS, AUTOMATED WEATHER--ETC(U)
FEB 79 S L BURKE F19628-77-C-0010
UNCLASSIFIED AFGL-TR-79-0047 NL

2 OF 2
AD
A067937

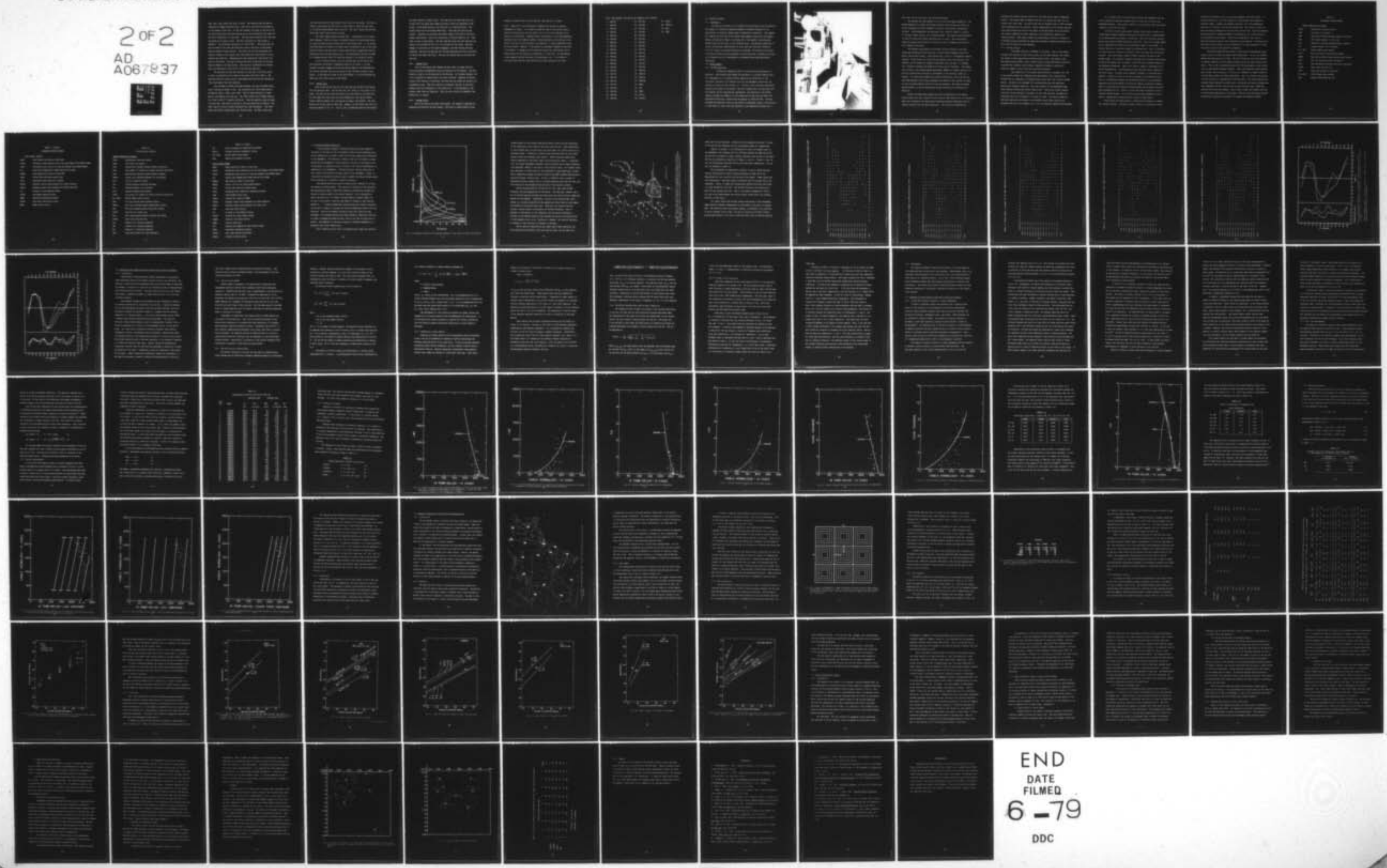

END
DATE
FILMED
6-79
DDC

Datn, Stor, Delt, Hard, End, Draw, or Eras. The overlays Quad and Draw or Zoom-Draw is always activated first. From one to four plots are already up on the screen at this time. In the Delt Overlay, the names of the sensors on the side of the plots are light buttons and can be activated by the light pen. The first instruction is "Pick Quad". The user must activate by the light pen the sensor he is going to edit. The next instruction is "Move Cross in Quadrant". The following instruction is "First Point". This means that the user by means of the light pen moves the cross to the point on the screen where he wishes to begin editing. This point will not be transferred into internal storage in the program until the instruction "First Point" is activated by the light pen. Immediately the next instruction "Last Point" will flash on the screen. The user now moves the cross to the point in the data where he wishes to end his editing. This point is transferred into storage after the instruction "Last Point" is hit with the light pen.

The user may not move the last point to the left of the first point. If done, an instruction will flash on the screen "Pick Point Again". The user must move the cross to pick a good second point and hit the instruction "Pick Point Again" with the light pen.

Once the span of editing has been selected, the user can decide which type of editing he wishes to use. The instruction will read "Which Option" followed by "Delt", "Subs", and "Intp". Each of these options is a light button, activated by the light pen. The "Subs" option has a further instruction "Type in XXX.X" To Specify Sub Value". When the specific value is typed in by the user, that value is plotted in the span specified for editing. The "Delt" option is used to delete erroneous data (bad instrument). The "Delt" option puts 9999 or missing data into the edit span. The 9999. value goes into the data array but some default value is put on the screen. The flag is either a value above the high value for the sensor or below the low value. It is easily distinguishable from true data. The "Delt" option must be used before the "Intp" option can be utilized.

The "Intp" option works on missing data. Interpolation is a routine which develops a "best fit curve" to estimate values for missing data points by using good data points on either side of the missing data. If not enough good data points (at least 10 on either side) are present to use in the interpolation routine, the user will be given instructions to expand the range by picking his first and last points again. The interpolation routine is based on a systems routine "SPLN FIT" which was adapted to our graphics routine.

In all of these options, after our editing span and our option has been selected, the screen is completely erased of all plots. In a few seconds, the plots reappear with the corrections added to our selected plot. Delt can be activated over and over again to edit the data as much as necessary. If the editing is done in the Zoom Overlay, it will be retained and shown when four plots are put on the screen.

2A-10 Overlay (8,0)

Hard is the overlay that puts the data that are plotted on the screen into the plotting queue. You can have one, two, three, or four plots on one graph. The user can put three exco plots up on the screen at the same time. All the graphs will have their own scale depending on the type of sensor. Clearly labelled symbols will distinguish one sensor from another. The time series will be real time for hard copy. However, on the screen, the user will see hours beyond 24 (26, 27). This is just a convenience used for the program and they indicate a change of day. The time scale for hard copy will only be the first five hours even though six hours of data are presented on the screen. As we stated earlier, the sixth hour is a duplicated hour. The Overlay Draw must be activated before Hard. (Draw puts the plots on the screen). Once Hard is activated, the sensor names on the side of the plots become light buttons. The first instruction is "Select Labels or Go". This label is also a light button. The user then must pick with the light pen the sensors to be plotted and hit "Go" on the bottom of the screen. When the message at the bottom of the screen disappears, the Hard Overlay has been completed. The plot has been put into the plotting queue and will be plotted at Central Site some time later. The user can usually pick up his plots the next day.

2A-11 Overlay (9,0)

Stor is the overlay that changes the data array to comply with the editing procedure accomplished during the execution of the program. Two data arrays are read in at the beginning of the program. For storing purposes, one file is labelled as unedited data; the other as edited. Whenever an editing routine (Delt Overlay) is activated, the data that are edited are stored in an intermediate array. When Stor Overlay is activated, the data in the intermediate array are transferred to the edited file. In the beginning of the program, both files are identical. After the Stor routine is completed, the edited file is altered.

2A-12 Overlay (10,0)

End is an overlay that exits the program. All graphic's jobs must be completed by activating the End overlay. This gives a normal ending to your program and assures that all your editing, hard copy etc. is saved.

2A-13 There are a few limitations to graphics and the user can easily compensate for these. It is better to keep the time on the initial control card set relatively low (25 sec) than to try to do all your editing in one exercise of the program. Graphics takes a large amount of core and supersedes anything else on the computer system. Since graphics has top priority in the system, once you put your program in the computer, it almost immediately comes up on the screen. However, if the system is overloaded, graphics is the first to be dumped. If graphics is not exited the normal way (End Overlay) but is either pulled off the system by an operator or a "com lost", all the editing or hard copying the user has done is irretrievably lost. It is better to load the program several times and do fairly small sections at one time.

2A-14 The original list set up for graphics is as follows:

1. FSM A15
2. FSM A10
3. FSM A05
4. FSM A01
5. FSM B10
6. FSM B05
7. FSM B01
8. FSM C01
9. FSM P10
10. FSM P05
11. FSM P01
12. FSM Q10
13. FSM Q05
14. FSM Q01
15. FSM X01
16. FSM Y01
17. FSM Z01
18. SPD P10
19. DIR P10
20. SPD P05
21. DIR P05
22. SPD A15
23. DIR A15
24. SPD A10
25. DIR A10
26. SPD A05
27. DIR A05
28. SPD X01
29. DIR X01
30. TMP A15
31. DPT A15
32. TMP A10
33. DPT A15
34. TMP A05
35. DPT A05
36. TMP X01
37. DPT X01
38. TRAN AB
39. TRAN BC
40. TRAN KL
41. TRAN MN
42. NEPH
43. VID
44. PYRG
45. PYR AI
46. PYR AII
47. PYRH I
48. PYRH II
49. BKG
50. RAIN

3.0 SATELLITE STUDIES

3.1 Introduction

The satellite program is a far ranging one that extends from the operation and support of interactive computer hardware to advanced concepts for the applications of satellite imagery data in operational forecasting. This chapter will address the work done on the McIDAS (Man-computer Interactive Data Access System) and the use to which it is being put in the research investigations. Research work has been done in the following areas: the physical properties of clouds; the objective specification of cloud type from very high resolution satellite imagery by advanced statistical techniques; the objective extraction of satellite sensed vertical soundings; and the collection, processing and analysis of imagery data for investigation of automated short-range forecasting techniques.

3.2 McIDAS Support

3.2.1 McIDAS operations

McIDAS was installed at AFGL in June 1974 by the University of Wisconsin. This system, which blends the precision of a digital computer with the convenience of a TV display and the ingenuity and imagination of the researcher, provides a very powerful tool for the management, processing and analysis of satellite data (Figure 3.1). In 1975, a real time data acquisition capability was added to the system. The 24-ft antenna with its associated 1687 mhz receiver and bit synchronizer, demodulator, and interface to the McIDAS computer allowed the reception of the visible and IR data from two GOES earth synchronous satellites, located over the equator at 135°E and 75°W. Coverage extended from Kwajalein Island in the Pacific to Ascension Island in the Atlantic. A 12-db signal to noise ratio was achieved in this acquisition system with a

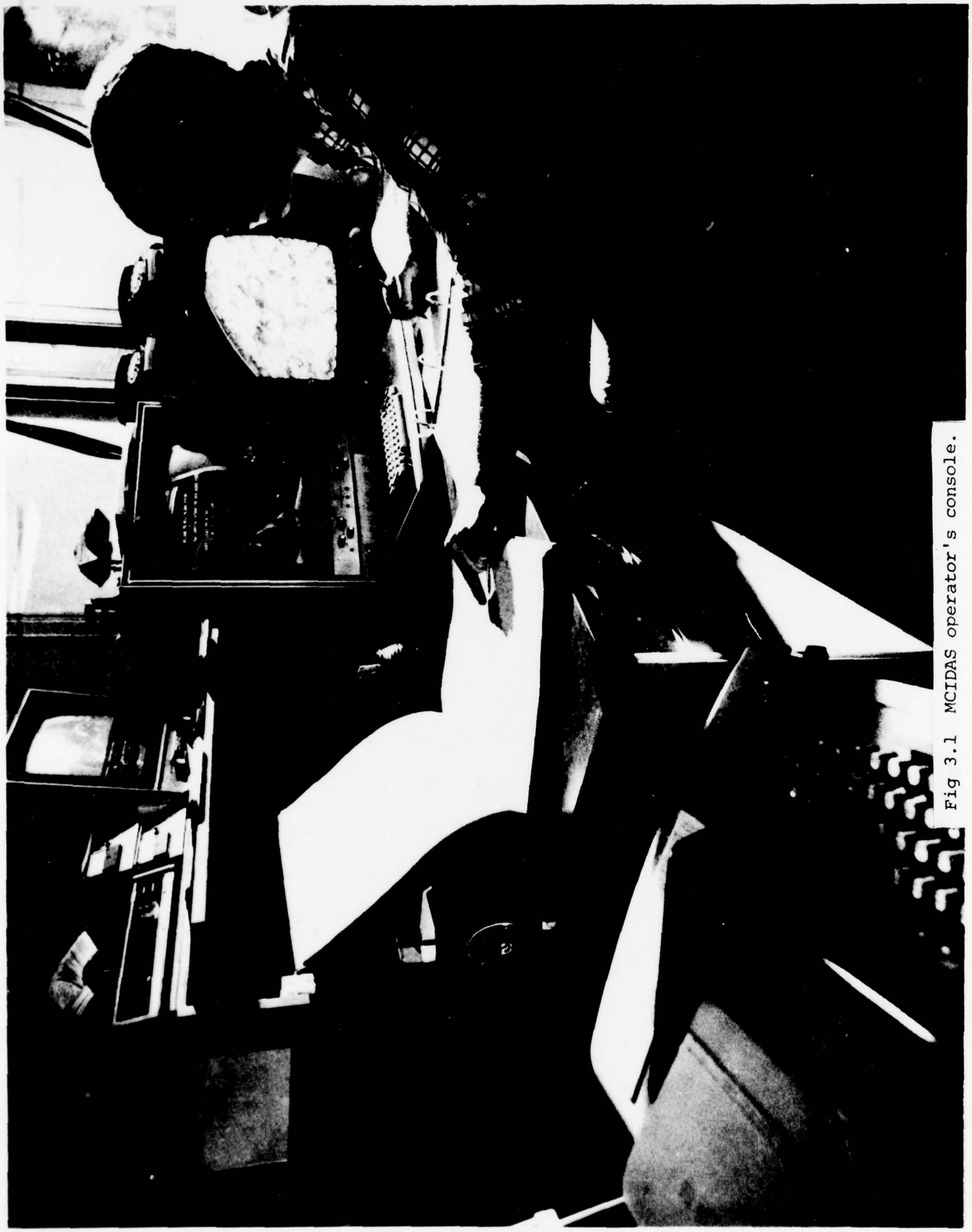

Fig 3.1 MCIDAS operator's console.

mean error rate of less than 1 per 100,000 characters.

The software was then updated to give a real-time system capability. The McIDAS capability to ingest and process satellite data includes the fitting of orbital parameters by known landmarks to achieve a high degree of positional accuracy. Tests showed that the positional error could be reduced to close to ± 1 picture element (pixel) in the acquired image. The average error measured on 235 sets of pixels with 4-mile resolution was 4.7 miles. This navigational capability permits the location of the data in areas of complete cloud cover or over landmark free oceans.

The hardware which makes up the McIDAS facility consists of the data acquisition system previously mentioned, a Harris 6024/5 computer with 65K of memory (24-bit word length), 5 disk drives with a total of 130 megabytes storage capacity, 2 tape drives for 9-track 800 bpi magnetic tape, line printer, card recorder, and TV console for operator interaction with the data. In December 1977 a second TV terminal was added by the University of Wisconsin. This update also provided a Write-Random Raster-Read Memory (WRRRM) to generate graphics and plotting presentations overlayed or independent of the satellite images, as desired. Following this hardware and software modification, data from the FAA high speed weather circuit were programmed into McIDAS so that surface and upper air data for North America could be stored and analyzed. The operating system used by McIDAS is a Harris Disk Monitor System modified by the University of Wisconsin.

During the period when support was given to operations in the western Pacific Ocean, data were required from the Pacific GOES satellite for the Kwajalein area, and in addition, the short-range forecasting program needed data from the Atlantic satellite for the New England area. This could be accomplished by switching the antenna from one satellite to the other during their transmission periods. The eastern GOES-2 transmits from 00 to 18 minutes and from 30 to 48 minutes after every hour. As long as data are not required south of 40°S latitude, both transmissions can be received. Manual repositioning of the antenna requires about three minutes and curtails the extent of the data which can be collected. Dual antenna command units were installed to give push-button selection of antenna position. This change reduced the repositioning time from 3 minutes to 40 seconds and has eliminated the operational problem of supporting missions with data from two satellites simultaneously.

3.2.2 McIDAS software

The McIDAS software is composed of two parts. First is the system software that consists of data files, control of the video display, data ingest and control of data applications software program files. The second is the data applications software, which includes cloud altitude algorithms, winds from cloud motions, pressure field displays, temperature displays, gridding of satellite imagery, curve-fitting and statistical analysis.

Upon completion of the system reconfiguration in December 1977, 99% of the system software was compatible but approximately 30% of applications software was not compatible or possessed logic faults when used in AFGL's McIDAS system. Included in the December 1977 reconfiguration were two additional applications software categories. The first category is the NOWCASTING group which displays conventional weather observations. Both hourly surface reports (100 hours of more storage is available for over 1100 stations) and upper-air radiosonde data can be analyzed in a variety of forms. The second category of additional applications software is the GRAPHICS group, which controls and processes data for a plot display file or for the electronic WRRM plotter/analyser.

As of October 1978, all applications software was compatible with the current system configuration although there are some logic faults in the NOWCASTING software. These faults, however, do not severely limit the display capability of the FAA line data.

In order to correct applications software logic faults, as well as to trouble-shoot hardware problems effectively and efficiently, an understanding of the McIDAS operating software is essential. There are two major software modules that control McIDAS' interactive capability. The first is named REMCOM and is responsible for handling all asynchronous inputs to the system. It handles ingestion of satellite imagery and teletype data. Also, it processes all inputs from the interactive terminals as well as inputs from the Acronym terminal. The second module, known as TVCTRL, controls the entire video display system. It recognizes requests from application software and proceeds to effect the display that is desired. These two major software modules are now completely documented. There still remain a number of sub-modules that require documentation. The documentation has taken the form of comments in the source input. Virtually every assembler statement is associated with a comment to explain its role in the entire ensemble of the software module. Thus, if an individual examines the documented modules, he can understand completely the software module's function by reading the detailed comments. Table 3.1 lists the major operating system modules and sub-modules that have been documented thus far. Table 3.2 lists most modules required to have a functional McIDAS system. It is easily seen that much documentation work remains. Applications software were not listed in these tables.

Efforts have also been devoted to developing new software to support the research programs. A McIDAS prototype version of a cloud-motion vector algorithm for eventual use on a large scale computer has been written. It provides printout of real-time analysis of cloud motions from consecutive satellite images. Another new software algorithm will yield probability estimates of visibility from current observations. The initial version computes visibility probabilities for Otis AFB and Scott AFB. Plans are presently being formulated to compute probability estimates for all military bases in the continental United States. They will be displayed in real time on a Mercator projection map for user interpretation and analysis. Provisions have been made in this software to allow manipulation of input parameters to study the effects on the final probability estimates.

Other McIDAS applications software, which has been designed and implemented, relate to collecting imagery and teletype data. In all, two software modules have been written for them. The first allows the main frame computer to schedule ingestion of GOES imagery through the Off-line Data Ingest System (ODIS). This module is necessary because the ODIS microcomputer cannot recognize any time beyond Greenwich midnight. Since the McIDAS main frame computer does not have this difficulty, it can set up a schedule for imagery ingestion into the ODIS, without any human intervention. This is a benefit particularly if data collection is required during off-duty hours. The second applications software module designed to collect data is concerned with hourly teletype data. Until September 1978 this was all done by hand from hard copy. McIDAS now performs this chore upon command. Future plans include the automatic editing of conventional observations in real-time. This will make the latest accurate observations continuously available for analysis and display by McIDAS.

TABLE 3.1

DOCUMENTED SYSTEM SOFTWARE

REMOTE COMMUNICATION CONTROL

ASYNC	Asyncronous interrupt handler
CALLC	FAA ingest file manager
COMM	Application software message handler (receiving)
CRBH	Card reader handler for RJE to UW
CQUE	Application software message handler (sending)
KBC	Keyboard handler (all terminals)
ND & NDAT	McIDAS common output handler
NUMC	FAA line current record address handler
REMPSA	Main loop of McIDAS remote communication control
RTAC	FAA line ingestion system initializer
SYSQ	Main applications software initiator loop module
SVCART	Input byte from FAA line
TTOH	Input byte handler for terminals
WD & WDAT	McIDAS common input handler
XMIT	Special COMM handler for KBC

TABLE 3.1 (CONT'D)

DOCUMENTED SYSTEM SOFTWARE

VIDEO DISPLAY CONTROL

AHEAD	Step forward one frame on video disk
CURJOY	Determines cursor position as TV line and element from McIDAS common
CURSIZ	Determines cursor size as TV line and element from McIDAS common
FIX	Build video command half words from two full words
FRMBAK	Step backward one frame on video disk
IADCW	Builds video disk main control word
IVSYS	Determines video system for terminal
KURPOS	Hardware control word processor for cursor position
KURSIZ	Hardware control bits processor for cursor size word
LTV	TV space to time mapping routine
SCHECK	Auto-sweep checking routine
TRMNL	Determines requesting terminal
TVCPSA	Main Video controlling routine
WRMIO	WRRRM output routine

TABLE 3.2

McIDAS System Software

REMOTE COMMUNICATION CONTROL	
ASYNC	Asynchronous interrupt handler
CALLC	FAA ingest file manager
COMM	Applications software message handler (receiving)
CRBH	Card reader "B" handler for remote job entry to/from UW
CQUE	Applications software message handler (sending)
DEBLAN	Output line righthand deblanker for CRT display
EXIR	Fax data ingestion handler
IR23	Arconym terminal interrupt subsystem
KBC	Keyboard handler (all terminals)
LOGH	Operator Communication handler
LPOBE	Line prints "E" handler for remote job entry to/from UW
ND & NDAT	McIDAS common output routine
NUMC	FAA line current record address routine
REMPSA	Main loop of McIDAS remote communication control
RTAC	FAA line ingestion system initializer routine
RTSVCC	Main FAA line ingest loop
SYSQ	Main applications software initiater loop module
SVCART	Input byte from FAA line
TAH	Terminal "A" interrupt subsystem
TBH	Terminal "B" interrupt subsystem
TCH	Terminal "C" interrupt subsystem
TTOH	Input byte handler for video terminals

TABLE 3.2 (CONT'D)

TTY	Key-in processor for applications software
TWAITS	Software execution suspension routine
WD & WDAT	McIDAS common input handler
XMIT	Application software initiator
VIDEO DISPLAY SYSTEM	
AHEAD	Steps forward one frame on video disk
CURJOY	Determines cursor position as TV line and element from McIDAS common
CURSIZ	Determines cursor size as TV line and element from McIDAS common
FIX	Builds video command half words from two full words
FRMBAK	Step back one frame on video disk
FRMSYN	Delays 1/30 sec for frame synchronization
IADCW	Builds video disk main control word
IVSYS	Determines video system for requesting terminal
IWRM	Builds WRRRM control word
IWRMIO	Controls all output to WRRRM
KURPOS	Hardware control word processor for cursor position
KURSIZ	Hardware control word processor for cursor size
LOOP	Auto-loop frame routine
LTV	TV space to time mapping routine
OVRLAY	Overlays two video output signals
SCHECK	Check for auto-loop time-out
SWEEP	Controls auto-loop
TCT	Obtains and prepares all video control words
TRMNL	Determines requesting terminal
TVCPSA	Main video controlling routine
VELCUR	Controls velocity cursor

3.3 Vertical Sounding Evaluation

Infrared sensors capable of detecting energy over small spectral intervals in the wings of the 15-micrometer carbon dioxide absorption band, can be combined into a system to sense the vertical temperature distribution in the atmosphere. The principle is based on the fact the amount of energy emitted by the atmosphere in narrow spectral intervals on the wings of the 15-micrometer CO_2 absorption band is related to the vertical distribution of temperature in the atmosphere. Different spectral intervals emit most of their energy from different altitude layers of the atmosphere. Figure 3.2 illustrates the weighting functions used to compute the energy reaching space from a selected set of spectral intervals (channels).

The problem facing the satellite meteorologist, however, is not how much energy is reaching space. That quantity is measured at the satellite. The meteorologist needs to know what temperature distribution created the amounts of energy sensed by the various channels. This is analogous to asking that given $2.37 in change, how many pennies, nickels, dimes, etc. are there in my pocket? There are any number of answers to the radiation problem also. A complex mathematical method called the inversion technique can be used, in theory, to recover the vertical temperature profile from the radiances. Statistical methods, building on past data, have also been developed. All proposed solutions for this problem of temperature retrieval are based on assumptions which are more valid at one time or place than at another. The selection of the best technique is therefore dependent on a comparison with direct observations.

Such a comparison would seem to be comparatively simple and straight-

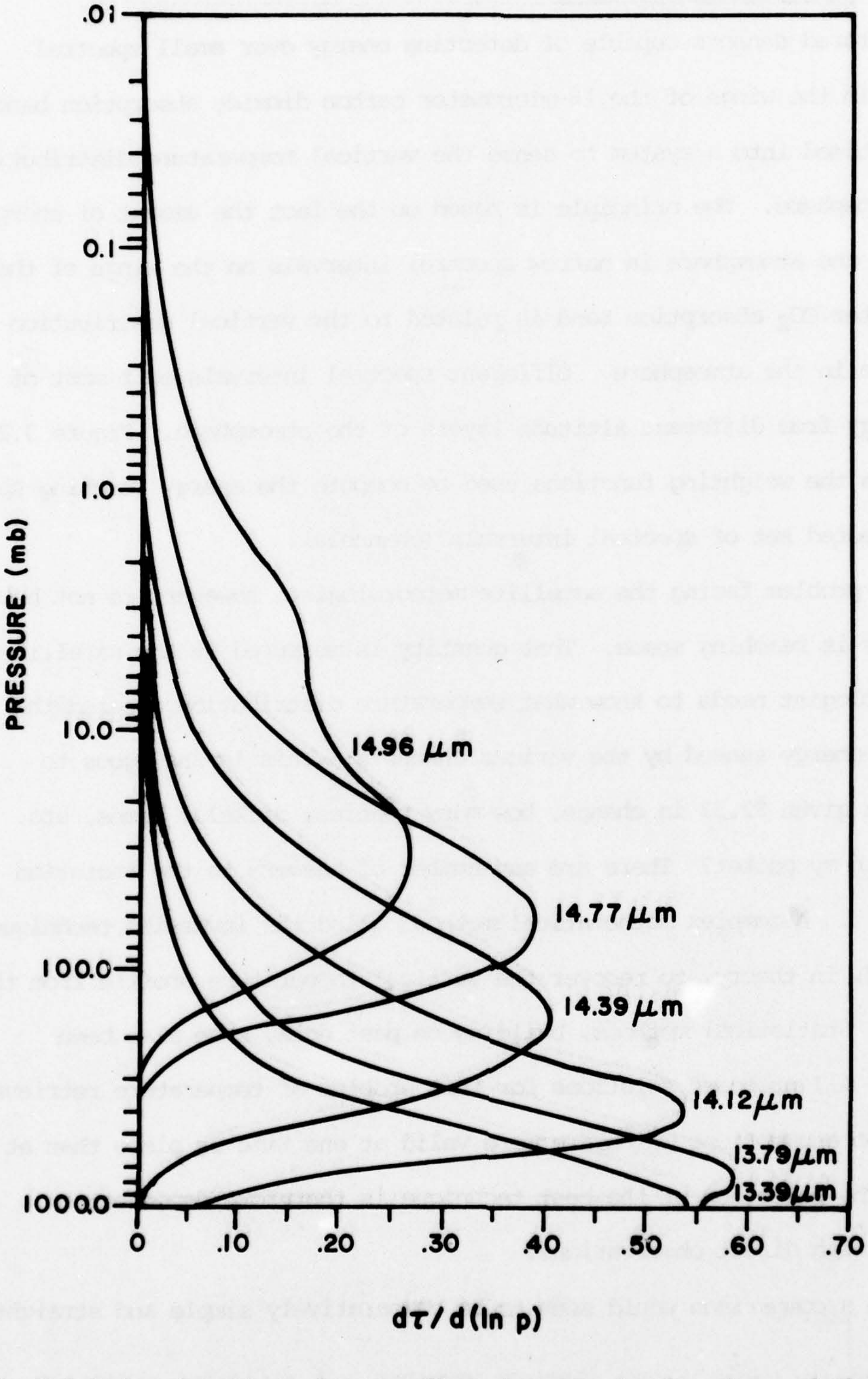

Fig 3.2 Weighting functions for sounding channels in the wings of the 15 um CO_2 band

forward except for one further complication which arises from the uncertainty of the emissivity of the ground at any given time or place. That complication is that sounding data are valid only over water where the surface emissivity is accurately known. Evaluation of sounding data have been made over the oceans against island and occasional ship reports. These occasional reports were usually separated in time and/or space from the satellite report. In February 1975, the Global Atmospheric Research Program conducted the Air Mass Transformation Experiment (AMTEX) in the Pacific Ocean south of Japan. Five weather ships were stationed in a small area and this presented a unique opportunity to make direct comparisons between radiosonde soundings and DMSP (Defense Meteorological Satellite Program) satellite data. Figure 3.3 shows the area, location of radiosonde stations, ground track of a typical satellite pass over the area, and the locations of the soundings along one scan of the satellite system.

During the period Feb 14 through Feb 28, 1975, there were 50 DMSP soundings that were appropriate for evaluation. The ship data, however, were not of the best quality and there was doubt about the value of direct comparison between the two systems. Accordingly, in place of the discrete ship radiosondes, temperatures extracted for the appropriate levels from U.S. Navy upper-air analyses of the Pacific were used. These data are called TT PAK and contain a certain amount of horizontal and vertical smoothing. This is probably not detrimental to the comparison since horizontal smoothing is inherent in the observed satellite data because the energy is integrated over a 33-km diameter circle at the satellite's subpoint and vertical smoothing is inherent in the conversion of radiance to sounding.

The 50 satellite observations were taken from 2 DMSP satellites, one with ascending and descending nodes near dawn and dusk, and the other with

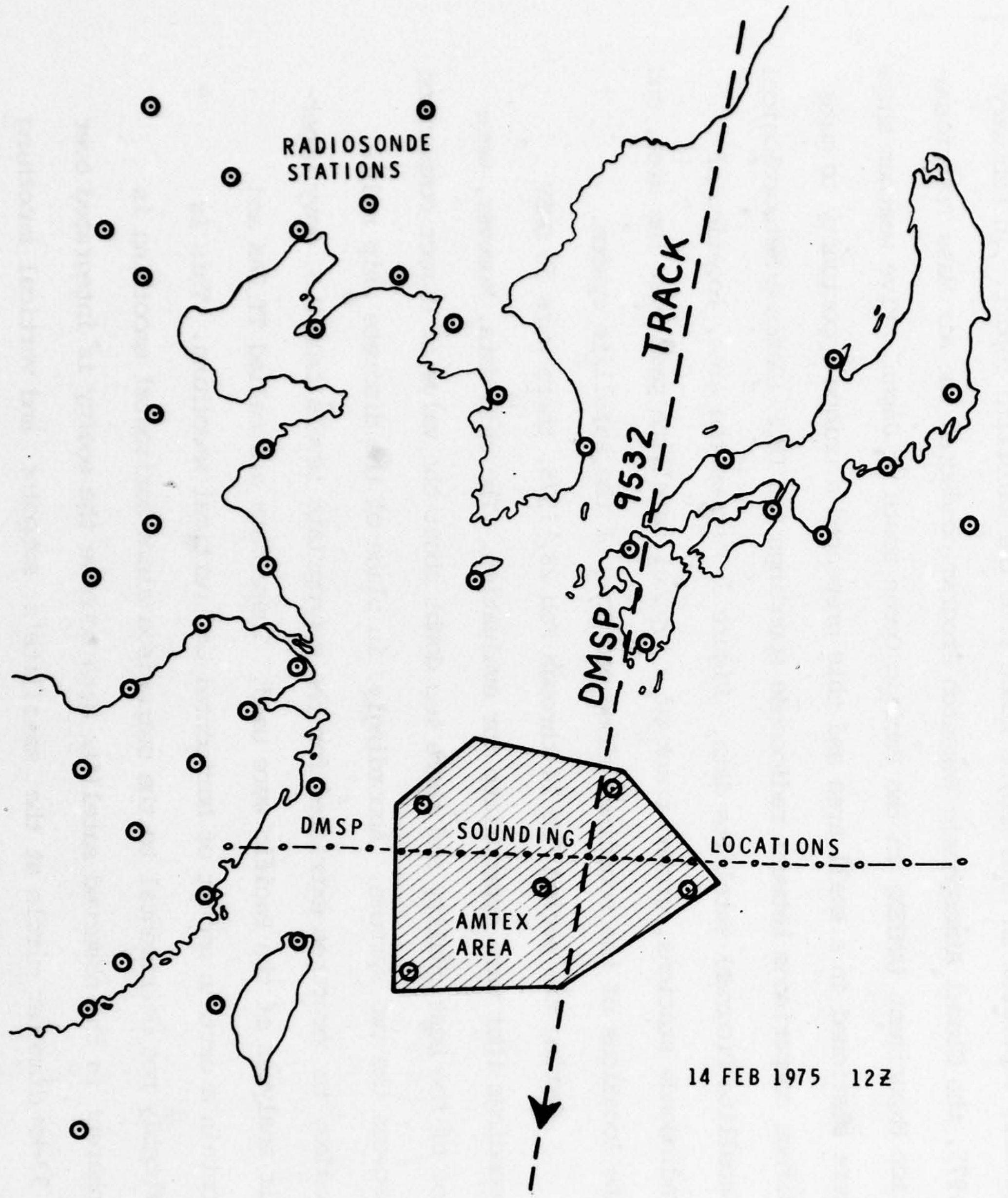
RADIOSONDE STATIONS
DMSP 9532 TRACK
DMSP
SOUNDING
LOCATIONS
AMTEX AREA
14 FEB 1975 12Z

Fig 3.3 AMTEX area in which radiosonde data was compared with satellite soundings is hatched. Circles with dots in center are radiosonde sites; dashed line is typical DMSP sub-point track; small circles are centers of satellite soundings along a typical DMSP scan.

nodes near noon and midnight. Satellite derived temperatures within ± 4 hours of 00Z and 12Z were compared with the corresponding upper-air temperatures.

Tables 3.3 through 3.7 are histograms that show, by pressure level in the atmosphere, the frequency that the difference between the DMSP and TT PAK occurred for the number of Celsius degrees indicated along the top of the table. The data are separated by satellite in Tables 3.3 and 3.4. Tables 3.5 and 3.6 list the distributions obtained from day and night data respectively. All the data are combined in Table 3.7.

This information is summarized in Figures 3.4 and 3.5 which show the vertical distributions of mean differences between the DMSP and TT PAK temperatures by time, satellite and the entire data sample. These results are very discouraging. They show largest differences near the surface and at the tropopause. Figure 3.4 shows the inconsistency between satellites and Figure 3.5, that between day and night. The standard deviation very seldom falls below 2°C and averages over 3°C. Even in the middle troposphere at 500 mb, not only is the range between the various average values large, the standard deviation is also large.

In summary, aside from the most general description of the atmosphere, these satellite sounding temperatures are unreliable to the point of uselessness. The study did serve its purpose, however, in bringing to the attention of the Air Weather Service (AWS), the need to reevaluate the whole sounder program from sensors to the uses to which such data could be reliably applied.

Table 3.3 Frequency,mean and standard deviation of temperature differences at standard levels between DMSP satellite No. 8531 and corresponding TT PAK data. (22 soundings)

	MEAN	SIGMA	****	-12	-11	-10	-9	-8	-7	-6	-5	-4	-3	-2	-1	0	1	2	3	4	5	6	7	8	9	10	11	12	****
10MB	.1	1.7												3	8	2	5	2		2									
30MB	4.1	3.5												1	2	2	2		2	2	3	2	1	3	1		1		
50MB	4.1	3.6												1	3	2	1			2	3	4	2	2	2				
100MB	3.5	2.5													3			6	2	1	5	2	2	1					
150MB	-2.9	3.0						1		5	3	1	4	1	1	2	2	2											
200MB	-4.8	1.9						1	4	2	6	6	2					1											
250MB	-4.9	1.5						2	3	1	5	7	3	1															
300MB	-3.4	3.1				1		1	4		2	1	2	3	5	1	2												
400MB	-2.6	2.7				1				3		5	2	4	1	3	3												
500MB	-1.6	2.7						1		1	1	3	2		3	8	2			1									
700MB	.8	2.2											1	3	2	4	3	4	3		2								
850MB	4.1	2.6														2	3	2	4	3	1	4	1	1		1			
1000MB	5.9	4.3												2	1		1		2	1	1	4	2	2	2	1	1		2
****MB	-2.1	4.7					1				3	4	9	1			1	1				1							1
TOTAL			0	0	0	2	1	6	11	12	20	27	25	20	29	26	25	18	13	12	15	17	8	9	5	2	2	0	3

Table 3.4 Same as Table 3.3 except for DMSP satellite No. 9532. (28 soundings)

	MEAN	SIGMA	****	-12	-11	-10	-9	-8	-7	-6	-5	-4	-3	-2	-1	0	1	2	3	4	5	6	7	8	9	10	11	12	****
10MB	-2.4	2.3								1	4	3	8	3	4	2		1	2										
30MB	2.9	4.0											4	2	3			4		3	4	3	2	2			1		
50MB	3.4	3.5											1	2	1	4	1		5	3	4	2	2	1	1	1			
100MB	1.5	3.3										1	1	2	4	7	2	2	3	1	2	1			1	1			
150MB	-5.3	4.4	1		1	4	1	2	4	2	2	2	2	1	2		1	1	2										
200MB	-6.1	2.8		2	1	2	2		3	6	4	5	2		1														
250MB	-4.1	3.1				1	1	1	5	4	2	1	5		5		3												
300MB	-1.4	5.0		1		1	1		3	1	2		2	2	1	4	3		3		1	1	1	1					
400MB	1.5	3.2								2				1	2	3	6	6	1	4		2				1			
500MB	.3	3.7							2		1	2	1	4	2	5	1	1	4		2	2	1						
700MB	.7	2.7										1	3	3	2	5	2	4	3	3	1		1						
850MB	3.4	3.4								1					2	2	2	2	5	6	1	2	1	2	1		1		
1000MB	4.2	4.6									1		1	2	1	1	2	3	2	1	3	3	2	1			4	1	
****MB	-.8	6.7					1	1	1	4	4	3	1	1	1	2	1	1	1	2			1			1			2
TOTAL			1	3	2	8	6	4	18	21	20	18	31	23	31	35	24	25	31	23	18	16	11	7	3	4	6	1	2

Table 3.5 Same as Table 3.3 except for 00Z (day) observations only of both satellites. (31 soundings)

	MEAN	SIGMA	****	-12	-11	-10	-9	-8	-7	-6	-5	-4	-3	-2	-1	0	1	2	3	4	5	6	7	8	9	10	11	12	****
10MB	-1.7	1.9								1	2	2	5	3	11	2	5												
70MB	3.4	3.9											1	3	5	2	1		2	2	4	4	1	4	1		1		
50MB	3.6	3.7											1	1	3	5	2			4	4	2	4	2	3				
100MB	3.0	2.7												1	4	3	1	5	4	2	5	3	1	1	1				
150MB	-3.2	3.7				1	1	1	3	6	2	1	4	2	1	2	3	3	1										
200MB	-5.2	2.5			1	2		1	7	1	7	7	3		1			1											
250MB	-5.2	2.0				1	1	2	6	3	6	5	5		2														
300MB	-3.7	3.8		1		2	1	1	6		2	1	2	3	5	4	2		1										
400MB	-1.5	3.1				1				5		3	2	2	3	4	7	3		1									
500MB	-1.4	2.9						1	1	1	1	4	1	3	5	9	1	1	2	1									
700MB	.4	2.3										1	2	5	2	6	4	5	4		2								
850MB	3.9	2.4														1	4	3	9	4	1	5	2	1		1			
1000MB	5.3	4.5									1			2	1	1	2	1	2	2	1	6	4	1	1	1	3		2
****MB	-2.2	4.3					1	1	1	2	4	5	7	2		1	1	1	1	1		1	1			1			
TOTAL			0	1	1	7	4	7	24	19	25	29	33	27	43	40	33	23	26	17	17	21	13	9	6	3	4	0	2

Table 3.6 Same as Table 3.3 except for 12Z (night) observations of both satellites. (19 soundings)

	MEAN	SIGMA	****	-12	-11	-10	-9	-8	-7	-6	-5	-4	-3	-2	-1	0	1	2	3	4	5	6	7	8	9	10	11	12	****
10MB	-.6	2.9									2	1	3	3	1	2		3	2	2									
30MB	3.5	3.8											3				1	4		3	3	1	2	1			1		
50MB	3.8	3.2												2	1	1			5	1	3	4		1		1			
100MB	1.3	3.5										1	1	1	3	4	1	3	1		2		1			1			
150MB	-5.9	3.9	1		1	3		2	1	1	3	2	2		2				1										
200MB	-6.1	2.4		2			2			7	3	4	1																
250MB	-3.2	2.8						1	2	2	1	3	3	1	3		3												
300MB	.1	4.3							1	1	2		2	2	1	1	3		2		1	1	1	1					
400MB	1.6	3.4										2		3		2	2	3	1	3		2				1			
500MB	.8	4.0							1		1	1	2	1		4	2		2		2	2	1						
700MB	1.3	2.7											2	1	2	3	1	3	2	3	1		1						
850MB	3.3	4.0								1					2	3	1	1		5	1	1		2	1		1		
1000MB	4.5	4.6											1	2	1		1	2	2		3	1		2	1		2	1	
****MB	.1	7.7					1			2	3	2	3		1	1	1	1		1									3
TOTAL			1	2	1	3	3	3	5	14	15	16	23	16	17	21	16	20	18	18	16	12	6	7	2	3	4	1	3

Table 3.7 Same as Table 3.3 except all observations from both satellites. (50 soundings)

	MEAN	SIGMA	****	-12	-11	-10	-9	-8	-7	-6	-5	-4	-3	-2	-1	0	1	2	3	4	5	6	7	8	9	10	11	12	****
10MB	-1.3	2.4								1	4	3	8	6	12	4	5	3	2	2									
30MB	3.4	3.9											4	3	5	2	2	4	2	5	7	5	3	5	1		2		
50MB	3.7	3.5											1	3	4	6	2		5	5	7	6	4	3	3	1			
100MB	2.4	3.2										1	1	2	7	7	2	8	5	2	7	3	2	1	1	1			
150MB	-4.3	4.0	1		1	4	1	3	4	7	5	3	6	2	3	2	3	3	2										
200MB	-5.5	2.5		2	1	2	2	1	7	8	10	11	4		1			1											
250MB	-4.5	2.5				1	1	3	8	5	7	8	8	1	5		3												
300MB	-2.2	4.4		1		2	1	1	7	1	4	1	4	5	6	5	5		3		1	1	1	1					
400MB	-.3	3.6				1				5		5	2	5	3	6	9	6	1	4		2				1			
500MB	-.5	3.5						1	2	1	2	5	3	4	5	13	3	1	4	1	2	2	1						
700MB	.8	2.5										1	4	6	4	9	5	8	6	3	3		1						
850MB	3.7	3.1								1					2	4	5	4	9	9	2	6	2	3	1	1	1		
1000MB	5.0	4.6									1		1	4	2	1	3	3	4	2	4	7	4	3	2	1	5	1	2
****MB	-1.3	5.9					2	1	1	4	7	7	10	2	1	2	2	2	1	2		1	1			1			3
TOTAL			1	3	2	10	7	10	29	33	40	45	56	43	60	61	49	43	44	35	33	33	19	16	8	6	8	1	5

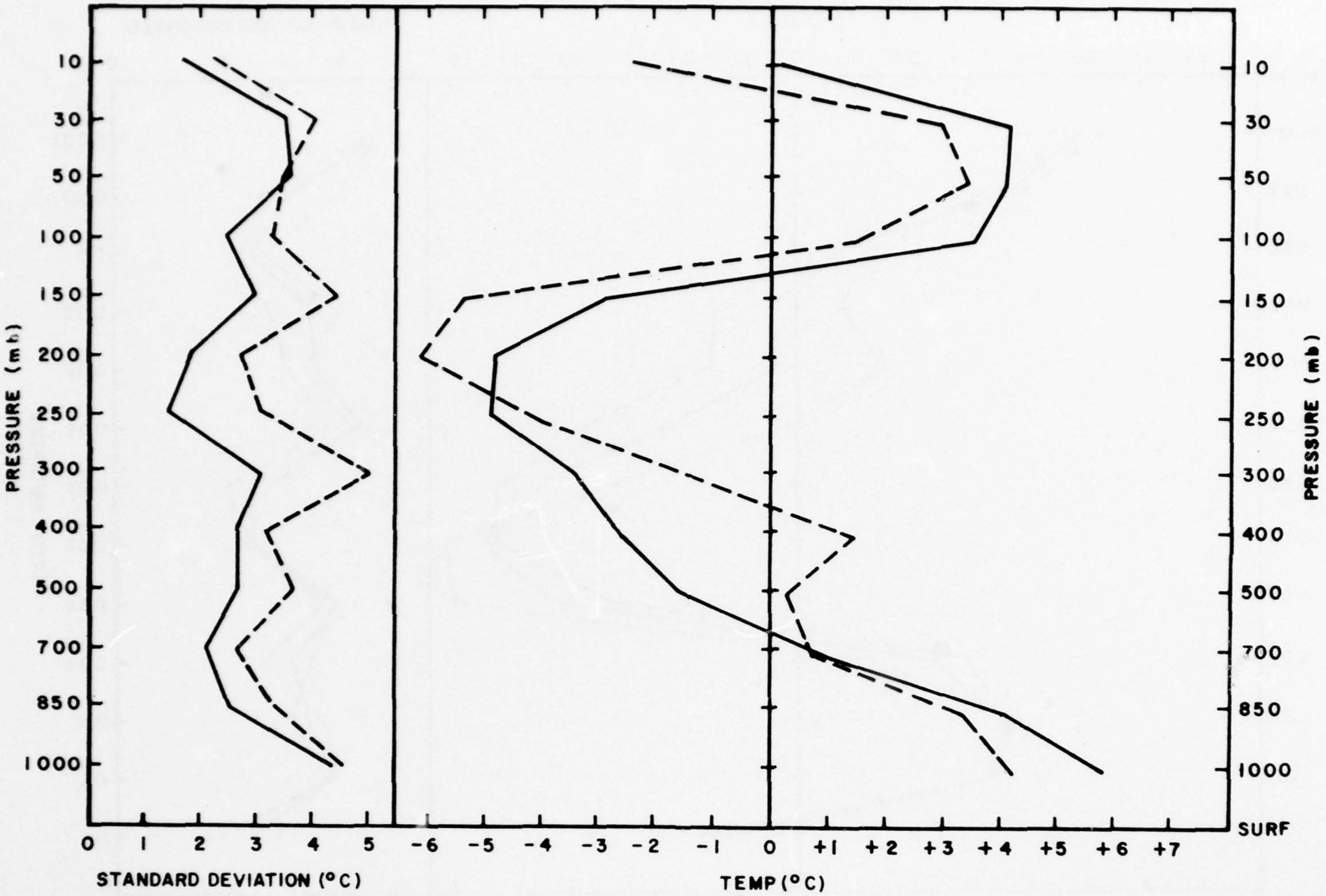

Fig 3.4 (Right) Average difference in the temperature soundings based on DMSP data and Navy TTPAK data. Solid line is satellite no. 8531 and dashed line is satellite no. 9532.

(Left) Standard deviation of temperature differences between satellite and TTPAK data at mandatory levels in the atmosphere.

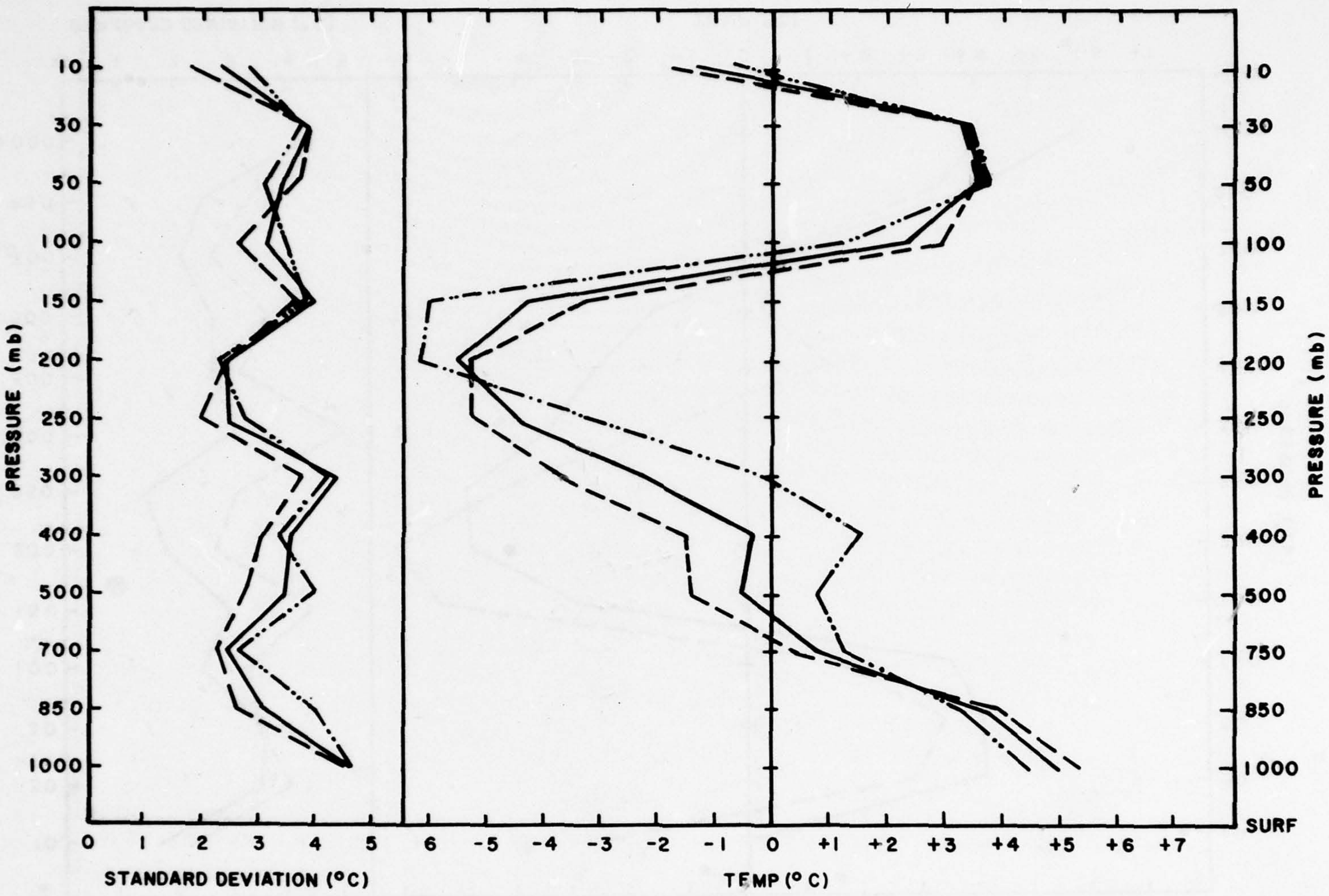

Fig 3.5 Same as figure 3.4 except dashed line 00Z (day) data; dot-dashed line is 12Z (night) data and solid line is all data.

3.4 Automated Cloud Identification by Second Order Statistical Methods

3.4.1 Introduction

Meteorology is characterized by enormous quantities of conventional data continuously pouring into weather centrals from all over the world. The addition of satellite data has augmented this data glut by orders of magnitude. For example, in one day 10^{11} data bits are collected by only one Geosynchronous Earth Orbiting Satellite (GOES). This high volume of data has a low information density. Methods are needed to reduce these data into a set with high information density.

Many computer systems and algorithms have been developed to assist in the efficient extraction of information from raw data. Interactive systems such as the Man-Computer Interactive Data Access System (McIDAS), have been developed to combine the electronic speed of a computer with the decision capability of a skilled analyst. At Air Force Global Weather Center (AFGWC) a computer data reduction algorithm has been developed. The algorithm produces a global cloud analysis, called 3-D Nephanalysis (3D NEPH), that is routinely generated for 15 levels in the atmosphere and for 25-mile square boxes. The cloud field is defined as clearly as possible using surface, radiosonde, aircraft, and satellite data as available. Observational modes are assigned priority in the computations by means of a decision tree process. Since global satellite data is routinely available, it is possible to generate a 3-D NEPH from satellite data alone. However, because of computational limitations, the data that are used have been degraded in resolution to reduce the quantity of the input. Consequently, there is a reduction in the quality of the output. AFGWC's operational commitments require the development of a new satellite processor, capable of handling increased amounts of satellite data with a higher level of sophistication and greater efficiency. This section briefly reviews the proposed method in the development of the new satellite processor for AFGWC.

3.4.2 Nature of the problem

Despite AFGWC's leadership in the application of satellite data, requirements placed on them by their customers exceed their processing capability. Smoothed mode satellite data at approximately 3-nm resolution are presently used as input to 3-D NEPH. Although fine mode data at 1/3 nm resolution are sensed by the satellite, they have not been used until recently. AFGWC computers are inadequate for processing satellite data in real time with the rates and volume of data involved. The fine mode sensor of the DMSP Block 5-D system generates over 100 times as much data as the high resolution sensor in the Block 5-C system.

Improvement in operational cloud specification at AFGWC implies the utilization of fine mode data. Thus, the new satellite processor's task would be data reduction of an enlarged data base containing 1/3 nm imagery while providing improved information content. Considering the quantity of data involved, sophisticated programming alone cannot come close to alleviating the problem. The approach selected by AFGWC and AFGL is to utilize sophisticated analytical techniques that are adaptable to hard wired computational devices. Specifically, utilization of Fast Fourier Transform (FFT) coefficients as indices of cloud types has been pursued.

3.4.3 The Fast Fourier Transform (FFT)

The Fourier Transform in the past has been used for characterizing linear systems and for identifying frequency components making up a continuous waveform. However, when the waveform is sampled, or the system is to be analyzed on a digital computer, it is the finite discrete version of the Fourier Transform that must be used. The Fast Fourier Transform (FFT), as developed by Cooley and Tukey, is simply an efficient method of computing the discrete Fourier Transform.

The discrete Fourier Transform pair can be written as:

$$\text{1a)}\quad Y(j) = \frac{1}{N}\sum_{k=0}^{N-1} X(k)\exp(-i2\pi jk/N)$$

$$\text{1b)}\quad X(k) = \sum_{j=0}^{N-1} Y(j)\exp(i2\pi jk/N)$$

where

$Y(j)$ is the frequency domain function

$X(k)$ is the time domain function

$i = \sqrt{-1}$

and N is the number of points sampled. The discrete Fourier Transform can be computed from equations 1a and 1b directly, but it is slower than using the FFT. For an N-point transformation, where N is some power of 2, ($N = 2^m$, m being positive), the number of complex additions and subtractions is given by N^2. For the FFT the number of complex additions and subtractions is reduced to $(N/2)\log_2 N$. For N = 1024 this represents a computational savings of 200 to 1.

The output of an FFT is simply the coefficients of a Fourier series representation of a function. A one-dimensional Fourier series representation of a function reduces to a simple harmonic expressed by:

$$2)\quad F(x) = A_o + \sum_{j=1}^{\infty} (A_j \operatorname{Cos} (\frac{2n\pi x}{T}) + B_j \operatorname{Sin} (\frac{2n\pi x}{T}))$$

where,

T = period of the function

X = sampled domain

j = phase

and A_o, A_j, and B_j are the coefficients. For a one-dimensional FFT of an 8-pixel (picture element) scan line the output consists of the 17 coefficients of A_o, A_j, and B_j, with j ranging from 1 to 8. In a two-dimensional FFT of an 8x8 pixel area the output would consist of 129 coefficients A_o, $A_{j,i}$ and $B_{j,i}$ with j and i ranging from 1 to 8.

The development of a new satellite processor for AFGWC involves the computation of the power spectrum from two-dimensional FFT coefficients. It is anticipated that proper processing of spectra will extract information from the satellite imagery field while functioning as a data reduction mechanism.

3.4.4 Computation of power spectra

Computation of power spectra from two-dimensional Fourier Transforms yields a new set of parameters in response to spatial distribution and frequency characteristics of the cloud field. If some cloud types generate reproducible power spectra parameters, one can classify clouds by using a discriminant function. Spectral signatures (reproducible cloud spectra) indicate size, shape and texture of a particular cloud type. Thus, power spectra are a measure of the amount of variance in an imagery field due to clouds of various sizes.

Power is defined as

$$3)\quad P_{j,i} = \sqrt{A^2_{j,i} + B^2_{j,i}}$$

if $A_{j,i}$ is the real part (Cosine term coefficient) and $B_{j,i}$ is the imaginary part (Sine term coefficient). Power spectra were initially computed by annularly integrating the FFT coefficients. Computation of power spectra in annular rings is permissible since the FFT retains the property of a periodic function allowing duplication of FFT output as a half-range expansion. The periodicity allows duplication of the FFT output in quadrant I of the frequency plane, into the II, III and IV quadrants. The duplication of the FFT output in the remaining quadrants simplifies the annular integration of the power spectra.

Power spectra that has been integrated annularly may be biased as a result of FFT aliasing. Aliasing is the result of high-frequency components impersonating low-frequency components. It is minimized by computing the last half of the FFT output by symmetric complex conjugates. Coefficients with frequencies higher than the linear Nyquist frequency ($f_s/2$, where f_s is the sample domain) are computed by the symmetric complex conjugates of frequencies lower than the linear Nyquist. Since the spectra are integrated on a two-dimensional plane, the spectra are computed up to what is termed the two-dimensional Nyquist frequency, given by:

$$\sqrt{\frac{(\text{sample size of first dimension})^2}{4} + \frac{(\text{sample size of second dimension})^2}{4}}$$

Thus, an area of 8x8 pixels will have a two-dimensional Nyquist frequency of 6. With an (j,i) Cartesian coordinate, a distance from the mean spectral coefficient ($P_{o,o}$) can then be computed. The remaining terms ($P_{j,i}$) with the same distance from $P_{o,o}$ are summed. Terms above the two-dimensional Nyquist (distance greater than 6 for an 8x8 pixel area) are folded back into lower distances. Integration of the FFT coefficients in each annular band, using this technique, is done by running through the FFT output array only once. Therefore, duplication of FFT output in Quadrants II, III, IV is not required.

3.4.5 Normalized averaged power spectra (NAA) computation

The computation that is made is not power in the strictest definition of the term, but what may be called normalized averaged amplitudes (NAA). The computations of NAA result by dividing the summed power of each annular band by the total number of terms entered into the sum. The square root of the quotient is then taken and normalization is achieved by dividing the averaged amplitudes by the number of pixels entered into the FFT. NAA can be expressed as:

$$\text{NAA}(f) = \frac{1}{J \text{x} I} \sqrt{\frac{1}{\text{NT}(f)} \sum_{i=1}^{I} \sum_{j=1}^{J} P^2{}_{j(f),i(f)}}$$

where $P_{j(f),i(f)}$ are power spectra that are dependent upon the distance they are located from $P_{o,o}$; NT(f) is the number of $P_{j(f),i(f)}$ terms entered into the sum that are the same distance from $P_{o,o}$; f is the distance from $P_{o,o}$;

J and I are the dimensional orders of the imagery array. For 8x8 pixels where J = 8 and I = 8 normalization is achieved by dividing by the product of J x I = 64.

3.4.6 A study of two cloud areas

NAA's were computed from the coefficients of FFT's of 3 nm resolution satellite imagery for 20 October 1976. Two well separated areas, each of which contained a roughly homogeneous cloud field over at least a 200-nm area, were selected for the data sample. Identification of the two cloud areas was made solely from a DMSP global mosaic transparency. The first area (area 1) was classified as a mixture of stratus (St) and stratocumulus (Sc) clouds and area 2 was classified as a uniform deck of stratus or fog. FFT's were performed on each 200-square nm area as well as on the 64-25 nm sq (8x8 pixels) area that made up the larger areas.

There were no great differences between means of NAA's for 64 (25 x 25 nm)boxes of the two areas, other than at frequency 0. The difference in frequency 0 indicated that the average brightness of area 1 is greater than that of area 2. The results were the same when the 200x200 nm areas were examined. A statistic was computed to determine whether the differences in mean NAA of the two areas as a function of frequency were significant, using each 25x25-nm box. The statistic, T' measured $\bar{u}_1 - \bar{u}_2$ for each frequency where $\bar{u}_1$ represents the mean NAA's for area 1 and $\bar{u}_2$ represents the mean NAA's for area 2. At the 0.01 level of significance, no significant differences in mean NAA for frequencies 1, 2, 5 and 6 were found. Significant differences for frequencies 0, 3 and 4 imply that in one of the areas, there is a fluctuation in brightness between pixels that does not exist in the other area.

Variation of NAA as a function of frequency for the 64 (25x25 nm) boxes of area 1 and area 2 was also computed. The variation of NAA for area 2 is what would be expected of a cloud deck with uniform tops that have essentially identical brightness between pixels. The higher variation for area 1 indicates a cloud deck with non-uniform tops and/or breaks above satellite sensor resolution. A statistic was computed to determine if the variation of NAA's between the two areas was significant. If S_1^2 and S_2^2 are the variances in NAA for area 1 and area 2 respectively, then the statistic F ($F = S_1^2/S_2^2$) could be computed for each frequency. At the 0.01 level of significance, frequencies 0, 4, 5 and 6 showed significant differences. The differences in variance for frequency 0 means that some of the 64 (25x25 nm) boxes in area 1 had a greater variation in cloud brightness from one pixel to another, while area 2 did not exhibit this variable cloud brightness. The ratios (F) of greatest interest and implication were for frequencies 4, 5 and 6. The reason is that, at higher frequencies, the sampling rate of the FFT is at a higher cycle than it is at lower frequencies. This means that the finer variable brightness in the imagery is being sampled. Thus, if one area has a finer variable brightness in its imagery than another area then the variance of NAA as a function of frequency will most certainly differ. This is what was seen for frequencies 4, 5 and 6. The finer texture may be a basis for cloud type discrimination, and thus the differences in variance of NAA may be a spectral signature. The important factor in this initial study is that enough difference was detected in FFT processing of the cloud-field imagery to justify further investigation of the problem.

3.4.7 Conclusions

The results discussed in the previous section (3.4.6) were based on 3-nm resolution data, primarily for test purposes. Nevertheless, there is an indication that processing of FFT coefficients will allow classification of cloud types in an automated scenario. Use of the 1/3-nm resolution imagery would undoubtedly enhance the high frequency distinctions of spatial cloud distribution. This would yield greater discriminating power among the class condition covariances of the spectra, improving reliability of the classification process.

3.5 Estimates of Cloud Properties derived from Satellite Sensors

3.5.1 Visible and infrared radiation in cloudy atmospheres

A number of published studies has suggested that a physical basis exists for the relation of cloud properties to satellite measurements. Satellite sensors measure radiation which has been emitted, absorbed, and scattered by surfaces, atmospheric gases, and clouds. These processes can be simulated by numerical models. The subject of radiative transfer in atmospheric gases above planetary surfaces has been treated in depth by Chandrasekhar[1]. The important case of radiative transfer in clouds composed of spherical particles has been summarized by van de Hulst[2], while extensive tables of calculated results have been published by Deirmendjian[3]. Both authors extend the work by Mie[4] which mathematically describes the interaction of a homogeneous sphere with a field of electromagnetic radiation.

The theory of radiative transfer in cloudy atmospheres has been applied to spectral regions suitable for cloud sensing from satellites. The principal regions are the visible spectrum from 0.5 to 1.0 µm, and the infrared (IR) spectrum from 8 to 12 µm. Both regions are suitable for cloud sensing since they are "window" regions for which gas transmission from cloud to satellite is very high and since the radiation fields are strong due to reflected sunlight (during daytime) at 0.5 to 1.0 µm and terrestrial emission at 8 to 12 µm.

Cloud particles absorb very little energy at wavelengths between 0.5 and 1.0 µm. Consequently, to relate cloud properties to radiation fields consistent with satellite viewing geometry one must primarily calculate the amount of sunlight scattered by cloud particles back toward the sensor. Such calculations have been performed for nominal distributions of cloud particles in a number of studies. Twomey, Jacobowitz, and Howell[5] found that cloud albedo, i.e., the ratio of reflected to incident sunlight, increased with the total cloud thickness or mass of cloud particles. The relationship was not linear, and for clouds with an integrated mass greater than 250 g/m^2, very little increase in albedo was found. The maximum albedo was about 90%. These calculations were for stratiform, non-precipitating water clouds. Plass and Kattawar[6] made calculations for both water and ice clouds at 0.7 µm. The reflected radiance was found to be less from ice clouds than from water clouds, primarily due to less efficient scattering per unit cloud mass by the larger ice particles. Multiple scattering was simulated by a Monte Carlo technique for computing the exact three-dimensional paths of scattered photons. The Monte Carlo technique has been adapted to non-stratiform clouds by McKee and Cox[7], among others. The important result here was that clouds of finite horizontal extent were not so bright as infinite clouds when viewed by a satellite due to a loss of scattered sunlight out the sides of the clouds. In these studies, however, the rather arbitrary assumption was made that ice cloud scattering could be approximated by a polydispersion of ice spheres since no general theory exists for scattering of non-spherical particles such as ice crystals. An important class of ice particles, namely, long hexagonal prisms which are frequently observed in cirrus clouds, was treated by Liou[8] by approximating the prisms as cylinders and applying a scattering theory first presented by Lord Rayleigh[9].

In the 8 to 12 μm IR window, scattering is much less important than absorption for modelling radiative transfer in cloudy atmospheres since water and ice particles intercept and reemit substantial energies at these wavelengths. The amount of incident sunlight at 8 to 12 μm is negligible, so that models are not dependent on solar illumination. On the other hand, the sources of upwelling IR radiation such as surfaces or water vapor must be known or approximated since they contribute the energy which is attenuated by clouds and also form the backgrounds against which clouds are observed by satellite IR radiometers. Two approximations are usually made in IR models. First, underlying surfaces are treated as blackbody emitters so that only their temperatures and not their reflective properties need to be put into the models. Second, many clouds are also treated as blackbody emitters, although this approximation is much more difficult to justify. In the case of thin ice clouds at high altitudes, it is a very poor approximation as shown by Kuhn[10]. For water clouds with particle mass densities on the order of 0.1 g/m^3 or greater most of the radiation measured by a satellite IR sensor originates within the upper 100 m of the cloud. In other words, the sensor "looks" into the cloud, but only for short distances so the blackbody approximation is acceptable if great precision is not required.

Models of radiative transfer have been developed for cloudy atmospheres in the 8 to 12 μm region. Shifrin[11] was one of the early investigators to predict the strong absorption effects in clouds at these wavelengths. Yamamoto, Tanaka, and Kamitani[12] did extensive calculations of radiative transfer in water clouds. Calculations for ice clouds were later done by Jacobowitz[13] and by Liou[14] for the important case of semitransparent or "greybody" cirrus clouds. The calculations indicated that the upwelling surface radiance would be so attenuated as to be undetectable from satellites when the integrated vertical cloud mass or optical path was on the order of 100 g/m^2. However, due to the low mass densities of ice clouds at cold temperatures, such a cloud might have a geometrical thickness of 5 km.

In summary, considerable progress has been made over the years in modelling radiative transfer in the window regions which are used to sense clouds from satellites. These studies are applicable to the forward problem of modelling, that is, given certain cloud properties such as particle size, phase, shape, number density, cloud thickness, etc., predicting what would be measured from the satellite. The forward models clearly indicate that satellite measurements should vary with cloud properties such as cloud thickness and mass and, in particular, that dense clouds or thick clouds should be highly reflective in the visible window and weak energy or cold sources in the IR window. Moreover, the satellite measurements would be related to cloud amounts in a highly nonlinear manner which depends on cloud physical properties, gas attenuation, and the viewing geometry from the satellite.

Even though progress has been made in forward models for estimating the reflectances and radiances observed by satellites for given clouds, very little progress has been made in inverse models for estimating the cloud properties for given satellite measurements and inverse models are the chief objective of the present study. The forward models are too simple to be readily adapted for use as inverse models. First of all, the radiation models assume homogeneous clouds although in situ samples from aircraft indicate substantial variations in vertical and horizontal dimensions. The radiation models assume that ice particles have some simple geometric shape, which is rarely observed in ice particle sampling. Also, inverse models would require some means of estimating the cloud particle size distribution, which is not directly measurable from satellites.

In the present study, it was not necessary to develop an inverse model by a theoretical approach since measurements were available from a lengthy experiment described by Conover and Bunting[15] and these measurements could be used to construct and analyze empirical models. Three cloud properties-Cloud Mass (LWC), thickness (ΔH), and Environmental Severity Index (ESI) were selected for extended study. A variety of cloud conditions was sampled from research aircraft over mid-latitudes of the United States and analyzed together with infrared (IR) and visible (VIS) measurements from National Oceanic and Atmospheric Administration (NOAA) satellite sensors.

3.5.2 Satellite measurements

The satellite instruments used were the Scanning Radiometers (SR) of the Improved TIROS Operational Satellite (ITOS). These broadband sensors simultaneously detected both VIS ($0.52 - 0.72\ \mu m$) and IR ($10.4 - 12.5\ \mu m$) radiation. Resolution at the satellite subpoint was approximately 3 km for the VIS channel and 6 km for the IR channel. Data from consecutive polar orbits were recorded in the form of a 2048 by 2048 element array for each hemisphere each day. These arrays were aligned with the conventional Numerical Weather Prediction grid (NWP) so that both IR and VIS were equally spaced on a polar sterographic projection. The spacing of adjacent grid points on the earth increases from about 6 km at the equator to about 13 km at the poles. SR data used in this study were thus mapped and sampled to provide a nominal 10 by 10 km horizontal resolution for both IR and VIS.

The VIS data were normalized for solar zenith angle and inconsistencies in brightness corrected at the swath edges between satellite passes using a bi-directional reflectance model as applied by Conover and Bunting[15]. Observations by the IR sensor were less sensitive to viewing geometry and therefore not normalized in a manner similar to the VIS. The IR data did include a correction for limb darkening due to water vapor abscrption. Also, since the original IR data set was recorded in counts, a conversion to temperature in degrees Kelvin was made:

$$\text{For counts} \leq 78, \qquad IR = 164 + \text{counts} \qquad (1)$$

$$\text{For counts} > 78, \qquad IR = 242 + \left[\frac{\text{counts} - 78}{2}\right] \qquad (2)$$

At locations where the aircraft recorded cloud information, IR and VIS data were averaged over about 50 NWP grid points which represented an area of about 70 by 70 km. This area was increased in size as a function of the satellite zenith angle. A maximum area thus averaged was 70 by 100 km.

3.5.3 Aircraft measurements

At the time of the satellite pass, an aircraft equipped with cloud physics instrumentation would descend from an altitude of 10 km in a 35 km diameter spiral at a descent rate of 0.3 km/min. Many instruments were used, including a "snow stick" for visual identification of crystal habit and size, Johnson-Williams liquid water sensor, continuous formvar replicator, cloud scene cameras, and particle measuring spectrometers. An onboard flight director observed altitudes of cloud tops and bases, estimated cloud tops when clouds were above the maximum aircraft ceiling, estimated the fractional coverage of cloud layers, noted optical effects such as halos, and described particles intercepted by the snow stick. This entire sounding schedule was completed in about 30 minutes.

Satellite measurements are sensitive to clouds at all altitudes and are recorded at a rapid rate - less than 15 seconds to cover the entire 70 by 70 km array. If the aircraft were to loiter to obtain a better estimate of cloud tops, clouds at a lower altitude might advect or change before the aircraft was able to descend for a sample. In all cases, the highest clouds were sampled closest to the satellite pass time. Because of the requirement for the aircraft sample to be rapid, often the number of cloud particles obtained was small. In this event other available data such as surface radar and rainfall reports were included in an effort to generate a profile of cloud mass density as a function of altitude. A total of 41 cases were thus recorded and Table 3.8 is a summary of the data.

The aircraft-measured cloud properties were calculated from the complete profiles of hydrometeor mass density according to the following definitions:

$$\text{LWC} = \int \rho \, dH \qquad (3)$$

$$\text{ESI} = \int \rho H \, dH \qquad (4)$$

$$\Delta H = \int \delta \, dH \qquad (5)$$

The symbol ρ represents hydrometeor mass density, H represents altitude, and δ equals one if ρ is greater than 0.0001 g/m^3, otherwise δ equals zero. LWC is the total cloud mass, integrated vertically, including all ice and

TABLE 3.8

Simultaneous Satellite and Aircraft Data Set

		SATELLITE DATA		AIRCRAFT DATA		
CASE NO.	DATE	IR (°K)	VIS (ft-L/40)	LWC (g/m^2)	ESI ($g\ km^2/m^3$)	ΔH (km)
1	11Jan74	281.3	161.0	45.	.35	1.2
2	14Jan74	259.0	91.0	63.	.18	.8
3	01Feb74	263.9	57.0	69.	.65	.8
4	01Mar74	230.3	204.0	2035.	7.44	9.0
5	03Apr74	281.7	40.0	0.	0.00	0.0
6	08Apr74	229.8	203.0	661.	2.79	8.4
7	24Apr74	265.3	184.0	56.	0.00	1.0
8	28Apr74	247.5	203.0	731.	2.29	8.6
9	02May74	234.2	176.0	325.	.77	2.8
10	15Jan74	283.7	137.0	25.	0.00	.8
11	12Jan75	223.0	211.1	1067.	3.65	8.8
12	14Jan75	261.1	112.8	486.	.16	2.6
13	20Jan75	217.2	204.8	1082.	4.38	10.4
14	22Jan75	248.4	141.2	178.	1.09	5.6
15	23Jan75	248.6	97.8	71.	.59	3.4
16	25Jan75	248.0	157.9	474.	2.24	8.6
17	27Jan75	262.9	123.1	60.	.01	1.6
18	29Jan75	257.9	191.4	752.	.23	4.6
19	04Feb75	251.1	175.2	736.	2.16	8.6
20	11Feb75	256.5	128.2	33.	.07	4.0
21	13Feb75	259.9	102.3	11.	.01	1.4
22	14Feb75	245.1	73.4	27.	.24	2.6
23	23Feb75	235.8	192.5	362.	.74	7.0
24	01Mar75	252.5	171.5	336.	.45	3.4
25	03Mar75	266.9	126.6	141.	0.00	1.6
26	16Mar75	223.7	182.0	595.	3.20	6.6
27	20Mar75	249.0	189.4	140.	.06	2.6
28	26Mar75	266.0	104.5	31.	0.00	.8
29	27Mar75	229.5	192.1	1314.	5.53	10.0
30	04Apr75	247.6	167.0	370.	.64	5.6
31	10Apr75	261.1	168.5	751.	1.26	5.0
32	22Apr75	259.7	135.0	41.	.04	3.6
33	23Apr75	230.5	200.1	1967.	7.30	9.2
34	29Apr75	260.9	145.2	129.	.05	5.2
35	30May75	244.1	220.1	817.	2.69	10.4
36	01Jun75	248.7	162.4	255.	.98	3.4
37	05Jun75	271.7	169.5	131.	.04	3.6
38	11Jan76	241.5	175.2	1042.	2.64	7.4
39	02Mar76	239.6	155.7	1127.	2.64	10.4
40	21Apr76	233.7	180.7	880.	6.25	10.2
41	08Oct76	241.4	155.7	1532.	2.68	10.0

water particles. ESI differs from LWC since altitude appears as a weighting factor and also since water particles with diameter less than 50 μm are excluded. ΔH is the total geometric thickness of all cloud layers.

3.5.4 Analysis of variance

Analysis of variance is a statistical technique that examines the relationship between a dependent variable (predictand or criterion) and independent variables (predictors). If the points on a scatter diagram (e.g., Figures 3.6-3.11) follow a line, that regression line may be considered the dynamic mean.

Although linear regression is generally adequate, it is a matter of observation that some data variates are not so connected. The investigation of a precise description of the concomitant variation of two or more quantities is one of the problems of curve fitting, known as curvilinear regression. The objective, then, is to test or discover a mathematical law which relates the variates.

The challenge of curve fitting the data of Table 3.8 was to determine a suitable equation. Many equation types were considered and four candidates were selected for analysis as shown in Table 3.9.

TABLE 3.9

General Equations - Clouds (Y) and SR (X)

Linear:	$Y = A + BX$	(6)
Inverse:	$Y = A + B/(X + C)$	(7)
Parabolic:	$Y = A + BX + CX^2$	(8)
Cubic:	$Y = A + BX + CX^2 + DX^3$	(9)

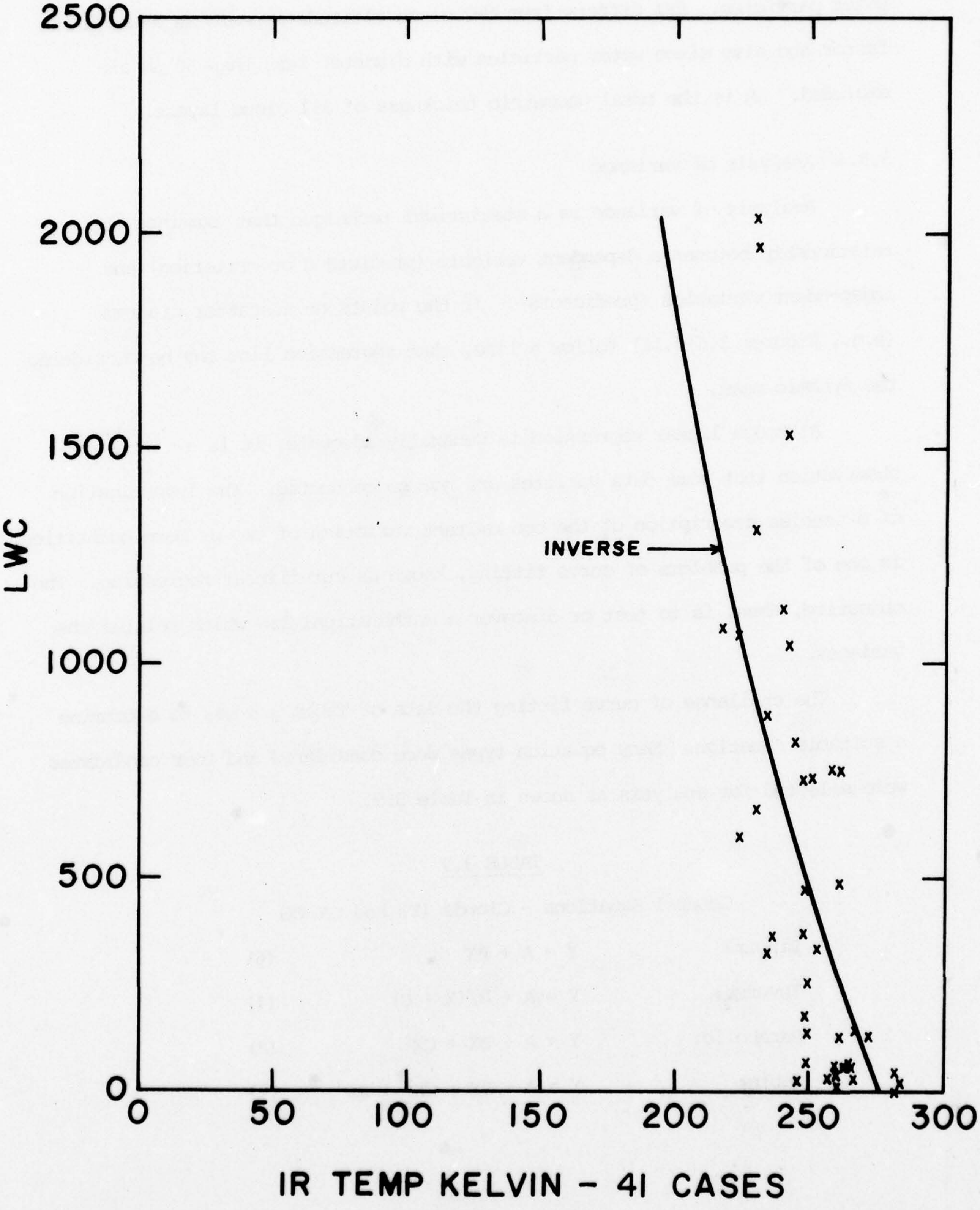

Fig 3.6 Scatter diagram relating aircraft measurements of total ice and water cloud mass (LWC) to satellite measurements of IR temperature A best fit curve according to Equation 7, an inverse form, is drawn.

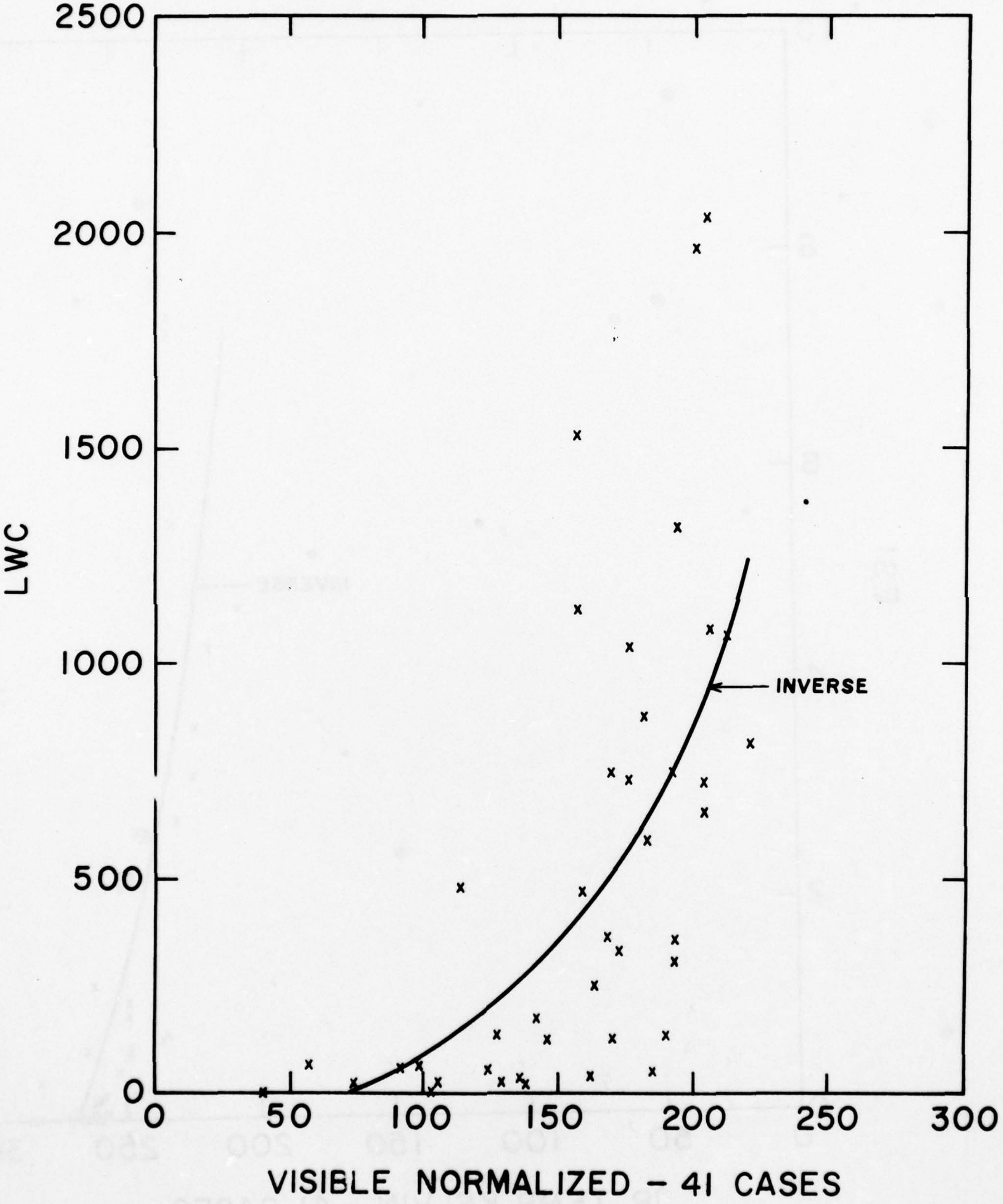

Fig 3.7 Scatter diagram relating LWC to satellite measurements of reflected sunlight normalized for viewing geometry and bidirectional reflectance.

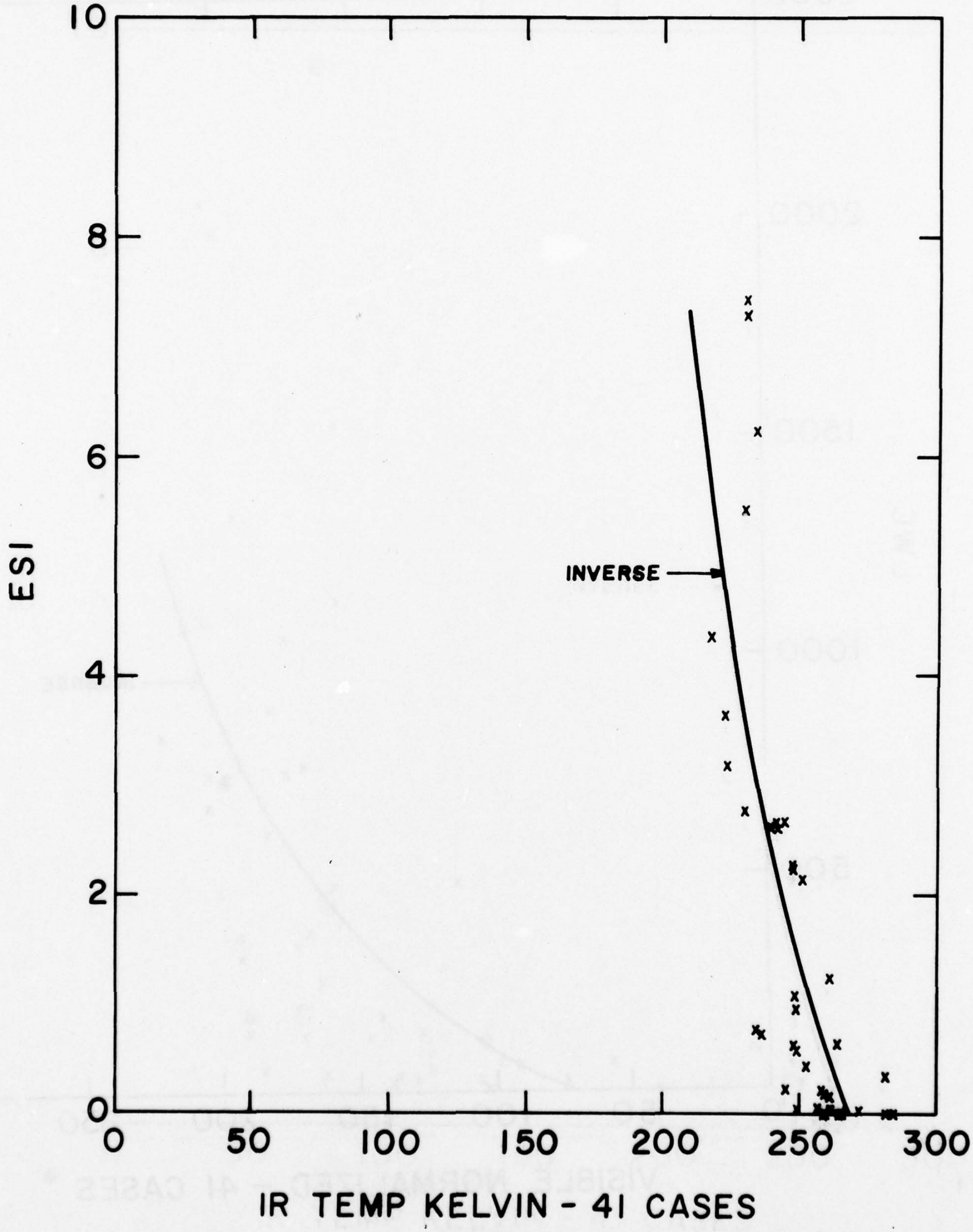

Fig 3.8 Scatter diagram relating ESI to IR temperature

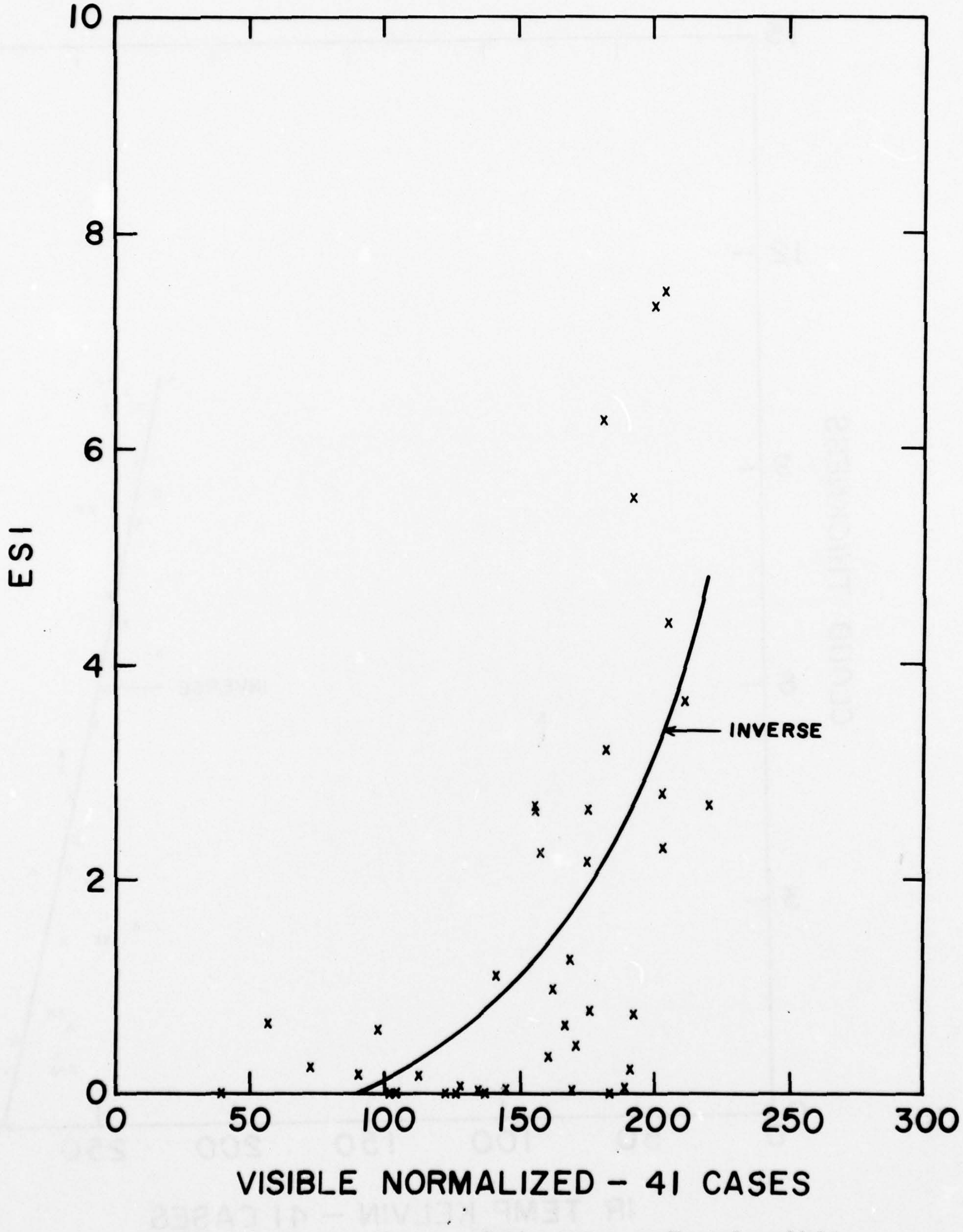

Fig 3.9 Scatter diagram relating ESI to reflected sunlight

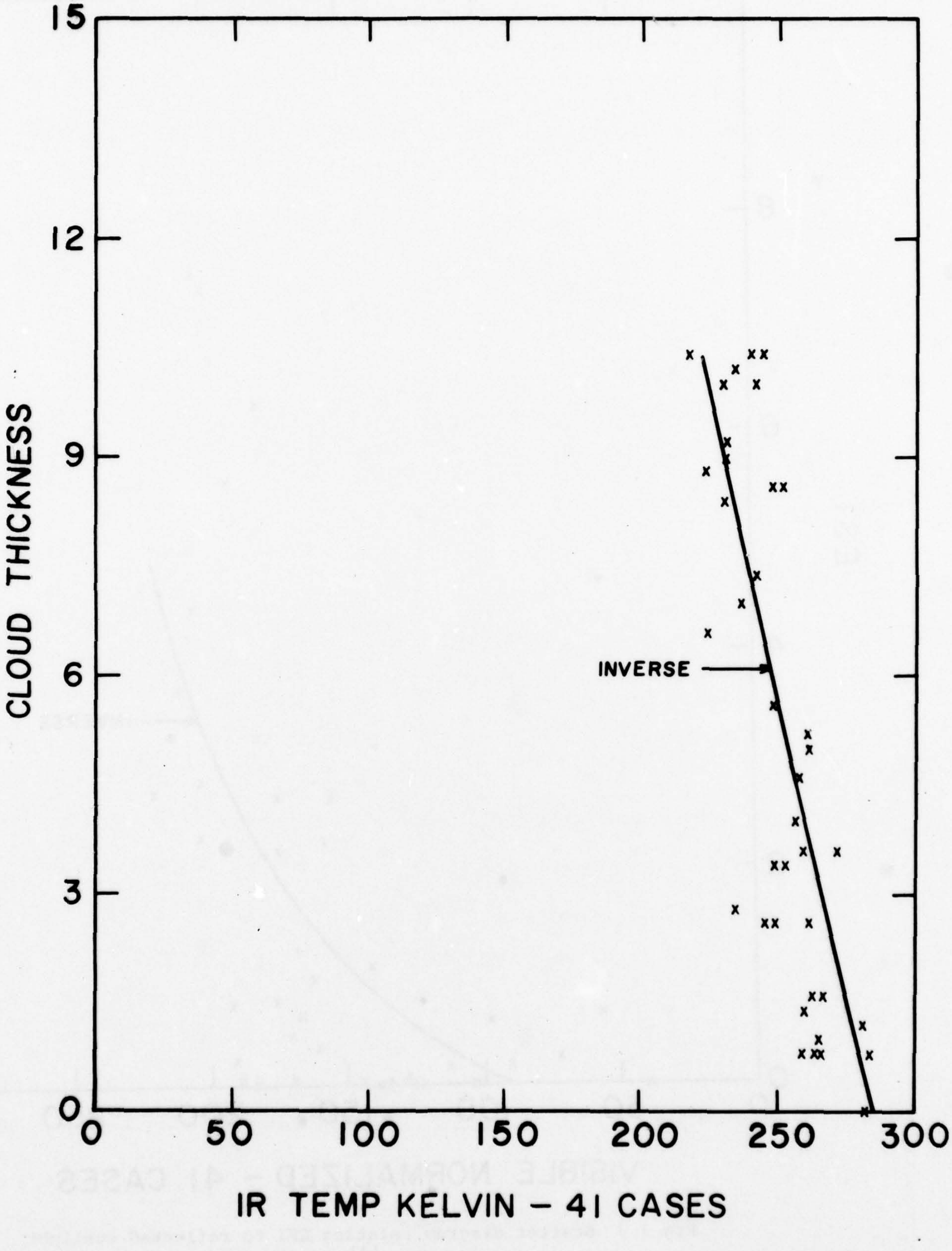

Fig 3.10 Scatter diagram relating total cloud thickness to IR temperature

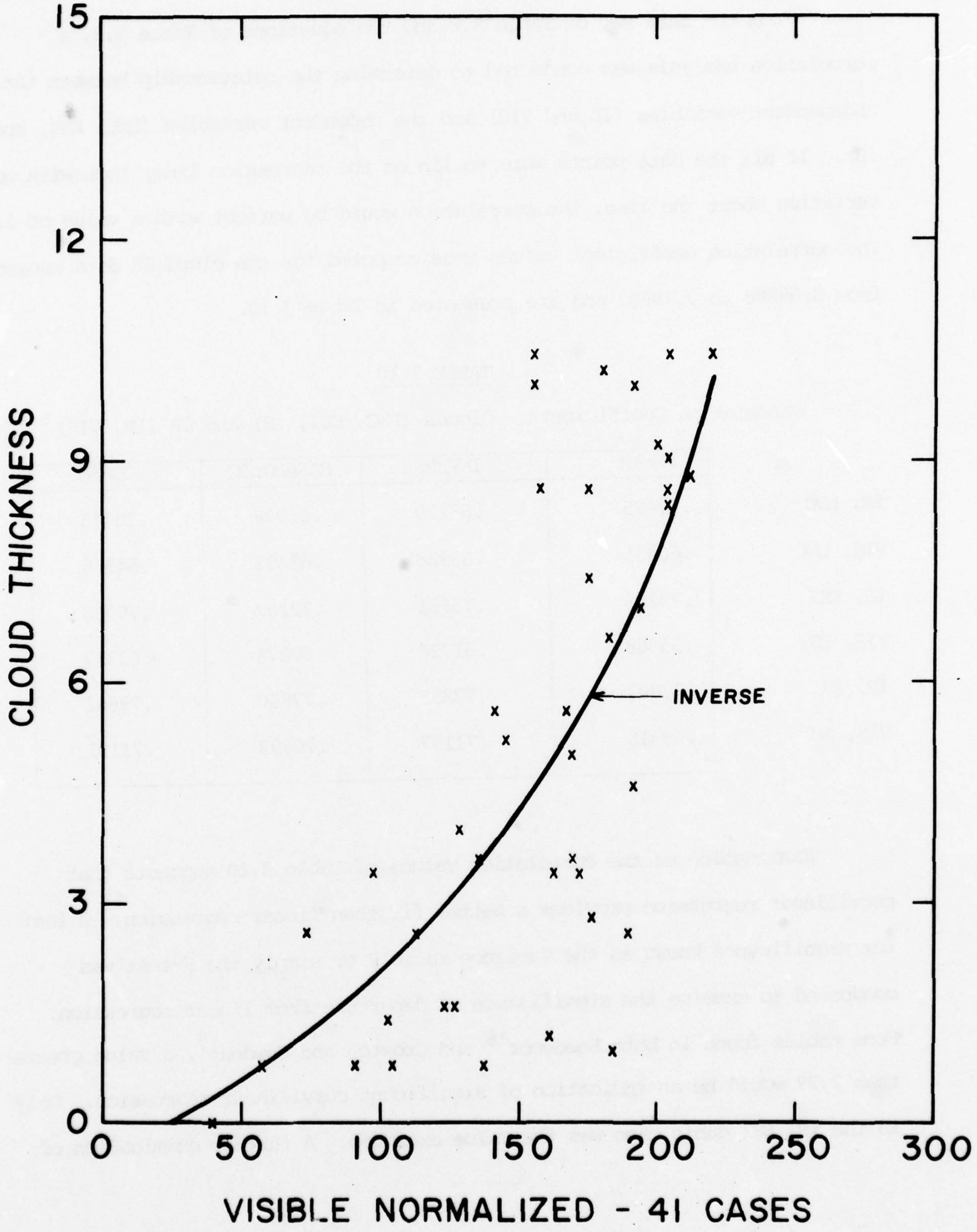

Fig 3.11 Scatter diagram relating total cloud thickness to reflected sunlight

From the data set of Table 3.8 and the equations of Table 3.9, a correlation analysis was conducted to determine the relationship between the independent variables (IR and VIS) and the dependent variables (LWC, ESI, and ΔH). If all the data points were to lie on the regression line, then with no variation about the line, the correlation would be perfect with a value of 1. The correlation coefficient values thus computed for the cloud-SR data ranged from 0.55868 to 0.79602 and are presented in Table 3.10.

TABLE 3.10

Correlation Coefficients - Clouds (LWC, ESI, ΔH) and SR (IR, VIS)

	LINEAR	INVERSE	PARABOLIC	CUBIC
IR, LWC	.67495	.68129	.66998	.70445
VIS, LWC	.60431	.63928	.63492	.64506
IR, ESI	.73253	.75681	.72262	.79000
VIS, ESI	.55868	.61726	.60278	.63317
IR, ΔH	.77887	.77853	.77850	.79602
VIS, ΔH	.69518	.71197	.70992	.71131

Examination of the correlation values of Table 3.10 suggests that curvilinear regression provides a better fit than linear regression. A test for significance known as the variance ratio F or simply the F-test was conducted to examine the significance of departure from linear regression. From tables found in both Snedecor[16] and Croxton and Cowden[17], a value greater than 7.29 would be an indication of significant curvilinear regression. Only in the IR, ESI cubic case was the value exceeded. A further examination of

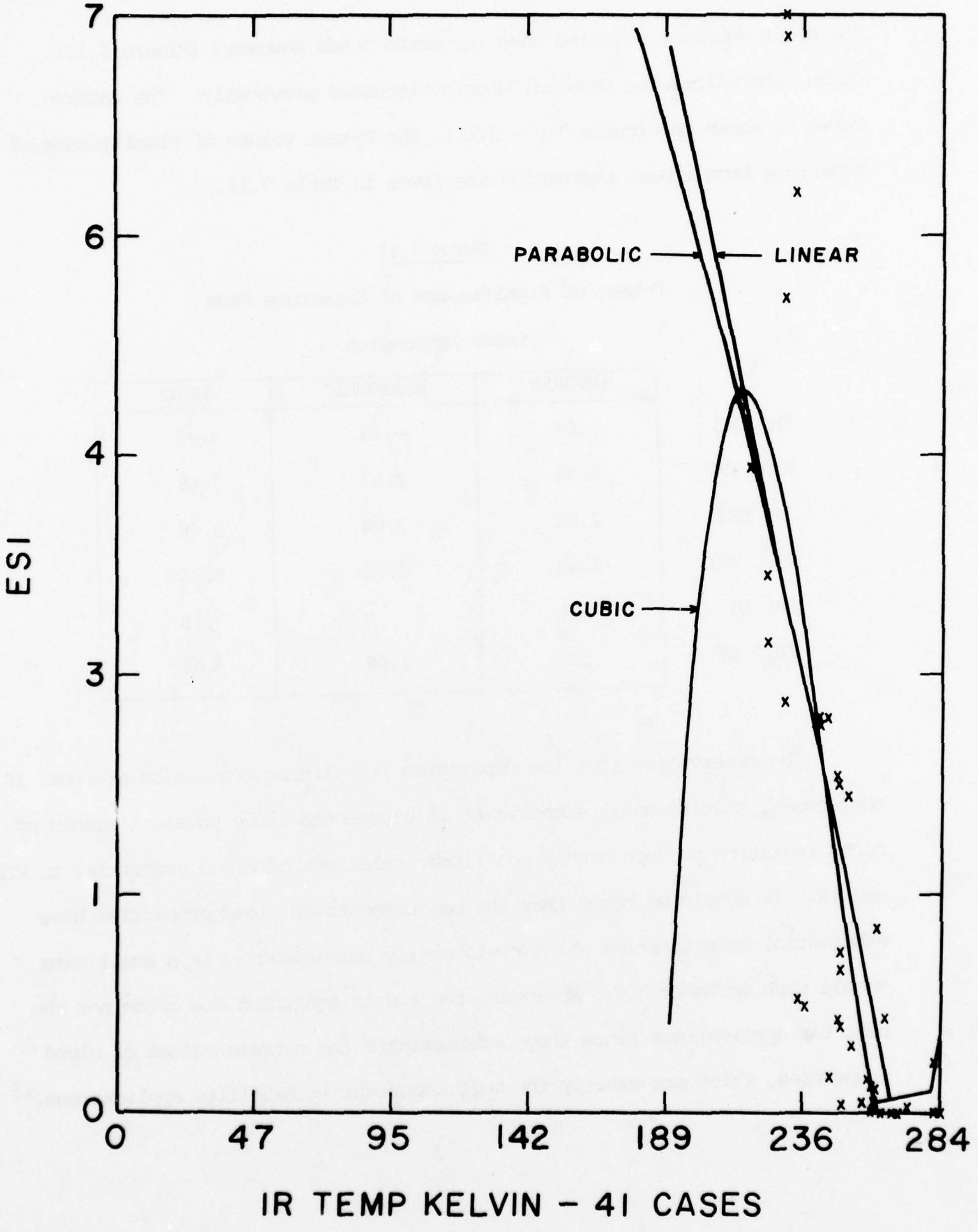

Fig 3.12 Three forms of curve-fitting for ESI as a function of IR temperature

the cubic equation revealed that the curve bends downward (Figure 3.12), which contradicts the physical models discussed previously. The inverse curve is shown on Figures 3.6 - 3.11. The F-test values of significance of departure from linear regression are given in Table 3.11.

TABLE 3.11

F-test of Significance of Departure from Linear Regression

	INVERSE	PARABOLIC	CUBIC
IR, LWC	.64	-.49	3.23
VIS, LWC	2.94	2.53	3.49
IR, ESI	2.04	2.04	9.48
VIS, ESI	4.07	2.72	5.76
IR, ΔH	-.04	0	3.18
VIS, ΔH	.53	1.69	2.04

The observation that the departures from linear regression are not, in most cases, statistically significant is unexpected since physical models of cloud radiation produce highly non-linear relations of cloud properties to VIS and IR. It should be noted that the measurements of cloud properties have substantial uncertainties which could easily be misleading in a small data sample such as Table 3.8. Moreover, the linear equations are often not the best for applications since they underestimate the extreme values of cloud properties, which are usually the most important in satellite applications.[15]

3.5.5 Multiple regression

Exactly the same principles are involved in multiple regression as simple regression, but the principles are extended to more than one independent variable. With the use of both independent variables IR and VIS, an estimate of LWC, ESI, and ΔH can be made more accurately than with one variable alone. A set of normal equations can be derived to estimate the coefficients A, B, and C in the equation of the form

$$Y = A + BX_1 + CX_2 \tag{10}$$

The resultant estimating equations from multiple regression based on the measurements in Table 3.8 are

$$LWC = 3950.851 - 16.157\ (IR) + 3.884\ (VIS) \tag{11}$$

$$ESI = 19.870 - 0.0785\ (IR) + 0.00904\ (VIS) \tag{12}$$

$$\Delta H = 30.597 - 0.119\ (IR) + 0.0283\ (VIS) \tag{13}$$

A summary of multiple correlation and standard error of the estimate is shown in Table 3.12.

Table 3.12

Multiple Correlation Coefficient and Standard Error of the Estimate for 41 Cases of Cloud Properties

	Multiple Correlation Coef.	Standard Error of Estimate
LWC	.72071	369.208
ESI	.74842	1.354
ΔH	.83073	1.889

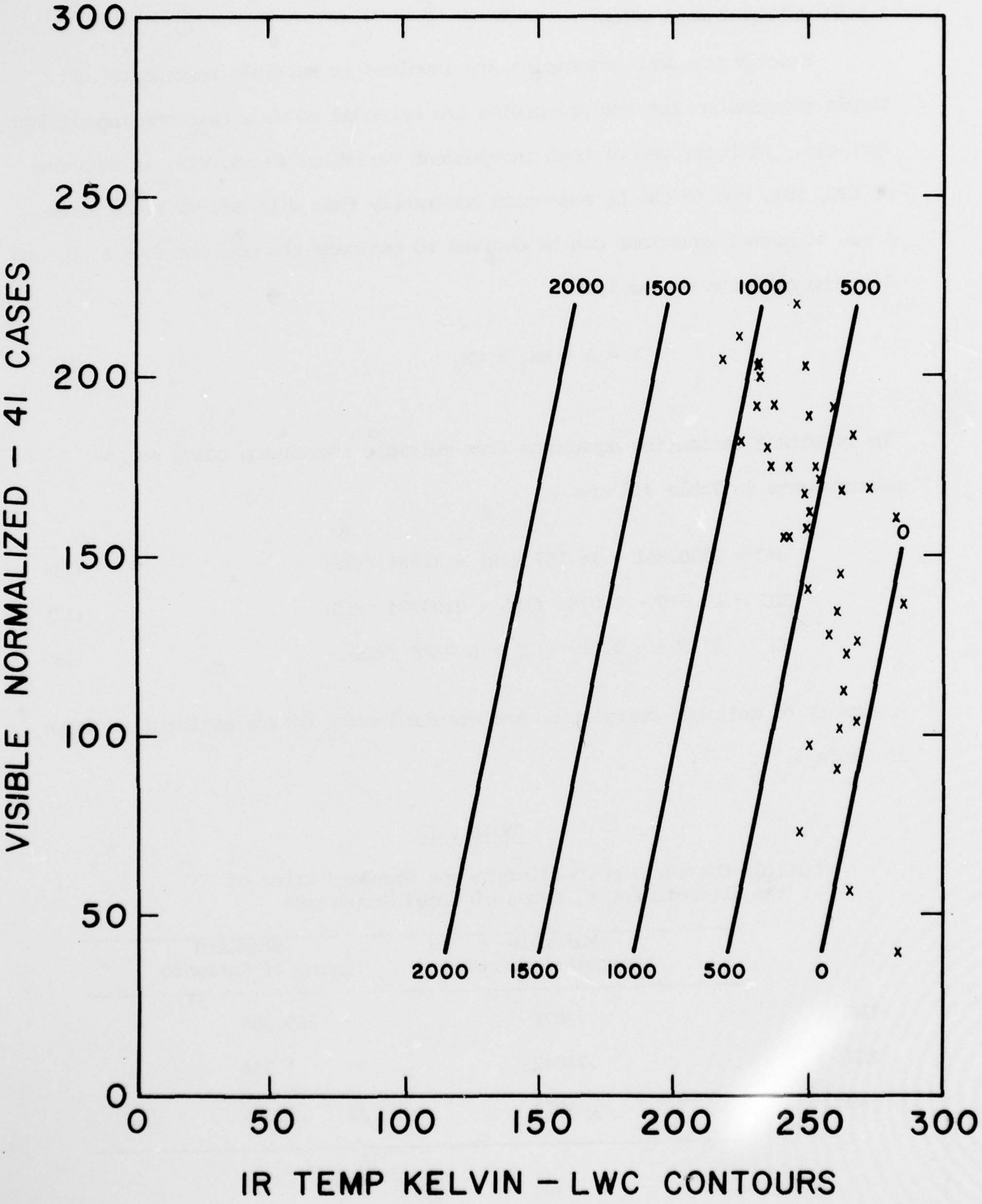

Fig 3.13 Scatter diagram relating LWC to both IR temperature and reflected sunlight. Solutions of the linear Equation (11) are also plotted.

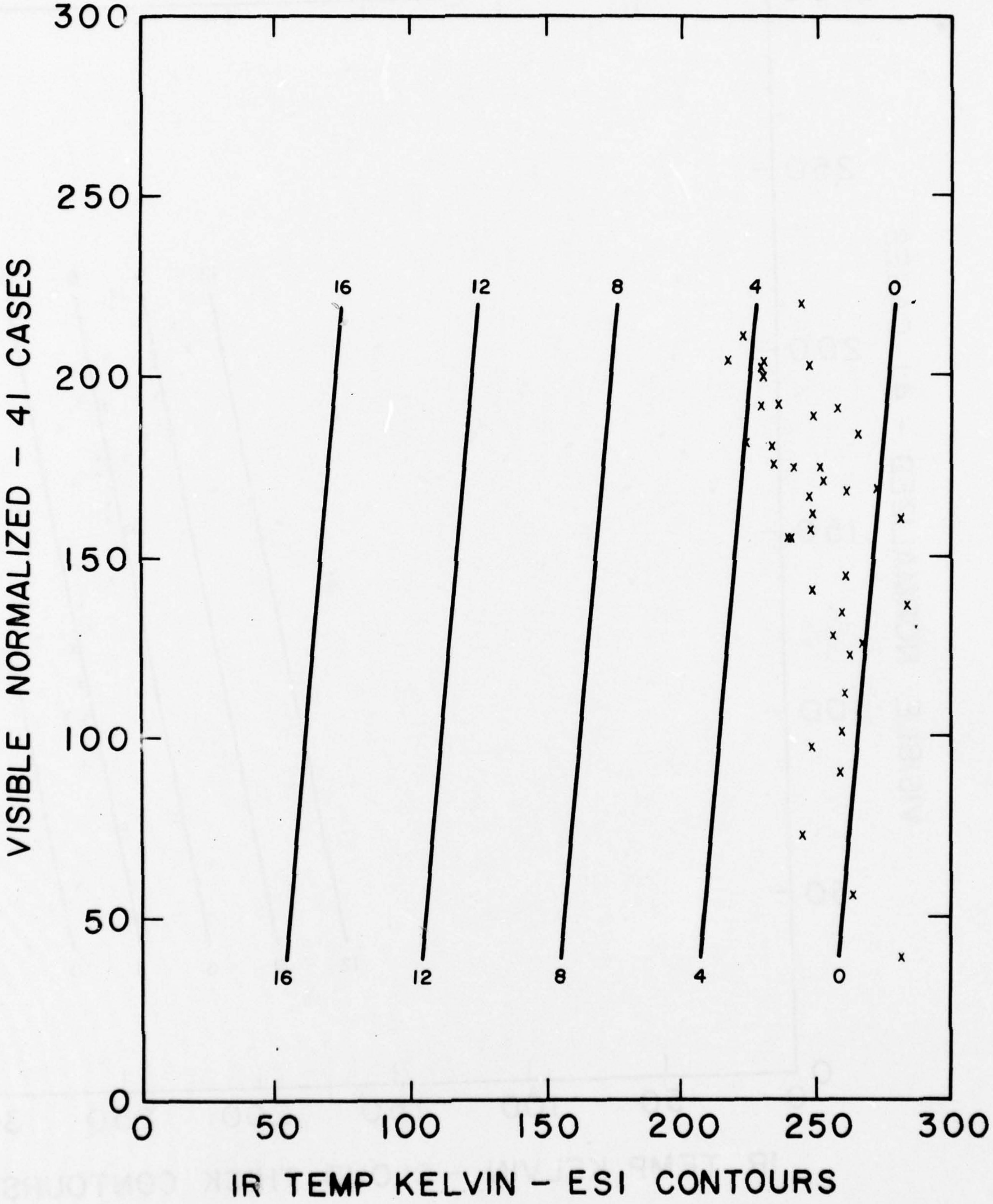

Fig 3.14 Scatter diagram relating ESI to both IR temperature and reflected sunlight.

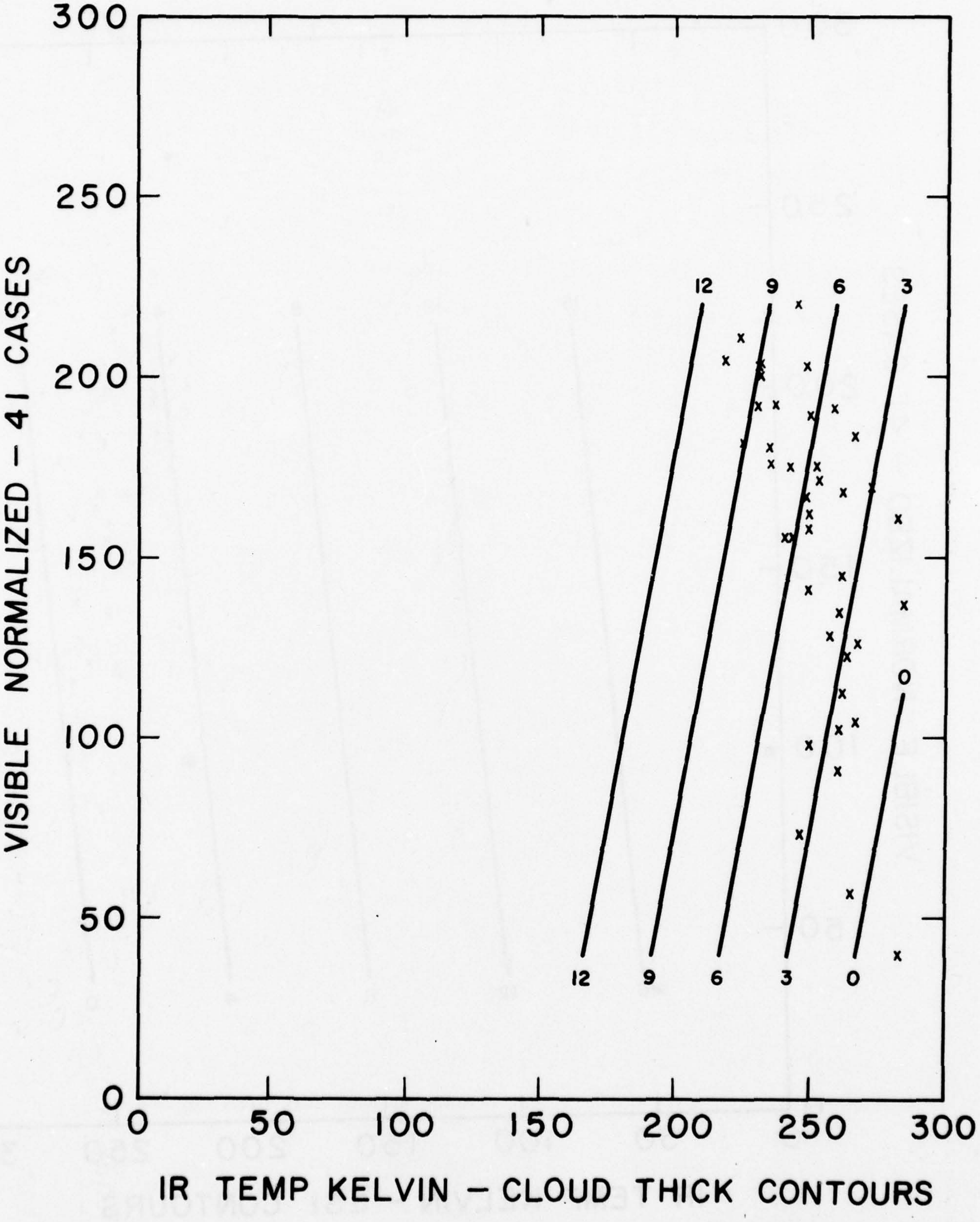

Fig 3.15 Scatter diagram relating total cloud thickness to both IR temperature and reflected sunlight.

The regression plane defined by the equation is designed to pass among the points so that the sum of squares of vertical distances from plane to points is a minimum. However, the statistics of multiple regression are subject to sampling variation and a final test of significance was conducted. An F-test similar to that conducted in Section 3.5.4 above proved highly significant. This means that IR and VIS as joint predictors of LWC, ESI, and ΔH are almost certainly valid and offer improved estimates over IR or VIS alone. Solutions of equations (11), (12), and (13) and shown as straight lines in Figures 3.13, 3.14, and 3.15. In multiple regression, as in single regression, the IR is a better predictor than VIS. This conclusion could be expressed in terms of statistical tests, but it is readily apparent by comparing the regression slope coefficients of IR and VIS in equations (11), (12), and (13).

Multiple regression was also done for inverse forms of the VIS and IR, as independent variables. These nonlinear forms generated slightly higher multiple correlation coefficients and slightly lower standard errors of estimate for the cloud properties LWC and ESI. There was less improvement in the case of ΔH.

3.5.6 Conclusions

Clouds which are brightest in the VIS and coldest in the IR have the largest LWC, ESI, and ΔH. IR temperatures are better predictors than VIS by a small amount. The equations to predict cloud properties from satellite IR and VIS have statistical significance according to established F tests. The simple form of the prediction equations lends itself readily to machine computation of cloud property estimates. Nonlinear forms of prediction equations offer slightly better predictions than the linear forms.

3.6 Objective Prediction of Cloud Cover and Precipitation

3.6.1 Introduction

The Air Weather Service is making significant changes in its operational format to meet demands for increasing services with fewer people. Among the goals being sought by the AWS are automation of observations, centralization of product preparation, and tailoring selected products to be used by the operator with a minimum of interpretation by meteorologists. In many cases, the technology needed to achieve these goals is readily available and needs only be modified for application to a specific problem.

At the present time sun-synchronous and geosynchronous satellites cover the globe many times per day providing large quantities of detailed, continuous information not readily available from other sources. However, two special problems are posed in the application of satellite data to automated processing. The first problem is handling the huge volume of data generated by the imagery sensors. An investigation of one aspect of this problem is reported in Section 3.4 of this report. A second problem is translating the necessarily subjective satellite photoanalysis into an automated objective form which can be processed by computers. The ability to achieve a primitive or partial solution to this second problem is implicit in the work reported herein.

3.6.2 Objective

The space and time scales of geosynchronous satellite imagery are consistent with the needs of short-range, mesoscale forecasting. The AWS has a requirement for continuously updated, automated, short range forecasts of weather events that are important to operational missions. The work in this investigation is one phase of a larger study concerned with the development

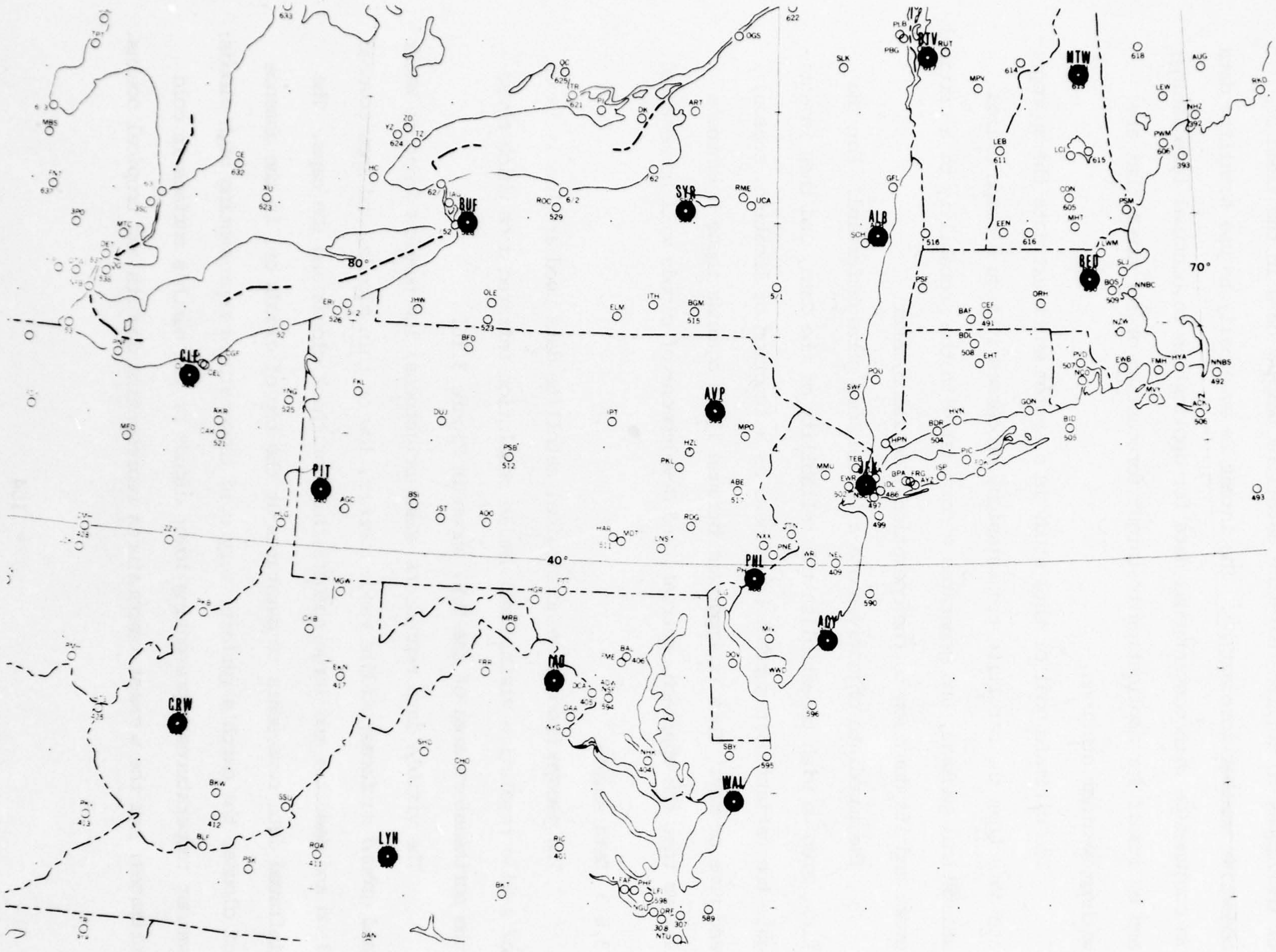
BTV
MTW
ALB
SYR
BUF
BED
AVP
JFK
CLE
PIT
PHL
ACY
IAD
CRW
WAL
LYN
70°
80°
40°
OGS
SLK
PLB
PBG
RUT
MPV
614
LEB
611
EEN
616
CON
605
MHT
PSM
PWM
AUG
LEW
NHZ
GFL
SCH
PSF
POU
SWF
BAF
CEF
491
BDL
508
EHT
ORH
BOS
509
NZW
PVD
507
EWB
FMH
HYA
NNBS
492
ACK
506
GON
BID
505
HVN
BDR
504
HPN
TEB
EWR
502
ISP
493
ART
UCA
RME
DK
OC
625
TR
621
ROC
529
ELM
ITH
BGM
515
OLE
523
BFD
JHW
ERI
526
FKL
DUJ
IPT
MPO
HZL
PKL
ABE
517
PSB
512
BSI
JST
AOO
HAR
511
MDT
LNS
RDG
PNE
NXX
WRI
NEL
409
590
596
MIV
DOV
WWD
SBY
595
MGW
HGR
MRB
FRR
BAL
406
DCA
405
ADW
NYG
CKB
EKN
417
SHD
CHO
BKW
412
BLF
SSU
ROA
411
PSK
RIC
401
BAT
DAN
ORF
308
307
NTU
589
AKR
CAK
521
MFD
CGF
ZD
YZ
624
TZ
HC
CE
632
XU
623
MBS
DET
MTC
FNT
637

Fig 3.16 Area of satellite imagery data. Surface reports saved for stations with bold markings.

of techniques to utilize real-time satellite imagery data in the field of objective weather forecasting. The intent is eventually to use satellite data in conjunction with conventional data for application to terminal forecasting; and by itself for application to target forecasting or for areas that are without weather stations.

The ultimate goal of this study is a system which extracts the appropriate data from the satellite transmission, processes it thru a computerized statistical package, and generates a forecast with the probability of a critical event and its duration to the operational decision maker.

The immediate objectives are a little more straightforward. For the first step we wish to establish the reliability of the data, and then investigate the variation in surface brightness as a function of location, season, and time of day. This is important because it is against these brightness values that the approach, retreat, and development of clouds will be measured.

3.6.3 Data sample

The geosynchronous meteorological satellite data used are hourly tapes of 1-mile resolution visible and 4-mile resolution infrared data which cover the northeastern area of the U.S. shown in Figure 3.16.

The visible data represents scene brightness: low numbers indicate water and ground surfaces; middle range numbers, low or thin clouds, and snow covered land and deserts; and large numbers, high or thick clouds and ice caps. The infrared data represents temperatures at the top of clouds or, in the absence of clouds, the earth's surface: very cold temperatures representing high clouds; warmer temperatures representing lower clouds or the earth's surface in cold climates; and the warmest temperatures representing deserts and tropical oceans.

In order to identify cloud amounts and predict their motion, the brightness signature of the earth's surface must first be determined. This in turn varies with the land/water configuration, the season of the year, i.e., color of the ground, and the time of day.

Two hundred fifteen essentially clear observations from March to December 1977 were chosen to determine the ground signature for a given day, time and location. The locations chosen for this study are Bedford, Boston, Albany, Pittsburg, and Dulles International Airport in Virginia. Plans called for collecting data throughout the working day. Preemption of the system by higher priority projects prevented the collection of afternoon data during May, June, and July.

With the given stations as the center points, visible data to cover 120 rows by 120 elements and infrared data to cover 30 rows by 132 elements were located and extracted from the archived data. Ranking these numerical sets of visible (VS) and infrared (IR) data into 24 classes, and assigning them the letters A - W,when printed out, gave a dramatic visual map of the chosen areas centered on the above locations. Land and water configurations could be easily seen and identified especially along the New England coastline. These printouts were initially used to verify the locations of landmarks in the data array.

3.6.4 Data corrections

The McIDAS system is used interactively to obtain a correction factor to fine-tune the navigation to a 2-mile or better accuracy necessary for the fine time and space scales required for mesoscale forecasting. This correction factor is determined by the difference between the line and element specified as the geographic coordinates of a landmark after the initial navigation, and

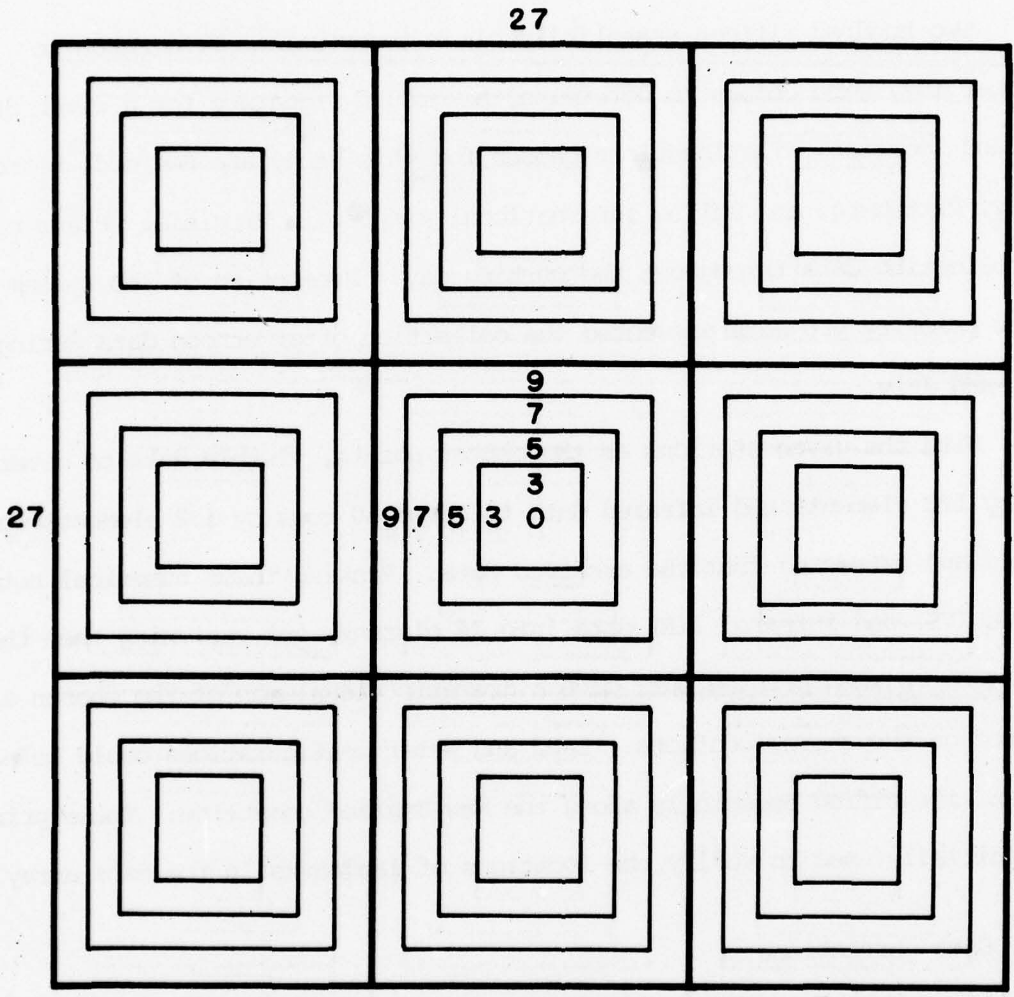

Fig 3.17 Geometric arrangement of image brightness statistics about a test station. Computations were made within each of the 9x9 pixel boxes for the smaller boxes as indicated at the center. The statistics were also computed for the entire 27x27 pixel area.

those obtained when the cursor is placed on that landmark on the screen. A 2-mile accuracy results when 3 good landmarks are visible, and 3-4 mile accuracy for 2 landmarks. This correction factor is valid for all points shown in Figure 3.16.

Examination of the averages of brightness for entire lines of data indicated systematic variations from line to line. These variations were indicative of slight differences in the sensitivity of the sensors. Although the variation amounted to only about 1%, the brightness values were adjusted. The average of all picture elements (pixels) sensed by each of the 4 scanners individually were made to agree by adding or subtracting appropriate constants from each brightness value.

Random RF noise was also taken into consideration and, if detected, an adjustment was made in the data. Noise was identified when the average brightness for a line departed more than approximately 13% from the average for the previous line. When this occurred, each pixel in the line was replaced by the average value of the pixel in the non-noise line above and the pixel in the next non-noise line below.

3.6.5 Data sampling

The spatial stability of the brightness data was examined by selecting an area of 27 x 27 pixels surrounding the selected site. This 27 x 27 (729) array was subdivided into nine 9 x 9 boxes, Figure 3.17. Each box was further subdivided into 7x7, 5x5, and 3x3 boxes. The total 27 by 27 box represents approximately 25 by 35 mile area which is close in size to the 3-D Nephanalysis unit.

For each 9, 25, 49, 81 and total 729-pixel box, the average, standard deviation, maximum, minimum, and range of brightness were computed. Figure 3.18

```
                        CENTER

BLOCK      ONE       TWO    THREE     FOUR

  AVG   21.528    20.990   21.235   21.228
   SD    3.495     3.158    3.524    3.779
  MAX       31        31       36       38
  MIN       19        19       19       19
RANGE       12        12       17       19
```

Fig 3.18 Sample of the format in which 9x9 pixel-box data, stored on tape, can be printed. Each printout-sheet contains this format for the central and 8 surrounding boxes arranged as in Figure 3.17.

is a sample of the output data for one 9x9 pixel box which is stored on tape for each hour used in the study.

A comparison of the average, standard deviation, maximum, minimum and range of brightness for the 9, 25, 81, and 729 pixel boxes centered on the selected site on clear days is shown in Table 3.13. The chart indicated that the statistics are relatively stable when computed from 9 to 729 pixels and that 9 pixels can provide sufficient accuracy for most uses.

Table 3.14 shows the brightness statistics for nine 9x9 pixel areas arranged as in Figure 3.17 for four clear observations at 16Z, and an observation with scattered clouds, shown in parentheses, on one of the same days at 14Z. The statistics of the clear observations show remarkable similarity from box to box. When scattered clouds were reported, the standard deviation was as much as 5 times larger and the maximum values were higher because of the clouds. The minimums were lower because the sun was lower in the sky.

This stability of the ground brightness values over a range of sample sizes and spatial distributions bespeaks an instrumental stability that should make possible the detection of subtle changes in clouds and cloud configurations.

3.6.6 Brightness analysis

An analysis was done of the average brightness for clear days at each of the 4 key stations, Bedford, Albany, Pittsburg, and Dulles. An example for July is shown in Figure 3.19. Low scattered clouds, newly forming, are indicated when the standard deviation is less than 10; more advanced scattered cloud development, denser scattered clouds, or bigger patches of cloudiness are indicated when the standard deviation is greater than 10. As can be seen,

TABLE 3.13 Brightness Statistics at Bedford MA at 1600Z as Function of Area on April 29, May 3, May 12 and May 23, 1977

No. Pixels		1	9	25	49	81	729
Average	4/29	18	17.2	17.3	17.3	17.5	17.4
	5/3	19	18.0	17.7	17.8	17.8	17.8
	5/12	19	18.1	18.1	18.0	17.9	17.8
	5/23	18	18.1	17.7	17.6	17.5	17.6
Stand. Dev.	4/29		0.5	0.7	0.7	0.7	0.8
	5/3		0.8	0.8	0.8	0.7	0.7
	5/12		1.1	0.9	0.8	0.7	0.8
	5/23		0.4	0.5	0.6	0.6	0.7
Range	4/29		1	3	4	4	6
	5/3		2	3	3	3	5
	5/12		4	4	4	4	13
	5/23		1	2	3	3	5

Table 3.14 Brightness Statistics over 9x9 Pixel Areas Surrounding Bedford at 1600Z

On April 29, May 3, May 12 and May 23, 1977. (1400Z on May 3, 1977 Shown in Parentheses)

	4/29	5/3	5/12	5/23	4/29	5/3	5/12	5/23	4/29	5/3	5/12	5/23
AVG	17.1	17.6 (16.1)	17.6	17.4	17.4	17.8 (16.0)	17.8	17.8	17.5	17.8 (16.5)	18.0	17.5
SD	.73	.70 (1.45)	.63	.58	.93	.73 (1.30)	.65	.68	.83	.73 (2.13)	1.53	.68
MAX	19	20 (24)	19	19	20	20 (22)	19	19	19	19 (27)	28	19
MIN	15	16 (14)	16	16	14	16 (14)	16	16	15	16 (14)	15	15
RNG	3	4 (10)	3	3	6	4 (8)	3	3	4	3 (13)	13	4
AVG	17.2	17.5 (18.1)	17.6	17.5	17.5	17.8 (17.9)	17.9	17.5	17.6	18.1 (16.7)	17.9	17.9
SD	.65	.68 (3.50)	.55	.55	.70	.73 (2.95)	.73	.60	1.0	.65 (1.43)	.68	.65
MAX	19	19 (32)	19	19	19	19 (27)	20	19	20	20 (21)	20	20
MIN	16	16 (13)	16	16	15	16 (14)	16	16	15	17 (14)	16	17
RNG	3	3 (19)	3	3	4	3 (13)	4	3	5	3 (7)	4	3
AVG	17.4	18.0 (15.9)	17.9	17.7	17.4	17.7 (16.1)	17.9	17.6	17.8	18.2 (15.9)	17.9	17.9
SD	.73	.58 (1.43)	.55	.68	.68	.55 (1.78)	.55	.60	.68	.63 (.75)	.53	.68
MAX	19	19 (25)	19	19	19	19 (26)	19	19	19	19 (17)	19	19
MIN	16	16 (13)	17	16	16	17 (14)	17	16	16	15 (12)	16	15
RNG	3	3 (12)	2	3	3	3 (12)	3	3	3	4 (5)	3	4

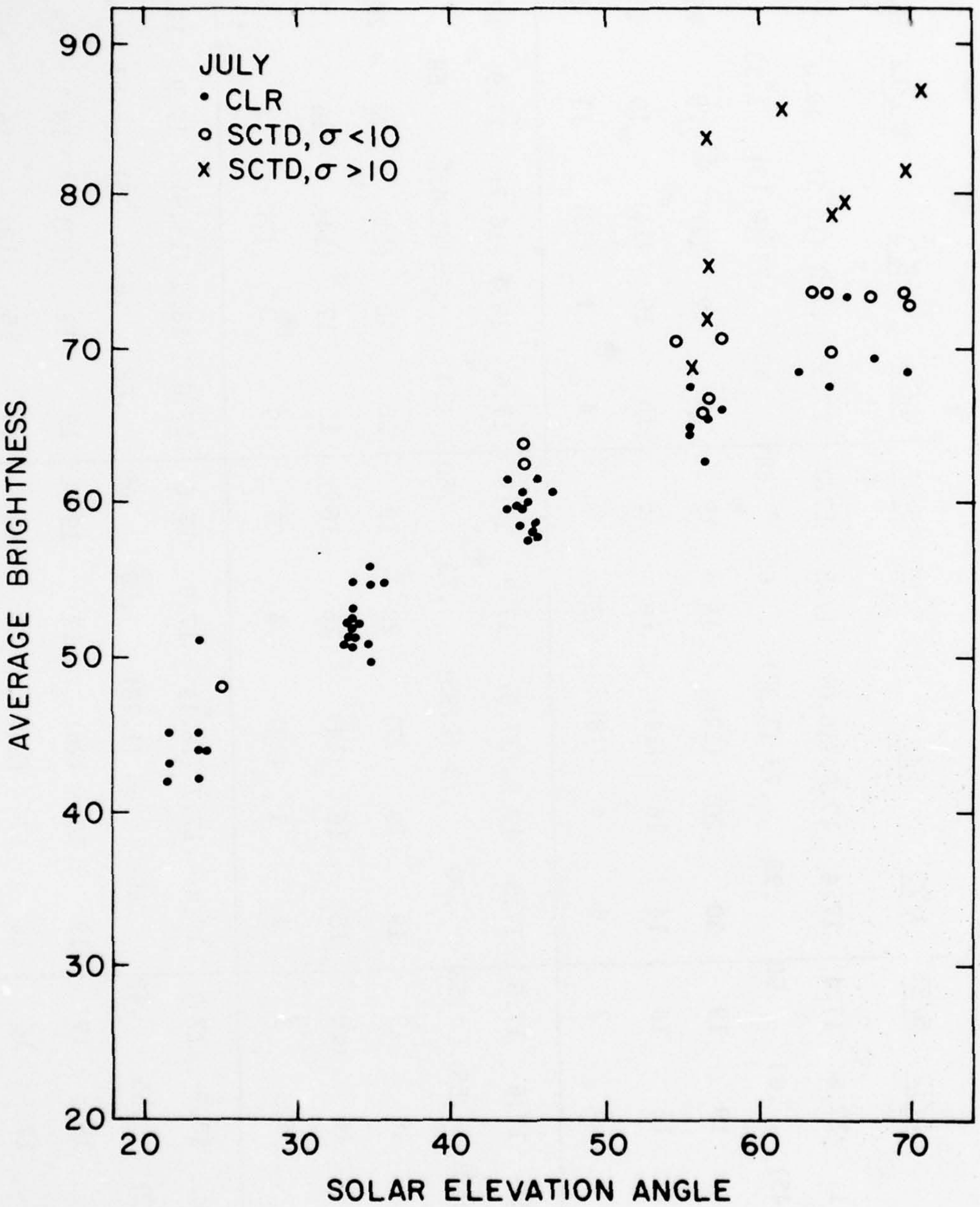

Fig 3.19 Scatter diagram of average ground brightness of a 9x9 pixel boxes centered at the 4 test stations during clear and scatter conditions.

when the standard deviation is small the points fall along the same line as the clear cases. Some of the widely scattered cases are included in the statistics to enlarge the sample for this initial study.

High, thin scattered clouds have little effect on the average brightness, and clear sky data may also include some of these cases. In contrast, haze did have a noticeable effect characterized by a brighter shade and a very small standard deviation. Haze cases were excluded and will be handled later.

In order to determine whether the minimum or average brightness is the better indicator of clear skys, both the minimum and average brightness for 729 pixels were correlated with solar elevation angle for selected days and hours at different locations.

The y intercepts and the slopes of the regression equations were computed, as was the standard error of estimate S_y. Figures 3.20 thru 3.24 show that the resulting correlation coefficients, standard errors of estimate, and the slopes are almost identical for both the minimum and average brightness.

3.6.7 Conclusions

There does indeed exist a stable relationship between background brightness and solar elevation angle from day to day and place to place. Variations result from seasonal changes in the characteristics of the surface texture and coloration. In this sample, brightness did not vary greatly among the 4 key locations, but a larger sample of data from this same region might change this conclusion. Certainly it will change as samples are analyzed from other than the northeastern United States.

A summary of average brightness over 729 pixels vs. solar angle is given in Figure 3.25. Almost all correlation coefficients were above 0.90 for

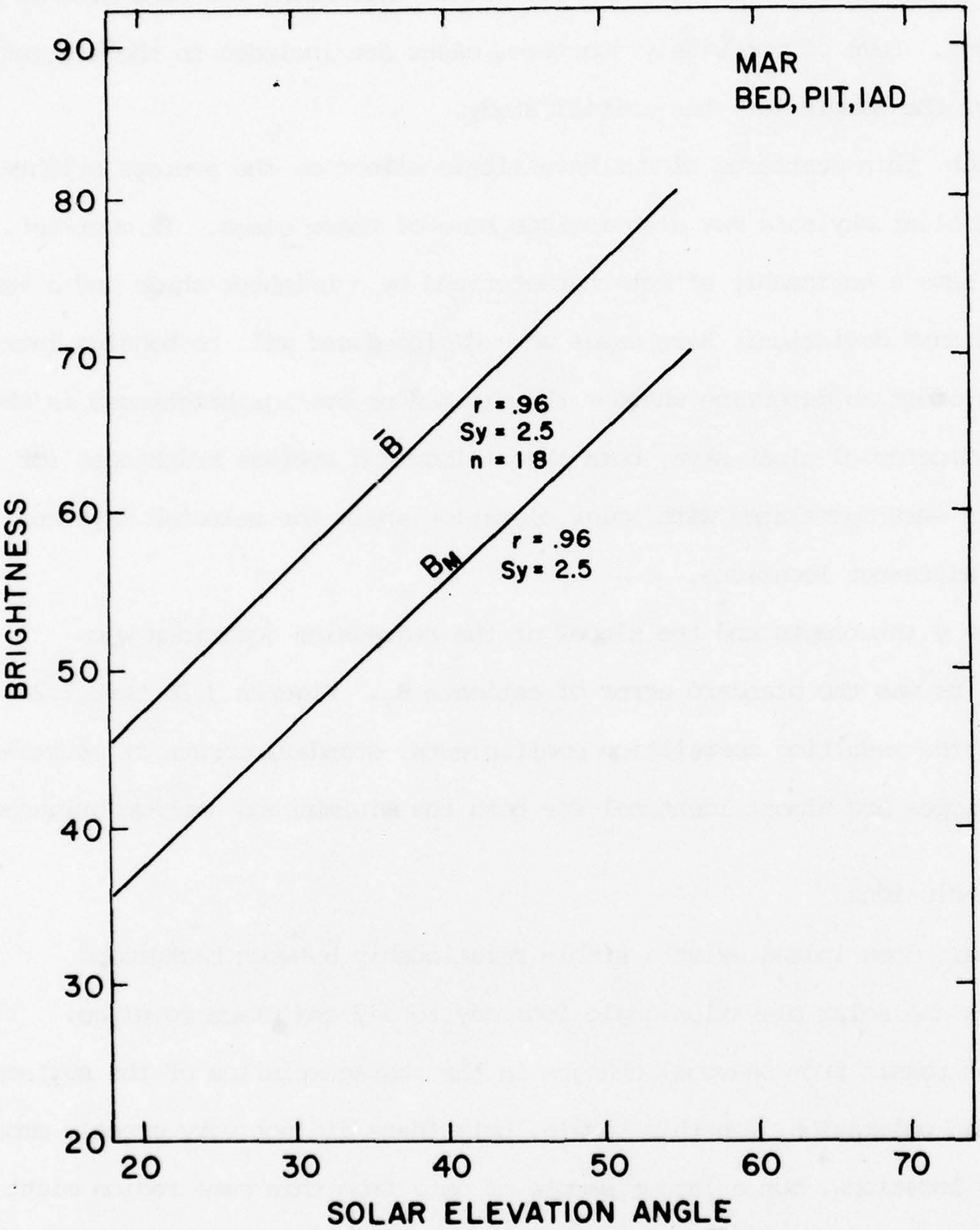

Fig 3.20 Graph of the regression equation for average ($\bar{B}$) and minimum (B_m) ground brightness vs. solar elevation angle on clear days for stations indicated on graph for March 1977. r is the correlation coefficient; S_y, the standard error of estimate· and n, the number of cases.

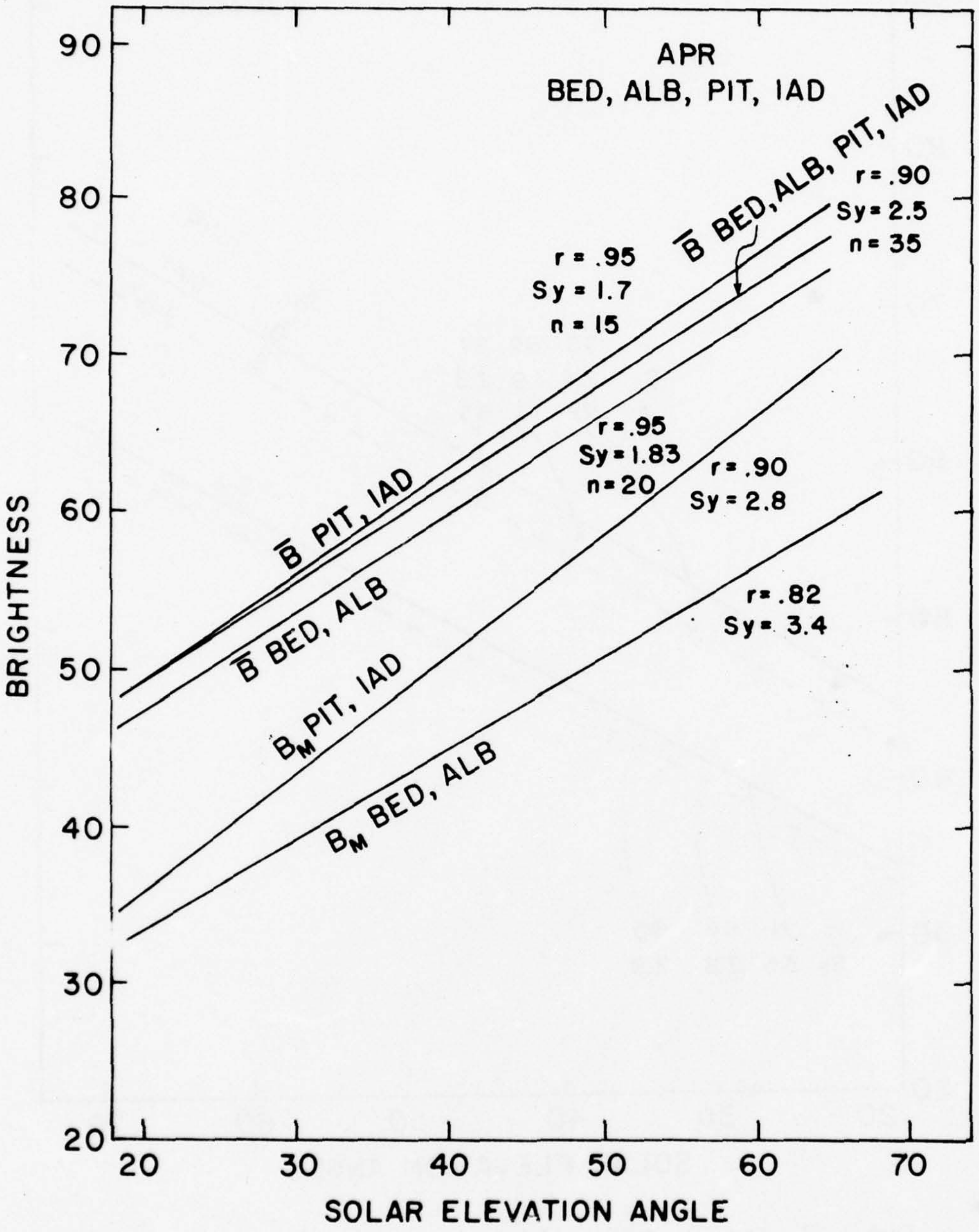

Fig 3.21 Same as Figure 3.20 except for April

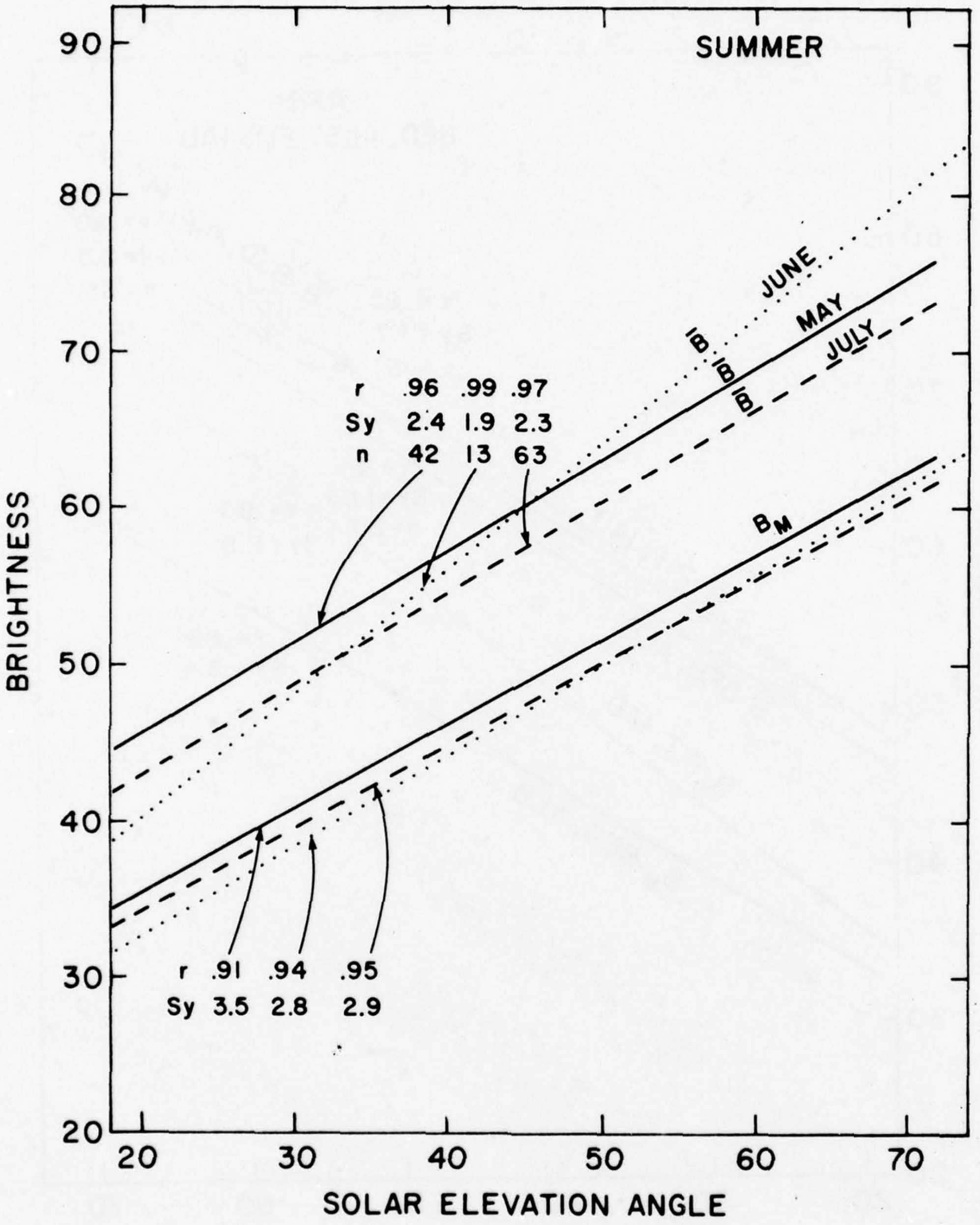

Fig 3.22 Same as Figure 3.20 except for May, June and July.

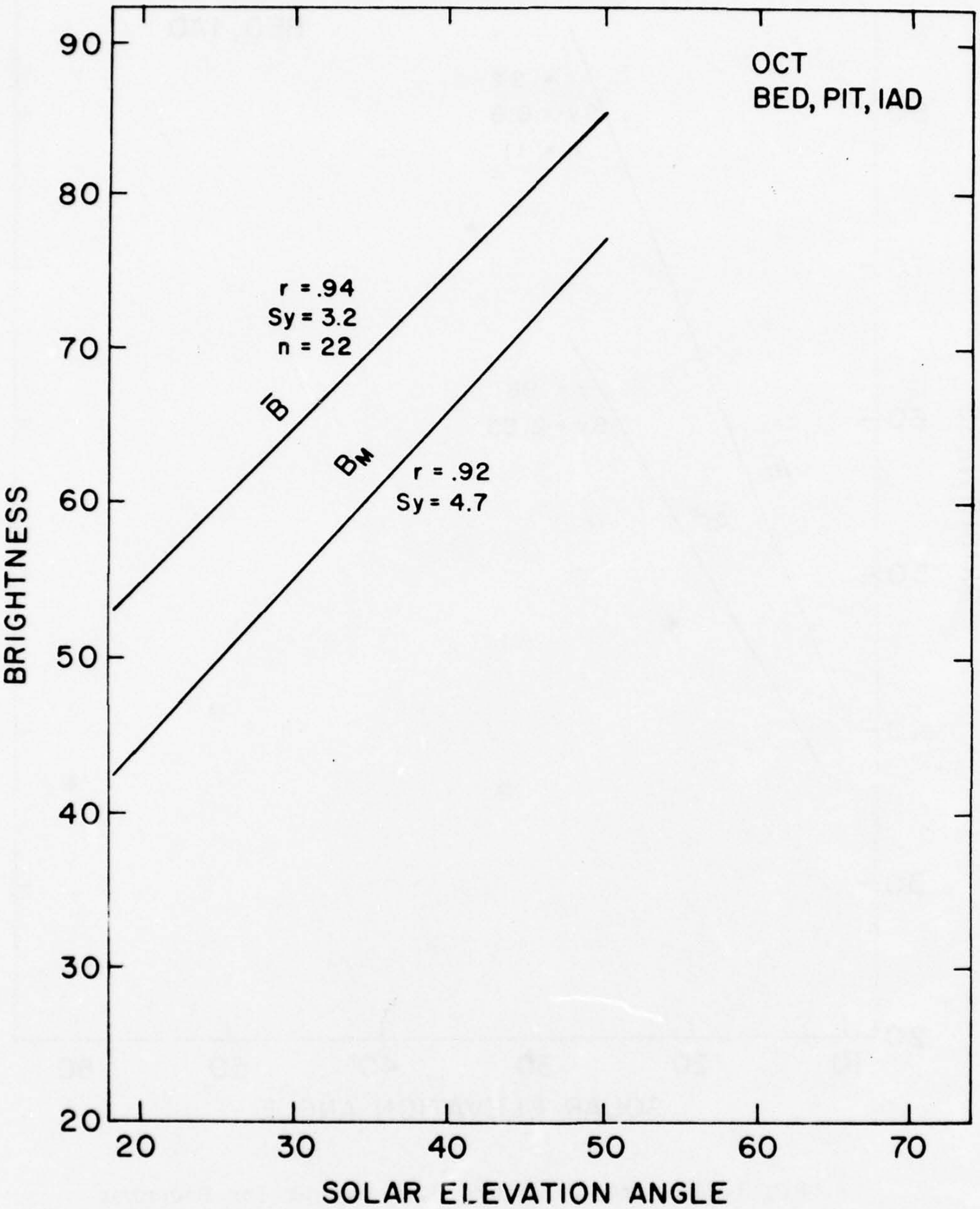

Fig 3.23 Same as Figure 3.20 except for October

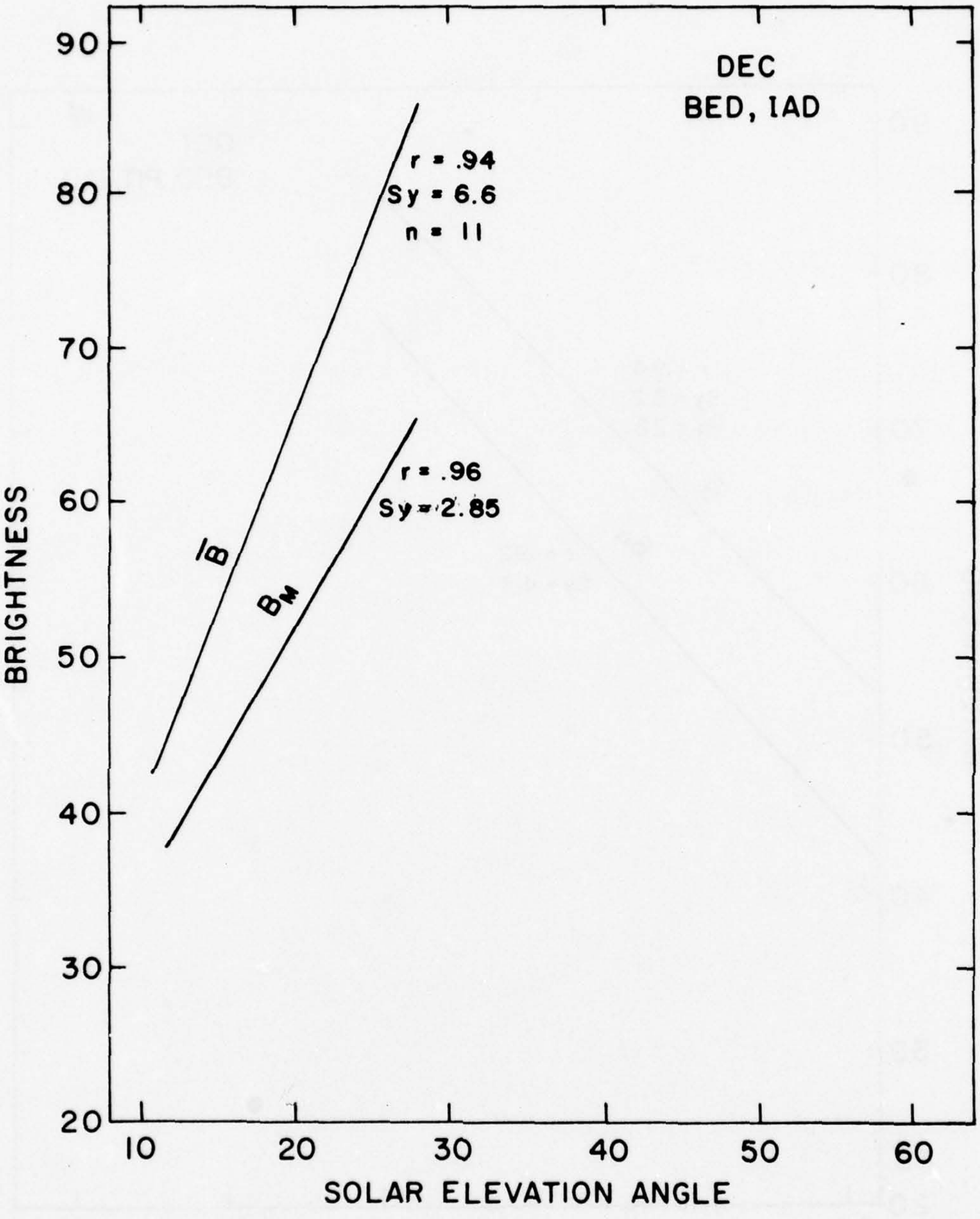

Fig 3.24 Same as Figure 3.20 except for December

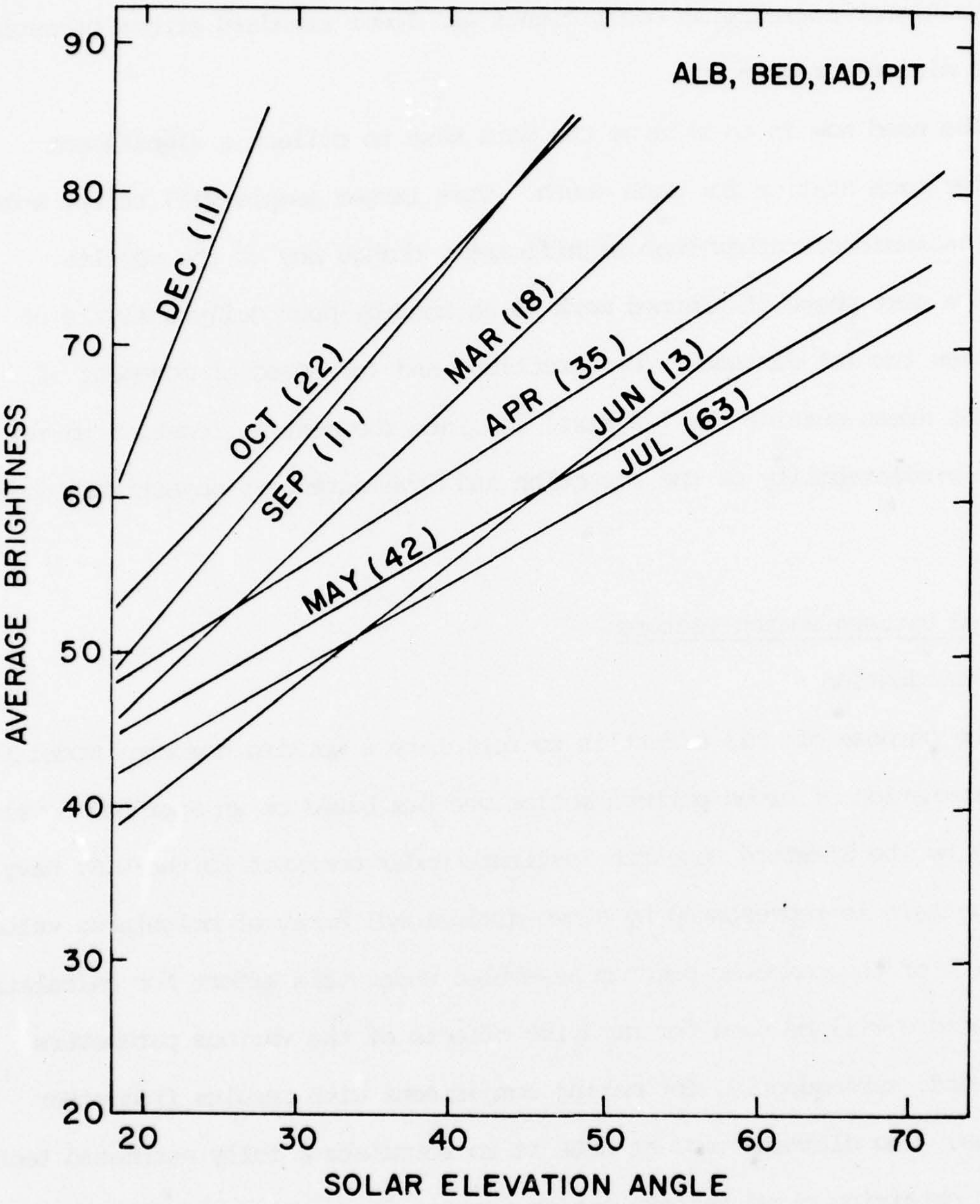

Fig 3.25 Monthly variation of average ground brightness as a function of solar elevation angle. Numbers in parentheses are the number of cases included in each month.

these combined locations. In all but one case, December, the average brightness have higher correlation coefficients and lower standard errors of estimate than the minimum brightness.

The need now is to enlarge the data base to collect a significant sample for each station for each month. This larger sample will refine some of the conclusions, rather than significantly change any of the results.

The next phase of planned work is an hour-by-hour daily analysis of cloud cases for (a) distance, (b) direction, and (c) speed of movement of brightness areas outside the 729 pixel box into the central location to estimate the predictability of the advection and development of objectively defined clouds.

3.7 Cloud Pattern Motion Vectors

3.7.1 Introduction

The purpose of this effort is to formulate a working computer model for the determination of cloud pattern motion vectors based on an approach developed primarily by the Stanford Research Institute under contract to the U.S. Navy. A cloud pattern is represented by a two-dimensional array of brightness values. The version of the computer program assembled under this effort for calculating motion vectors will be used for studying effects of the various parameters involved and, subsequently, for making comparisons with results from other approaches. The ultimate goal at AFGL is to formulate a fully automated technique for obtaining cloud pattern motion vectors for use in shortrange sensible weather prediction studies.

The requirement that the technique be automatic, being accomplished from beginning to end by computer, greatly increases the difficulty of such a development as compared to those requirements which can settle for a semi-automatic approach. However, there are a few candidates for the automatic approach to motion vectors which show promise. The one formulated here is patterned after the one developed at the Stanford Research Institute (SRI) and described by Endlich et al.[18]

Much of the work in recent years on calculating cloud motion vectors has either explicitly or implicitly had as a goal the estimation of wind velocities. This is not our goal either explicitly or implicitly. Cloud pattern motion vectors have a raison d'etre apart from their implication of winds; namely as an aid in generating cloud and other weather element forecasts. The word pattern is used to emphasize the fact that the goal is that of tracking arrays of brightness instead of individual elements of brightness.

The object pursued here is somewhat different from that which gave rise to the SRI model. A single velocity vector which is representative of an area of the order of 90x90 n.mi. is sought. SRI seeks synoptic or sub-synoptic motion vectors over large areas (where clouds permit of course). The Navy (NEPRF, Monterey CA) has recently begun an operational use of an interactive version of a more recent SRI model. Although this more recent model undoubtedly includes experience gained over the past few years, the principal change has been toward a simplification of the clustering process for the sake of computer time savings rather than for improved clustering. Clustering techniques are usually developed and applied to assist in the analysis of large amounts of data. Their development and use has been very rapid in recent years. Briefly, clustering techniques are computational means of grouping data. They are usually thought of as techniques for finding natural groupings of data since most of the research activity and applications occur in this area.

Our approach to motion vector analysis uses brightness centers to represent cloud patterns. Given two consecutive cloud pictures, brightness centers are obtained for both, and then the two sets of centers are matched. From this matching an overall vector is obtained. Ball _et al_[19] are accredited with developing this approach around their ISODATA clustering algorithm. No effort has been made here to improve on the technique of Endlich _et al_ (1971); an effort has been made to interpret it as accurately as possible from their report. Differences most likely do exist since the write-up does not give enough details to be certain what was done. This applies especially to the routine for finding brightness centers. Strengths and weaknesses of the steps taken will show up in experiments with the model and comparisons of it with other techniques.

3.7.2 Three significant steps to motion vector analysis

There are three significant steps to motion vector analysis in this approach: (a) Simplification of cloud images by truncating at some brightness level or by some other process such as spacial averaging; (b) Application of a clustering procedure to obtain representative brightness centers; (c) Pairing off of members of two sets of brightness centers to obtain motion vectors. A discussion of each of these is in order before laying out the details of the computer version assembled for AFGL. The flexibility of this approach is, as might be expected from the above steps, considerable.

(a) Simplification of Cloud Images

Simplification of the images is necessary because of limitations imposed by computer storage and running time. Even with simplification by truncating to a one-bit brightness level and taking, for example, every other element of every other row, the problem of obtaining good sets of brightness centers by clustering is no minor process in terms of computer time. Simplification is a necessity. There are many ways this can be done other than truncation. The main idea here is to obtain a simplification that best represents those features that are of interest for tracking. This step has received little comment in the literature. How best to simplify? This is a good question but, so far, there have been no good answers. The answer could be important in any efforts to improve the model such as separating cloud motions at different levels or obtaining the motion most significant in terms of station forecasts. In addition to this, there are many more unknowns which require extensive experiments in order to understand them well. Different channels could be used separately or composited in some way. The possibilities for this step seem unlimited. The first step, to save time and energy, for an indepth exploration would naturally be time spent at an interactive graphics console to narrow down the field of possibilities.

(b) Clustering Brightness Areas

The clustering of brightness areas and use of their centers to represent cloud patterns is the core of this approach and is at the same time its weakest link. Simplifications in the clustering process are required at the expense of completeness. The guiding idea here is to take the simplified cloud images and obtain locations of major brightness centers. Then two consecutive images would be expected to resemble each other except for the shift resulting from motion of the cloud pattern. The procedure must contend with complications such as (a) patterns moving partially off (or over) the area of interest, (b) changes in brightness areas or number of brightness centers due to growth or dissipation, (c) brightness centers splitting or combining, and (d) coping with the flimsy, irregularity of what we refer to as "clouds" and "cloud patterns".

(c) Pairing the Two Sets of Brightness Centers

Once brightness centers are obtained the remaining problem is to pair, where possible, centers on the first image with centers on the second image in such a way that they would be judged the same points in the pattern at different times. The difficulty here lies in designing the model to cover a very wide range of cases. First of all, the number of points in the two sets need not be the same for the reasons mentioned in the previous paragraph. Important factors in this analysis is the distance between brightness centers, the number of centers, and the area associated with the centers. These factors are obviously interrelated. Another important consideration is the interval of time between the two images. The distance between centers relative to motion distance is an important factor in the process of pairing. Best results are expected when center separation distances are large relative to the motion distance and vice versa.

Each of the three important steps in the analysis, simplification, clustering and pairing, can be upgraded without serious impact on the other two. Which parts are in need of improvement, if any, can be determined from rather simple comparisons with more reliable semi-automatic methods.

3.7.3 Computational details of motion vector model

Details of the computational model will now be given in sufficient detail to permit duplication. As compared to the actual implementation by SRI, the model developed here is simple and straightforward. This simplicity of structure permits modifications and improvements where necessary without getting into complications that require an unreasonable amount of experimentation. It seems to us there is little reason to employ a clustering routine that goes to as great a depth of precision as does the SRI ISODATA routine when the problems of accounting for cloud pattern changes other than translation are a major source of error. Recent developments at SRI of their model indicates an agreement on this point. In any event, the technique developed here will yield improvements in whatever components that might be needed. It will also yield readily to adjustments to different images, image sizes, and pattern scales.

a. Preparation of Arrays

The first step was to develop a procedure that would permit computer runs of the model on many different kinds of cloud patterns. A program was written (COZHA) which takes a prescribed array from a data tape of the Geostationary Operational Environmental Satellite (GOES) and places it into a permanent file at the AFGL Computer Center. These arrays are kept in the same resolution as is recorded on the satellite data tapes. For the visible data channel, which is of current interest, there is approximately one picture element per mile. These images consist of every other element and every other line of the initial one-half mile resolution GOES data. Simplifications in these data are needed that are most advantageous to the model.

The array size chosen for current studies is 90x90 n.mi. The selection of this size area represents an effort to obtain a balance between (a) small enough to be representative of small scale changes, (b) large enough to include enough cloud pattern to obtain a representative reading of motion.

The computer program COZHB takes arrays at two different times and obtains from them a motion vector.

b. Simplification by Truncation

There are many ways to simplify an image for further processing and little is known so far about advantages and disadvantages of them. Simplification is needed here to bring the data within a size that is reasonable in terms of computer storage capacities and times required for execution.

From the 90x90 picture element array every third column and every third row is taken. This results in a 30x30 array. The hundred brightest points are selected from this array for further use. An element is either in the hundred brightest or it is not. Actually, since there may be more than one point that ranks one-hundred, there may be a few points more than a hundred in this brightest category.

c. Calculation of Brightness Centers

Brightness centers are obtained from the arrays of truncated brightness by a clustering procedure using Euclidean distance as a measure of proximity of points. Passes are made through the data points to select brightness center locations. Each pass operates on the data in a similar way. The difference or improvement from one pass to another lies in the fact that some center locations (clusters) which do not have enough points in them are dropped. This provides a means for filtering out small areas of brightness. We have found that two passes of the routine for finding centers, are sufficient to obtain stable results. A minimum requirement of six points per brightness center gives results that smooth out small irregularities.

The procedure for locating centers rests on the computational operations of a pass through the list of x, y components of the data set composed of those hundred-plus highest brightness values.

A description of such a pass will be given. The center of gravity of all the points is obtained. This represents the location of the first brightness center. The points assigned to this center are those which lie within half the average distance of all points from the center of gravity. This fraction (one-half) is often referred to as the sphere factor. The value of one-half was found to work well from experience by SRI. The small amount of experimenting we have done indicates that it is a good value for this model. The next center is the first x, y encountered (reading left to right, top to bottom) that does not lie in the first cluster. The points assigned to this center are those which fall within the average distance but are not already assigned to the first cluster. Subsequent centers are found in the same way until all the points are exhausted. Clusters having fewer than six points in them are discarded. New centers of the clusters, excluding the first, of course, are defined as the average of the coordinates of the points within the clusters. Splitting of large clusters or combining of small ones occurs on the second pass only as a result of changes due to the dropping of the very small clusters. It has been found that a second pass through the data is all that is required to obtain good results. Additional passes through the data set do not change results enough to make them worthwhile.

d. Matching of Brightness Centers

The cluster centers for the two image times require a means of pairing off, where possible, to obtain measures of displacements. The number of centers for the two image times may be different and there may be centers without matches, i.e., those that have moved on or off the area of the image. The approach to matching centers followed here relies heavily on the center of gravity of the brightness field.

The motion of the center of gravity is taken as an initial displacement. This is always one component of the final motion vector. Other components are obtained when pairs of points lie within 20 grid intervals of each other relative to this displacement. This method follows SRI's approach and rests on their experimentation. It is expected that this parameter (20 grid intervals) will require some refinement by making it a function of both grid interval size and time between images. It is also expected that the center of gravity carries too much weight and that modification to lessen its influence would improve the results.

e. Example

Figures 3.26 and 3.27 show arrays of points (after two passes of the subroutine for obtaining cluster centers) obtained from two GOES images taken one hour apart. The grid size is approximately 6 n.mi. in both the x and y direction. The coordinates, row and column numbers, appear on the left and at the top, respectively. The difference in the column numbers resulted from a relative gridding error between the two images. This error was found by making comparisons of geographical features. The centers of brightness are marked by a C and a subscript which is a cluster number for referencing purposes. Table 3.15 shows the distance of separation of the two sets of centers relative to the motion of the center of gravity. Distances are in grid intervals. Pairs selected are shown on the right side of the table. Having obtained these pairs, an overall motion vector is obtained from the vectors defined by each pair of points. An average of the x and y components of these vectors produce components of an average vector. A velocity of 7.4 n.mi./hr with motion from 315 degrees was obtained for this case.

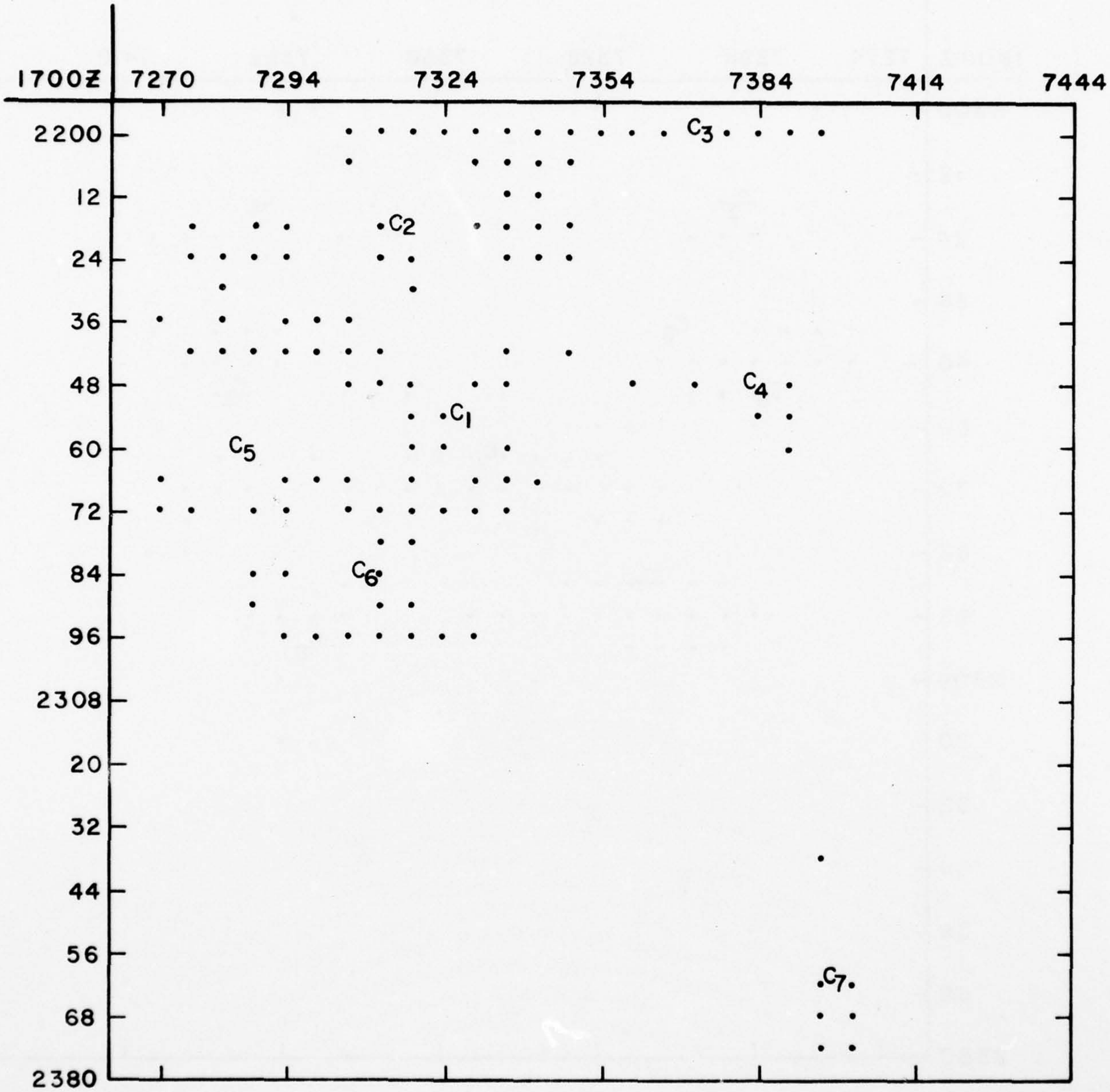

Fig 3.26 Centers of brightness for 1700Z and the "hundred brightest" points which remain after two passes through the routine for finding centers. See text for details.

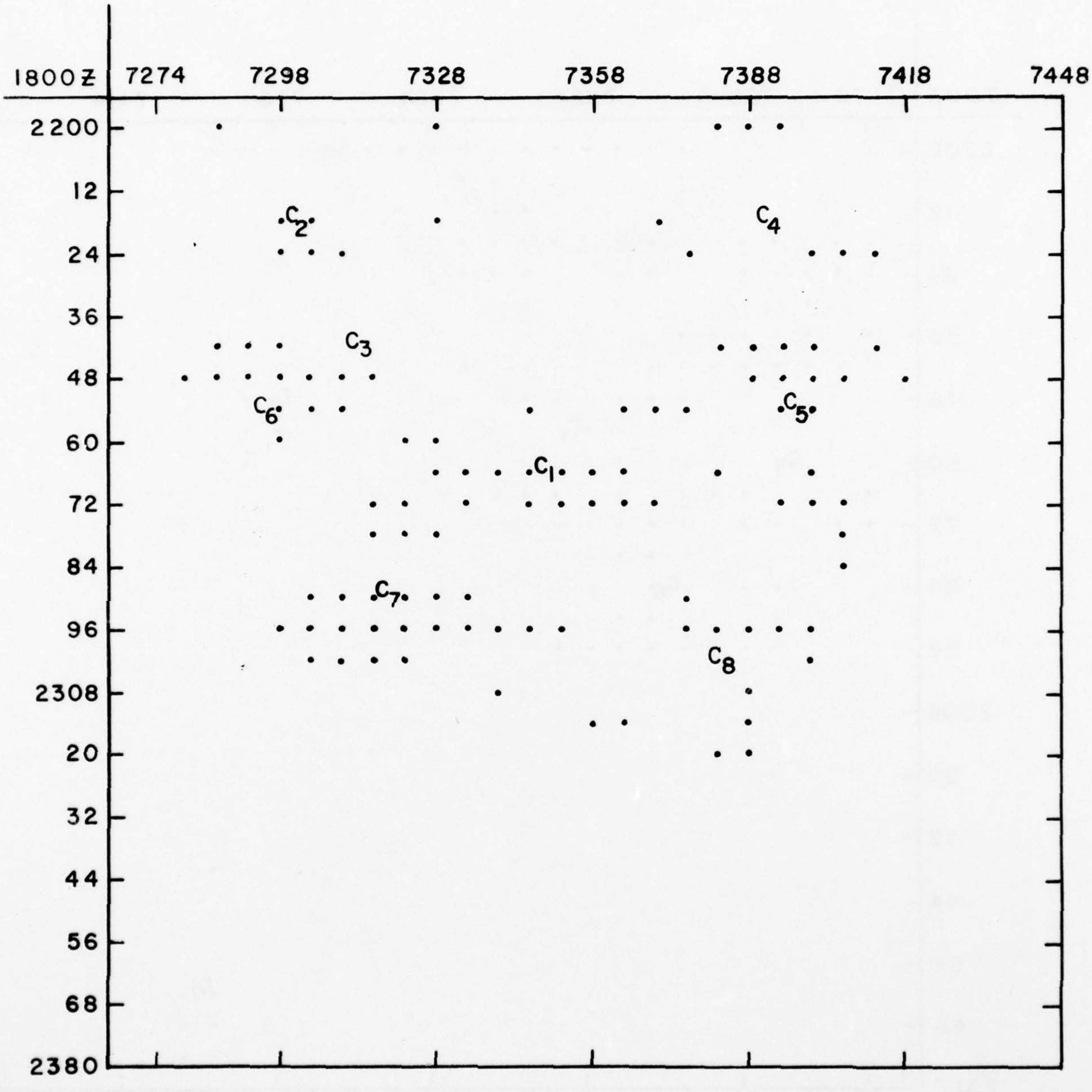

Fig 3.27 Same as Figure 3.26 but for 1800Z.

Table 3.15 Matching centers of brightness for the two images (See text for details)

		CLUSTER CENTERS FRAME TWO								
		1	2	3	4	5	6	7	8	PAIRS
CLUSTER CENTERS FRAME ONE	1	0	65	42	62	49	55	38	52	1/1
	2	39	37	31	55	67	49	65	88	--
	3	70	95	90	9	44	108	107	92	3/4
	4	52	112	93	50	13	107	82	38	4/5
	5	48	44	23	102	97	14	33	91	5/6
	6	33	61	35	93	81	36	12	68	6/7
	7	121	184	158	149	112	163	118	71	--

VELOCITY = 7.4 n.mi./hr.

DIRECTION = 315 degrees

3.7.4 Summary

The model for the automatic calculation of motion vectors described here was based on an early version of the SRI model. There are several parameters which are poorly understood and require experimental results for their clarification. The more important ones have been mentioned here. The greatest asset of this approach is its flexibility. It should be rather easy to pick out those areas which require more sophisticated ideas to improve the results. Development of such ideas are not expected to be terribly difficult.

REFERENCES

1. Chandrasekhar, S., 1950: Radiative Transfer, Oxford University Press, London and New York, 393 pp.

2. van de Hulst, H. C., 1957: Light Scattering by Small Particles, John Wiley and Sons, Inc., New York, 470 pp.

3. Deirmendjian, D., 1969: Electromagnetic Scattering on Spherical Polydispersions, American Elsevier Publishing Co., Inc., 290 pp.

4. Mie, G., 1908: Ann. Physik., 25, pp 377-445.

5. Twomey, S., Jacobowitz, H., and H. B. Howell, 1967: Light Scattering by Cloud Layers, J. Atmos. Sci., 24, pp 70-79.

6. Plass, G. N., and G. W. Kattawar, 1971: Radiative Transfer in Water and Ice Clouds in the Visible and Infrared Region, Applied Optics, 10, pp 738-750.

7. McKee, T. B., and S. K. Cox, 1974: Scattering of Visible Radiation by Finite Clouds, J. Atmos. Sci., 31, pp 1885-1892.

8. Liou, K.-N., 1972: Light Scattering by Ice Clouds in the Visible and Infrared: A Theoretical Study, J. Atmos. Sci., 29, pp 525-536.

9. Lord Rayleigh, 1918: The Dispersal of Light by a Dielectric Cylinder, Phil. Mag., 36, pp 365-376.

10. Kuhn, P. M., 1963: Measured Effective Long-Wave Emissivity of Clouds. Mo. Wea. Rev., 91, pp 635-640.

11. Shifrin, K. S., 1954: To the Theory of the Radiative Properties of Clouds., Proc. Acad. Sci. USSR, 94, No. 4.

12. Yamamoto, G., Tanaka, M., and K. Kamitani, 1966: Radiative Transfer in Water Clouds in the 10-Micron Window Region., J. Atmos. Sci., 23, No. 3.

13. Jacobowitz, H., 1970: Emission, Scattering, and Absorption of Radiation in Cirrus Cloud Layers, PhD. Thesis, MIT, 181 pp.

14. Liou, K. -N., 1974: On the Radiative Properties of Cirrus in the Window Region and Their Influence on Remote Sensing of the Atmosphere, J. Atmos. Sci., 31, pp. 522-532.

15. Conover, J. H., and J. T. Bunting, 1977: Estimates from Satellites of Weather Erosion Parameters for Reentry Systems, Air Force Geophysics Lab Tech Rept 77-0260, 85 pp.

16. Snedecor, G. W., 1950: Statistical Methods, the Iowa State College Press, Ames, Iowa; pp. 221-225 and pp 351.

17. Croxton, F. E., and D. J. Cowden, 1940: Applied General Statistics, Prentice-Hall, New York, NY, Appendix G2.

18. Endlich, R. M., D. E. Wolf, D. J. Hall, and A. E. Brain (1971), Use of a Pattern Recognition Technique for Determining Cloud Motions from Sequences of Satellite Photographs, Journal Applied Meteorology, Vol 10, pp 105-117.

19. Ball, G. H., A. E. Brain, G. H. Burch and D. J. Hall (1964), Graphical Data Processing Research Study and Experimental Investigation, Rept. 16, Contract DA 36-039-AMC-03247 (E), Stanford Res. Institute, Menlo Park, CA, 53 pp.

ACKNOWLEDGMENT

Recognition must here be made of the coordinated team effort of the Regis College Research Center Staff whose members were: mathematicians Thomas Leonard and Jack Mettauer; mathematical analysts Lucy Aharonian, Gail Bertolini, Donald Cozzens, Ronald Fournier, Roy Glasser, Mary Hermann, Dorothy Moran and Joan Ward; physicists Harold Pratt and Thomas Foremen; engineers Barry Mareiro, Steven Telsey, John Jasionis and physical scientist John Powers. Preliminary status reports were typed by Jean Tremblay. Scientific reports were typed by other students assisting Jean Tremblay. Frances Fernandes, technical typist, has typed the final report.